AERODYNAMICS

The quality of the materials used in the manufacture of this book is governed by continued postwar shortages

Aerodynamics

by

A. WILEY SHERWOOD, M.E., M.S.
Professor of Aerodynamics
Glenn L. Martin College of Engineering
and Aeronautical Sciences
University of Maryland
Formerly Aeronautical Project Engineer
David Taylor Model Basin

First Edition
SECOND IMPRESSION

New York: London
McGRAW-HILL BOOK COMPANY, INC.
1946

PREFACE

Since the beginning of this century, the science of aerodynamics has been paced by the ever-increasing demands of the aviation industry. Much progress has been made in the improvement of experimental techniques and facilities, particularly in the construction of extremely large and powerful wind tunnels. Fully as important, though less spectacular, have been the contributions of theoretical methods which have proved invaluable in interpreting and correlating experimental results, in pointing the way toward future advances, and in aiding the understanding of aerodynamic phenomena. There is, however, no cause for complacency on the part of the aerodynamicist, for, even after the most judicious application of theoretical and wind-tunnel results, many new high-performance airplanes require costly alterations before they exhibit satisfactory flying qualities.

In this book, an effort has been made to cover the more practical phases of both theory and experiment. Unusual emphasis has been placed on the physical aspect of the theory in order to cultivate the interest of the student and to provide a general background suitable for later more intensive mathematical work in the field. This approach makes feasible the introduction of such normally advanced topics as compressibility and flutter. Experimental methods are discussed at considerable length because of the importance of model tests in airplane design. A description of the more important wind-tunnel corrections is included. An understanding of these corrections should prove of practical value, particularly if a laboratory course in aerodynamics is employed to supplement the text.

Experience in using most of the material of this book for several classes at the University of Maryland and for a

class at the David Taylor Model Basin was drawn on in a effort to make the book more teachable. The problen were originated for these courses and were selected on tl basis of practical significance and breadth of application.

Although use has been made of elementary calculus in few derivations in the text, it is believed that the studei who has no training in calculus will not be seriously han pered. Prior work in physics and mechanics will great benefit the student in studying this book.

The author wishes to express his indebtedness to Dr. J.] Younger of the University of Maryland for his assistan and encouragement in the early stages of the writing; Commander C. J. Wenzinger for his cooperation and gui ance; and to Messrs. M. J. Bamber, G. C. Hill, M. E. Lon J. N. Fresh, W. B. Barnett, and C. L. Poor III for the helpful criticisms and suggestions.

The author also wishes to acknowledge the kindness Dr. G. W. Lewis of the National Advisory Committee f Aeronautics for permission to use material from the pub cations of the Committee.

A. Wiley Sherwood.

College Park, Md.,
August, 1946.

CONTENTS

CHAPTER 1

PHYSICAL PROPERTIES OF AIR

The science of aerodynamics covers a broad field, dealing with both the flow of gases and the forces arising from the motion of a body relative to a gas. Preeminent in this field are the problems of flight, which overshadow all other applications in interest and practical importance. Indeed, most of the fundamental principles of aerodynamics can best be studied in relation to aeronautics, particularly in connection with the airplane.

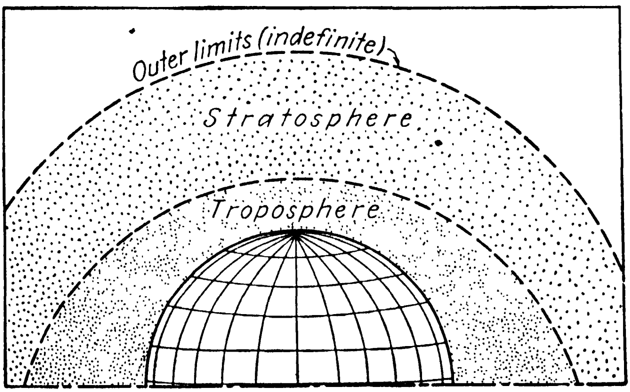

FIG. 1.1.—Divisions of the atmosphere.

The Atmosphere.—Basic to aeronautics are the properties of the atmosphere, the medium in which all flight takes place. The atmosphere is divided by the meteorologist into two layers, as shown in Fig. 1.1, of which the *troposphere* is nearest the earth. The troposphere is characterized by irregular fluctuations in temperature, wind velocity, and pressure. Average temperatures are highest at the ground where the air is heated through direct contact with the earth. Barometric pressures decrease with an increase

of altitude, not only in the troposphere but throughout the atmosphere, since the pressure at any altitude is due to the weight of a column of air of unit cross section extending vertically upward from that altitude to the outer limits of the atmosphere. The upper layer or *stratosphere* may be reached at an elevation of approximately 35,000 ft., the exact elevation depending on latitude and season. The air is unusually free from turbulence in the stratosphere with a temperature that remains quite uniformly at −67°F. regardless of altitude.

Since the performance of an airplane and the accuracy of commonly used instruments such as the altimeter and the air-speed indicator depend on atmospheric conditions, it is important that a standard or reference atmosphere be established. The National Advisory Committee for Aeronautics (N.A.C.A.) has defined a "standard atmosphere" which is presented in the form of tabulated values of temperatures and pressures at various altitudes. These values are based on the yearly average of temperatures and pressures at a latitude of 40 deg. in this country. Table I

TABLE I.—VALUES OF TEMPERATURE, PRESSURE, AND DENSITY AT VARIOUS ALTITUDES IN THE N.A.C.A. STANDARD ATMOSPHERE

Altitude, ft.	Temperature, deg. F.	Pressure, in. Hg	Mass density ρ, slugs/cu. ft.	$\frac{\rho_{alt}}{\rho_{sea\ level}}$
0	59.0	29.92	0.002378	1.000
1,000	55.4	28.86	0.002309	0.9710
2,000	51.8	27.82	0.002242	0.9428
3,000	48.4	26.81	0.002176	0.9151
4,000	44.8	25.84	0.002112	0.8881
5,000	41.2	24.89	0.002049	0.8616
6,000	37.6	23.98	0.001987	0.8358
7,000	34.0	23.09	0.001928	0.8106
8,000	30.6	22.22	0.001869	0.7859
9,000	27.0	21.38	0.001812	0.7619
10,000	23.4	20.58	0.001756	0.7384
20,000	−12.3	13.75	0.001267	0.5327
30,000	−48.1	8.88	0.000889	0.3740
40,000	−67	5.54	0.000582	0.2447
50,000	−67	3.44	0.000361	0.1517

presents this information in a form convenient for practical problems. It may be noted that standard sea-level values of temperature and pressure are

$$T = 59°\text{F.}$$
$$P = 29.92 \text{ in. Hg} = 14.69 \text{ lb./sq. in.}$$

Properties of Air.—Dry air is a physical mixture consisting approximately (by volume) of 78 per cent of nitrogen, 21 per cent of oxygen, and 1 per cent of carbon dioxide and other inert gases. The density of dry air varies with both temperature and pressure. Experiment shows that this variation conforms very closely to the laws of Boyle and Charles which may be combined and used most conveniently in the form of the *perfect gas equation*

$$PV = WRT \tag{1.1}$$

where P = absolute pressure, lb. per sq. ft.
V = volume, cu. ft.
W = weight, lb.
R = gas constant (53.34 ft. per deg. F. for air)
T = absolute temperature (459.6 + deg. F.)

The weight density w, in pounds per cubic foot, can readily be calculated by using Eq. (1.1).

$$w = \frac{W}{V} = \frac{P}{RT} \tag{1.2}$$

Of more frequent utility, however, is the mass density ρ (rho), in slugs per cubic foot. Recalling that

$$\text{mass} = \frac{\text{weight}}{\text{acceleration of gravity}}$$

we have

$$\rho = \frac{w}{g} = \frac{W}{Vg} = \frac{P}{RTg} \tag{1.3}$$

Applying this equation to the problem of finding the mass density of dry air corresponding to *standard* sea-level

conditions of temperature and pressure,

$$\rho = \frac{P}{RTg} = \frac{14.69 \times 144}{53.34 \times (459.6 + 59) \times 32.2}$$
$$= 0.002378 \text{ slug/cu. ft.}$$

This standard sea-level value of the mass density of dry air is frequently employed in aeronautical problems.

Atmospheric air may contain as much as 5 per cent (by volume) of water vapor which modifies the density as calculated on a dry-air basis. Water vapor is 37.8 per cent lighter than air under the same conditions so that neglect of the effect of moisture in density calculations leads to results that are slightly high. Since a barometer reads the total of the pressure of the dry air and the vapor pressure of the moisture in the atmosphere, the pressure P of Eq. (1.3) must be reduced by a factor involving the vapor pressure e, and the difference in density between water vapor and dry air to express accurately the density of atmospheric air, that is,

$$\rho = \frac{P - 0.378e}{RTg} \tag{1.4}$$

where ρ = mass density of atmospheric air, slugs per cu. ft.
P = barometric pressure, lb. per sq. ft.
e = vapor pressure of atmospheric moisture, lb. per sq. ft.

The vapor pressure is generally determined from psychrometric charts based on wet- and dry-bulb thermometer readings.

Since the effect of humidity in the calculation of mass density seldom exceeds 1 per cent, humidity corrections are generally neglected except in accurate wind-tunnel tests.

Absolute Viscosity.—Viscosity is of the utmost importance in influencing the resistance to motion of an immersed body through a fluid. In developing a mathematical expression for the action of viscosity, a simple experiment will be analyzed.

Consider the upper plate of Fig. 1.2 in motion parallel to the lower fixed plate with a velocity V, through the action of a constant force F. The fluid tends to adhere to each plate so that the top surface of the fluid between the plates travels to the right with the velocity of the upper plate V, and the bottom surface remains stationary, with a uniformly varying velocity between. Any layer of the fluid must therefore move with a *relative* velocity to the adjacent layers on either side. Thus any layer of the fluid tends to slide over its neighbors, producing viscous forces in the fluid to resist the applied force F.

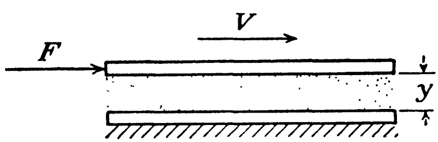

FIG. 1.2.—Experimental study of viscosity.

A systematic investigation conducted with this apparatus by changing only one variable at a time would disclose the following:

1. The force F varies with the test fluid (such as air, water, or oil).
2. F varies with the temperature of the test fluid.
3. F is independent of the pressure of the fluid (within the range of practical application to aeronautics).
4. F varies directly with the speed with which one layer tends to slide past its neighbors. This sliding speed may be expressed as the change of velocity per unit distance between the plates V/y, or more generally as dV/dy, the *velocity gradient*.
5. F varies directly with the area A of the plates.

Therefore,

$$F \propto A \frac{dV}{dy}$$

and

$$F = \mu A \frac{dV}{dy} \tag{1.5}$$

where μ (mu), the coefficient of proportionality, is called the "absolute viscosity" of the fluid. Using consistent English units in Eq. (1.5), (F in pounds, A in square feet, dV in feet per second, dy in feet), μ must have the units of pound-seconds per square foot.

The absolute viscosity of air increases with temperature as shown by the curve of Fig. 1.3. This is due to the greater agitation of the air molecules at higher temperatures

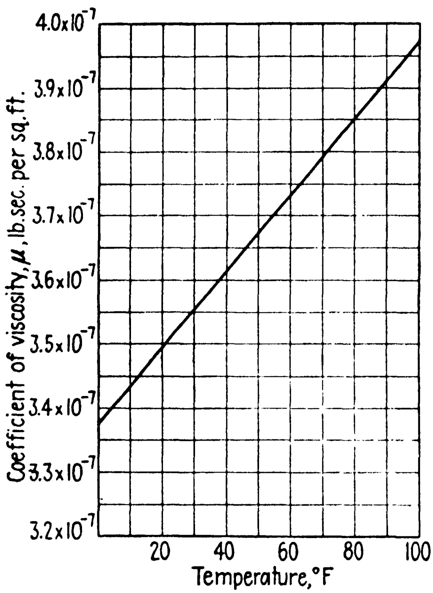

FIG. 1.3.—Variation of the coefficient of viscosity of dry air with temperature.

which promotes the interchange of particles between adjacent layers. In the apparatus of Fig. 1.2, such an interchange would tend to speed up the slower layers and drag back the faster ones to increase the viscous drag on the upper plate.

The ratio of absolute viscosity to mass density frequently enters into aeronautical calculations. We accordingly define

$$\nu \text{ (nu)} = \text{kinematic viscosity} = \frac{\mu}{\rho} \qquad (1.6)$$

Since ν involves density, its value for air changes with pressure as well as with temperature.

For standard conditions $\nu = 0.0001566$ sq. ft./sec.

PROBLEMS

1. Compute the weight density w and the mass density of dry air at a temperature of 100°F. under a pressure of 28 in. Hg.

2. Calculate the percentage variation from standard sea-level density ($\rho = 0.002378$ slug per cu. ft.) corresponding to assumed extreme atmospheric conditions of (*a*) $T = -20$°F., $P = 31$ in. Hg; (*b*) $T = 100$°F., $P = 27$ in. Hg. (Assume dry air.)

3. Calculate the percentage error introduced into the calculated mass density by assuming dry air at 70°F. and 30 in. Hg as being at standard sea-level density.

4. What percentage error is introduced by the assumption of standard sea-level density for dry air at 59°F. and 30.5 in. Hg?

5. What force is required to move the upper plate of the apparatus of Fig. 1.2 at a speed of 300 ft. per sec.? The area $A = 2$ sq. ft., $y = 0.010$ in., and the fluid between the plates is air at a temperature of 60°F.

6. What is the kinematic viscosity of dry air at a temperature of 100°F. and a pressure of 31 in. Hg?

CHAPTER 2

PRINCIPLES OF FLUID FLOW

As an aid to visualization, any fluid may be considered as composed of innumerable particles of very small size. In flowing around an immersed body, these fluid particles generally take various paths and assume differing velocities as they proceed. The velocities of successive particles taken at any *fixed* point in the flow pattern may vary from one instant to the next producing *unsteady flow* or, in the more usual condition of *steady flow*, the velocity of the fluid at any point may remain constant as successive fluid particles file past. This latter condition of steady flow not only exists in most practical problems but affords considerable simplification in theoretical developments as well, so that steady flow will be assumed throughout subsequent discussions.

Streamlines and Stream Tubes.—Lines representing the paths followed by fluid particles in passing through a field of flow are known as "streamlines." The velocity of a particle at any point must consequently extend along a tangent to the streamline passing through that point. The intersection of two streamlines is plainly impossible since a particle at such an intersection could not move along each streamline at the same time. For convenience in interpretation, only a few streamlines are generally used to describe a flow pattern about an immersed object. These are selected at uniform intervals in the approaching *undisturbed* flow to the object. A streamline flow pattern about an airfoil is shown in Fig. 2.1.

A stream tube is made up of the streamlines, an infinite number, which may be drawn tangent to any closed curve located in the fluid, as shown in Fig. 2.2. A stream tube

acts like a conduit with impervious walls for no fluid can enter or leave without creating the impossible situation of an intersection of streamlines. In the flow pattern of Fig. 2.1, stream tubes of unit width bounded on their upper and lower sides by adjacent streamlines may be chosen, provided the flow is known to proceed in parallel planes to that of the figure in a *two-dimensional* manner.

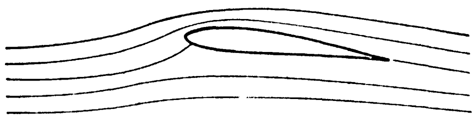

FIG. 2.1.—Streamline-flow pattern around an airfoil.

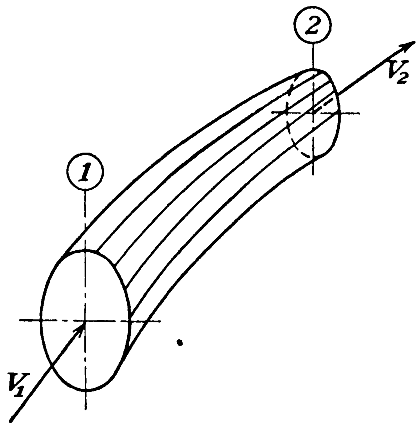

FIG. 2.2.—Stream tube.

The Equation of Continuity.—Since there can be no flow through the walls of a stream tube, the mass of fluid flowing per unit of time past any one section must equal the mass per unit time past any other section, that is (Fig. 2.2),

$$\frac{\text{Mass}_1}{\text{Unit time}} = \frac{\text{mass}_2}{\text{unit time}}$$

and

$$\frac{(\rho \times \text{quantity})_1}{\text{Unit time}} = \frac{(\rho \times \text{quantity})_2}{\text{unit time}} \tag{2.1}$$

but $\frac{\text{quantity}}{\text{unit time}}$ past any section of a stream tube can be represented by the volume of a cylinder with the area of the section A as the base and the average velocity at the section V as the altitude (Fig. 2.2). Substituting in Eq. (2.1),

$$\rho_1 A_1 V_1 = \rho_2 A_2 V_2 \tag{2.2}$$

If the density remains constant between sections 1 and 2, $\rho_1 = \rho_2$ and

$$A_1 V_1 = A_2 V_2 \tag{2.3}$$

where A_1 and A_2 are the cross-sectional areas at any two sections of a stream tube, sq. ft., V_1 and V_2 are the velocities of flow through the steam tube at sections 1 and 2, ft. per sec.

The foregoing expressions are alternative forms of the *continuity* equation, so named because its derivation is predicated on the condition of steady, continuous flow. For most aerodynamic applications the constant density form [Eq. (2.3)] may be employed since usual pressure changes in the air flowing around an immersed body make only negligible differences in the air density.

The continuity equation may be applied to the flow pattern of Fig. 2.1 to evaluate the velocity of the fluid at any desired point in terms of the streamline spacing. As stated previously, stream tubes of unit width enclosed between adjacent streamlines may be considered, as long as the flow is two-dimensional. Writing the continuity equation between any two sections of one of these stream tubes,

$$A_1 V_1 = A_2 V_2$$

Letting S_1 and S_2 represent the streamline spacing at sections 1 and 2,

$$S_1 \times \text{unit width} \times V_1 = S_2 \times \text{unit width} \times V_2$$

and reducing,

$$S_1 V_1 = S_2 V_2 \tag{2.4}$$

Under the usual conditions of constant velocity and uniform spacing of streamlines in the undisturbed fluid approaching the airfoil, the product SV in the undisturbed portion of the flow pattern is the same for all stream tubes; so, under these circumstances, points 1 and 2 of Eq. (2.4) need not be confined to a single stream tube but may be taken as any two points in the field of flow. The velocity of fluid flow therefore varies inversely as the streamline spacing throughout the flow pattern. Thus, the convergence of the streamlines above the leading edge of the airfoil indicates a higher velocity in this region than that

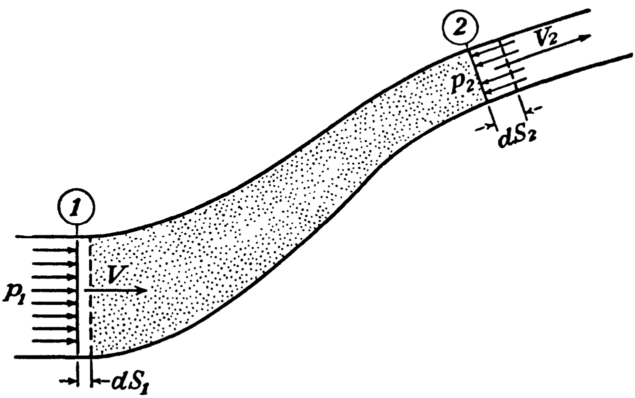

FIG. 2.3.—Development of Bernoulli's equation.

of the free stream, while the relatively large spacing directly in front of the airfoil denotes a lower velocity than that of the free stream.

Bernoulli's Equation.—The development of the general form of the continuity equation [Eq. (2.2)] required only the assumption of steady flow conditions. By further restricting our analysis to an *ideal* frictionless fluid of constant density, a very important relation between the pressures and velocities in a fluid can be derived, known as "Bernoulli's equation."

In the development of Bernoulli's equation, a portion of the fluid flowing within a stream tube will be considered. The work done on this portion by the external pressure

forces during a short time interval, dt, will be equated to the change of energy of the fluid within this volume, in accordance with the principle of the conservation of energy.

In Fig. 2.3, the initial position of the isolated volume of fluid under consideration is shown by solid lines and its final position (at the end of time dt) by dotted lines. The fluid progresses a distance ds_1 in the large section 1 of area A_1 and a distance ds_2 in section 2 of area A_2. For continuity of flow,

$$A_1 ds_1 = A_2 ds_2$$

The work done by the external pressure forces is positive at section 1 where the pressure p_1 and the displacement ds_1 are in the same direction and negative at section 2 where pressure p_2 and the displacement ds_2 oppose. The work done by the pressure forces normal to the walls of the stream tube is zero, since these forces are not displaced during the flow through the stream tube. The net work is therefore

$$W = p_1 A_1 ds_1 - p_2 A_2 ds_2$$

where p_1 and p_2 are the pressures at sections 1 and 2.

The change of energy within the isolated volume is confined to differences in the energies of the end sections since the total energy of the shaded volume does not change during the chosen time interval dt. The change of potential energy due to differences in elevation between the end sections can safely be neglected in aeronautical problems since it is relatively insignificant in magnitude when compared with the difference in the kinetic-energy terms. The change in kinetic energy may be written

$$\Delta E = \tfrac{1}{2} m_2 V_2^2 - \tfrac{1}{2} m_1 V_1^2$$

and, therefore,

$$\Delta E = \frac{\rho}{2} A_2 ds_2 V_2^2 - \frac{\rho}{2} A_1 ds_1 V_1^2$$

Equating the external work done on the fluid to its change of kinetic energy,

$$W = \Delta E$$

and

$$p_1 A_1 ds_1 - p_2 A_2 ds_2 = \frac{\rho}{2} A_2 ds_2 V_2^2 - \frac{\rho}{2} A_1 ds_1 V_1^2$$

Dividing by $A_1 ds_1$ or its equivalent $A_2 ds_2$,

$$p_1 - p_2 = \frac{\rho}{2}(V_2^2 - V_1^2)$$

Rearranging,

$$p_1 + \frac{\rho}{2} V_1^2 = p_2 + \frac{\rho}{2} V_2^2 \qquad (2.5)$$

where p_1 and p_2 are the pressures at any two points, 1 and 2, in a single stream tube, lb. per sq. ft.; V_1 and V_2 are the velocities at 1 and 2, ft. per sec.; ρ is the mass density of the fluid, slugs per cu. ft.

The term $\rho V^2/2$ has the units of kinetic energy per cubic foot of the fluid, as may be seen by writing the units of its equal $wV^2/2g$.

$$\text{Units of } \frac{wV^2}{2g} = \frac{\text{lb./cu. ft.} \times \text{ft.}^2/\text{sec.}^2}{\text{ft./sec.}^2} = \frac{\text{ft.-lb.}}{\text{cu. ft.}}$$

In the same way p has the units

$$\frac{\text{lb.}}{\text{sq. ft.}} = \frac{\text{lb.}}{\text{sq. ft.}} \times \frac{\text{ft.}}{\text{ft.}} = \frac{\text{ft.-lb.}}{\text{cu. ft.}}$$

Since the term p has the units of energy, it is often called the "pressure energy" of the fluid. Considered from an energy standpoint, Bernoulli's equation states that the sum of the pressure and the kinetic energies at any point along a stream tube is equal to the sum of the two energies at any other point—that the *total energy* of the fluid is constant along a stream tube.

In many applications, it is convenient to regard the terms of Bernoulli's equation as pressures rather than as

energies per cubic foot of the fluid. This interpretation is permissible since the units of both p and $\rho V^2/2$ may be either foot-pounds per cubic foot or its equivalent pounds per square foot. Viewed in this manner, p is termed the "static pressure" of the fluid and $\rho V^2/2$ the "dynamic pressure" of the fluid, usually designated by the letter q.

Application of Bernoulli's Equation.—The pressure distribution in a flow pattern like that of Fig. 2.1 may now be determined, provided the flow conforms to the three basic conditions underlying Bernoulli's equation: steady flow, zero viscosity, and constant density.

To meet the first requirement of steady flow it is only necessary that the air approach the airfoil at a constant velocity and that the position of the airfoil with respect to the air stream remain unchanged.

The second requirement is not directly fulfilled, however, since air does not have zero viscosity. On the other hand, the viscous forces within the fluid depend upon the velocity gradient dV/dy, as well as upon the coefficient of viscosity, so viscous effects may be small where the velocity gradient is small. Experimental investigations generally show extremely low velocity gradients throughout any flow pattern except in a thin *boundary layer* of fluid covering the surface of an immersed body and in the turbulent *wake* behind the body. Outside of these two regions the effect of viscosity may be considered negligible.

The final requirement of constant fluid density is very nearly realized since the variation of pressure over the airfoil, although of the utmost importance in creating lift, produces only minor variations in density.

As in the application of the continuity equation, a condition of constant velocity and pressure in the undisturbed flow approaching the airfoil of Fig. 2.1 is of considerable advantage. With this condition fulfilled the total energy of the fluid, $p + \rho V^2/2$, is the same for all stream tubes and Bernoulli's equation may be written between any two points in the flow pattern. It becomes evident that with

the total energy constant the pressure of the air must be high where the velocity is low and vice versa. For instance, the convergence of the streamlines over the leading edge of the airfoil indicates a higher velocity through the continuity equation and a lower pressure through Bernoulli's equation than the velocity and pressure of the undisturbed flow.

If a body like that of Fig. 2.4 is pointed directly into an air stream, the streamlines will assume the general form shown. The streamline coinciding with the axis of sym-

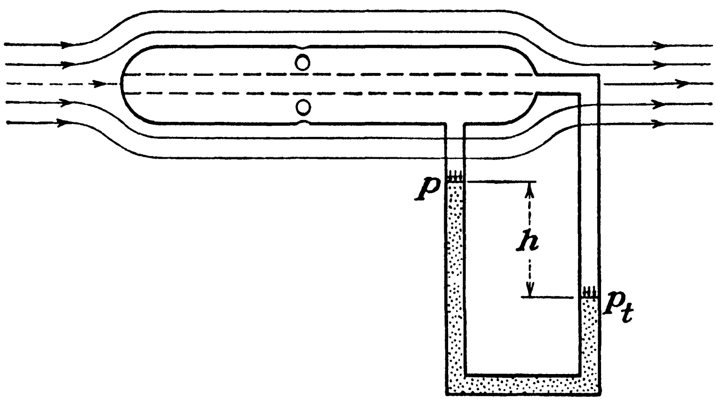

FIG. 2.4.—Diagram of a pitot-static tube.

metry of the body represents the path of particles coming to a complete stop before proceeding around the body. This point where the fluid particles have zero velocity is known as the "stagnation point." A similarly situated point occurs on the after end of the body. A short distance behind the nose of the body the streamlines again become straight and parallel with velocities and pressures equal to those of the free stream.

Writing Bernoulli's equation between the stagnation point and a point in the parallel section of the body of Fig. 2.4,

$$p_t + 0 = p + \frac{\rho V^2}{2}$$

Solving for V,

$$V = \sqrt{2(p_t - p)/\rho} \tag{2.6}$$

where p_t = pressure of the fluid at the stagnation point, often called the "total pressure," lb. per sq. ft.
p = static pressure in the undisturbed fluid, lb. per sq. ft.
V = velocity of the undisturbed fluid, ft. per sec.
ρ = mass density of air throughout the flow, slugs per cu. ft.

The pressure difference $p_t - p$ can be conveniently measured with a differential manometer, as shown in Fig. 2.4, connected to openings at the stagnation point and in the side wall of the body. The relation between the manometer reading h, in feet of manometer liquid of weight density w_1, and the pressure difference $p_t - p$ may be derived by considering the equilibrium of the weight of the unbalanced liquid column of the manometer with the unbalanced pressure force, that is,

Difference in pressure forces = weight of liquid column and so

$$(p_t - p)A = Ahw_l$$

Canceling,

$$p_t - p = w_l h$$

Substituting in Eq. (2.6),

$$V = \sqrt{\frac{2w_1h}{\rho}} \tag{2.7}$$

where w_1 = weight density of the manometer fluid, lb. per cu. ft. (62.5 lb. per cu. ft. for water)
h = manometer deflection, ft.
ρ = mass density of the fluid flowing past the tube, slugs per cu. ft.

The pitot-static tube forms a simple, direct, and accurate method for measuring the velocity of fluid flow. Since the

accuracy of pitot-static tubes depends to a large degree on general proportions and the size and location of the pressure

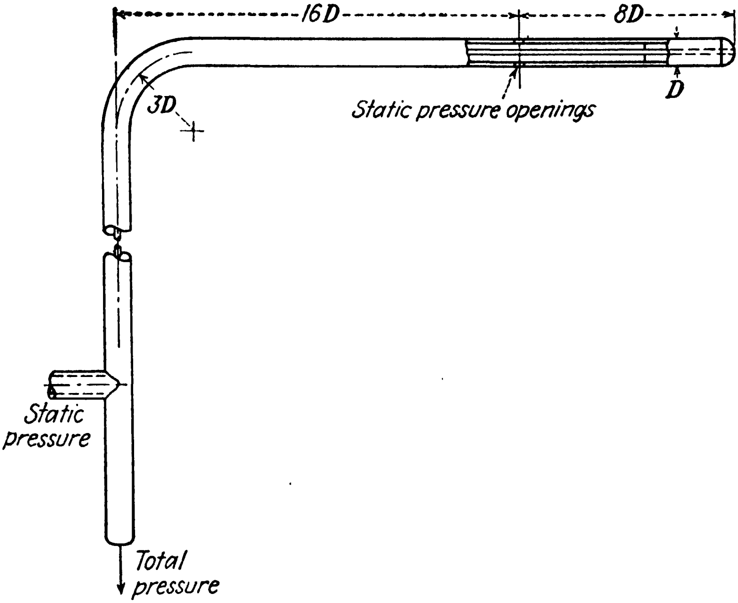

FIG. 2.5.—General proportions for a pitot-static tube. (*N.A.C.A. Technical Note* 546.)

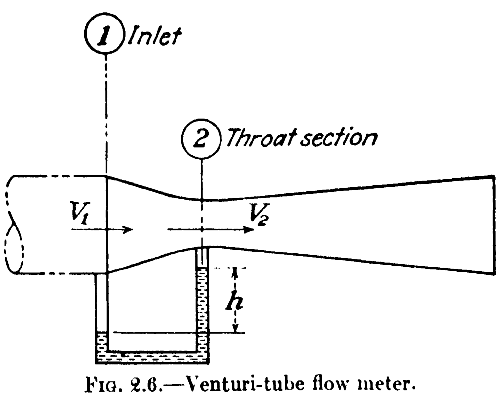

FIG. 2.6.—Venturi-tube flow meter.

openings, it is advisable to follow a proved design like that of Fig. 2.5 in the construction of a new instrument.

The Venturi Tube.—A channel with converging walls followed by a more gradual diverging portion, as in Fig. 2.6,

is known as a "venturi tube." The useful properties of the venturi tube can be made evident through an application of Bernoulli's equation and the continuity equation between the entrance, section 1 of Fig. 2.6, and the narrowest or *throat* section at 2,

$$\frac{\rho V_1^2}{2} + p_1 = \frac{\rho V_2^2}{2} + p_2 \tag{2.8}$$

and, according to the continuity equation,

$$V_2 = \frac{A_1}{A_2} V_1$$

Substituting in Eq. (2.8) and solving for $p_1 - p_2$, we have

$$p_1 - p_2 = \frac{\rho V_1^2}{2}\left[\left(\frac{A_1}{A_2}\right)^2 - 1\right] \tag{2.9}$$

This equation shows that air flowing through the inlet of a venturi tube will be reduced in pressure at the throat by an amount depending upon the inlet velocity and density and the relative dimensions of inlet and throat sections. The reduced pressure at the throat of a venturi tube is employed in most aircraft carburetors for drawing gasoline through tiny jets into venturi-shaped air passageways. An approximate proportionality between air and fuel is obtained in this way.

A further inspection of Eq. (2.9) shows that the velocity of flow of a fluid of known density through a given venturi tube can be calculated if the pressure difference between inlet and throat sections is measured. Flow measurements in fluid pipe lines are frequently made in this way.

Momentum of Air Streams.—An understanding of the application of Newton's second law to fluid-flow problems is an important prelude to the study of wing and propeller theory. This law can be stated

$$\text{Impulse} = \text{change of momentum}$$

or

$$Ft = M'(V_1 - V_2) = M'\Delta V$$

Dividing both sides by the time t,

$$F = \frac{M'\Delta V}{t} \tag{2.10}$$

where the force F must act in the same direction as the change of velocity ΔV of the mass M'. Since in flow problems, we employ the symbol M as the mass flowing *per unit time*,

$$M = \frac{M'}{t}$$

and, therefore,

$$F = M\Delta V \tag{2.11}$$

Assuming that the mass of air deflected per second, M, through an angle θ (theta) by a deflecting vane is known

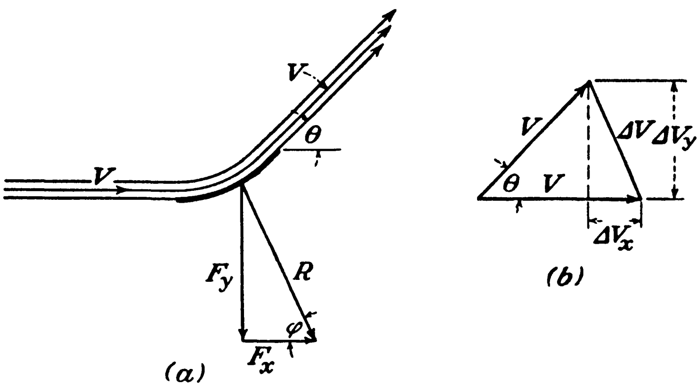

FIG. 2.7.—Force exerted by an air jet on a deflecting vane.

(Fig. 2.7), the horizontal and vertical components of the resultant force can be computed. Since the passage of the air stream over the blade is assumed to be frictionless, $V_1 = V_2$ in *magnitude* and any change in velocity ΔV must result from a change in the *direction* of flow of the fluid in passing over the vane. Referring to Fig. 2.7, the force exerted by the fluid in the horizontal or X direction may be written

$$F_x = M \times (\text{horizontal component of the velocity change, } \Delta V_x)$$

that is,

$$F_x = M(V - V\cos\theta) = MV(1 - \cos\theta)$$

Similarly, the vertical component of the force on the blade F_y becomes

$$F_y = M \times \Delta V_y = MV\sin\theta$$

The resultant force R is equal to the square root of the sum of the squares of its two components F_x and F_y.

$$R = \sqrt{F_x^2 + F_y^2} = \sqrt{[MV(1 - \cos\theta)]^2 + (MV\sin\theta)^2}$$
$$= MV\sqrt{2(1 - \cos\theta)} \quad (2.12)$$

The angle φ (phi) between R and the horizontal may be related to the deflection angle of the vane θ,

$$\tan\varphi = \frac{F_y}{F_x} = \frac{\sin\theta}{1 - \cos\theta} \quad (2.13)$$

Momentum methods are successfully used in the determination of the drag force on wind-tunnel models of airplane

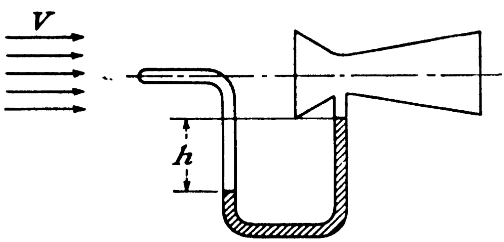

FIG. 2.8.—Combination pitot and venturi tube.

wings to secure more accurate data than may be obtained with the usual force-measuring system. The technique involves taking a series of pitot-static readings directly before and behind the model to furnish sufficient information for the calculation of the mass of air affected and its retardation in velocity. The same system has been employed on airplane wings during actual flight where direct force readings were not feasible.

PROBLEMS

(Assume standard sea-level conditions unless otherwise specified.)

1. Air passes through the 8-ft. circular test section of an atmospheric wind tunnel at an average velocity of 200 m.p.h. Compute the weight of air circulated in pounds per second and the quantity of flow in cubic feet per second.

2. If the streamlines of Fig. 2.1 are spaced 0.25 in. apart in the undisturbed flow in front of the airfoil and converge to a minimum spacing of 0.18 in. above the airfoil, compute the maximum velocity of flow corresponding to an undisturbed relative velocity of 100 m.p.h. What is the minimum pressure above the airfoil?

3. The minimum pressure above an airfoil falls to 0.1 lb. per sq. in. below the pressure of an 150-m.p.h. air stream. What is the maximum velocity above the airfoil?

4. A U-tube manometer attached to a pitot-static tube shows a deflection of 6 in. of water. What is the velocity of flow past the head of the tube in feet per second? in miles per hour?

5. A pitot-static tube exposed to the air stream approaching an airfoil produces a deflection of 6 in. of water in an attached manometer. If the minimum pressure above the airfoil is 0.25 lb. per sq. in. below the pressure of the undisturbed air stream, what is the maximum velocity of flow over the airfoil?

6. The pointer of an air-speed indicator reads 100 m.p.h. at an elevation of 10,000 ft. What is the true air speed? (The pointer is actuated by the differential pressure from a pitot-static tube. The dial is calibrated according to standard sea-level air density.)

7. Air enters a carburetor venturi tube with a velocity of 100 m.p.h. and a pressure of 14.7 lb. per sq. in. What is the pressure at the throat if the ratio of inlet to throat diameter is 2:1?

8. A wind tunnel with an 8-ft. circular test section is equipped with a circular return passage 25 ft. in diameter. What is the difference in pressure in inches of water between the test and return sections corresponding to a test air speed of 200 m.p.h.? Neglect friction and assume standard sea-level air density at both sections.

9. A pressure of 0.25 lb. per sq. in. below atmospheric is desired to operate a gyroscopic compass. What is the required throat diameter of a venturi tube to furnish this pressure at an air speed of 100 m.p.h.? The inlet diameter of the tube is 4 in.

10. A venturi tube with a 4-in. diameter entrance and a 3-in. throat is exposed to an air stream. A water manometer connected between inlet and throat shows a deflection of 7 in. What is the weight of flow in pounds per second?

11. A combination venturi and pitot tube as shown in Fig. 2.8 has been proposed for increasing the pressure differential of an air-speed indicator for a given air speed. If the value of h is 10 in. of water corresponding to a venturi tube area ratio of 4:1, what is the air speed? For this air speed, what would be the value of h if the venturi tube were used alone? the pitot tube alone? Assume that the entrance velocity to the venturi tube is equal to the air speed.

12. What force is required to deflect a 4-ft. diameter horizontal air stream moving with a velocity of 100 m.p.h. downward through an angle of 60 deg.? At what angle does the resultant force act?

13. The 90-deg. corner vanes in a wind tunnel are 20 ft. long and spaced 8 in. apart. What is the resultant force on each of these vanes corresponding to an air velocity of 50 m.p.h.?

14. A propeller fan 3 ft. in diameter accelerates air from rest to a speed of 15 m.p.h. If the velocity through the propeller is 7.5 m.p.h., what is the end thrust on the fan? What horsepower does the fan impart to the air?

CHAPTER 3

DIMENSIONAL ANALYSIS AND DYNAMIC SIMILARITY

Dimensional analysis affords a mathematical approach to a wide range of engineering problems which would prove difficult, if not impossible, to solve by other means. With only elementary algebraic equations, dimensional analysis assists in the systematization of laboratory experimentation, the checking and derivation of physical equations, and the correlation of model and full-scale results.

The Fundamental Dimensions.—In dimensional analysis the word "dimension" refers to the nature or kind of a physical quantity; common usage, on the other hand, associates the word with an arbitrary standard of measurement. A line, for instance, can have only the dimension *length* in dimensional analysis, although, in nontechnical language, its "length dimension" might be expressed as 1 yd., 3 ft., or 91.4 cm., depending upon the ratio of its length to the standard yard, foot, or centimeter. Thus the word "dimension" has a more fundamental meaning in dimensional analysis which is independent of numerical units.

In examining the natures—that is, the dimensions—of the physical quantities that enter into aeronautical problems, many similarities and interrelationships become apparent. In particular, the dimensions of *mass* (M), *force* (F), *length* (L), and *time* (T) are generally sufficient to express the dimensions of all the other quantities. To cite a few examples:

$$\text{Area} \equiv \text{length} \times \text{length} = L^2$$

$$\text{Volume} \equiv \text{length} \times \text{length} \times \text{length} = L^3$$

$$\text{Velocity} = \frac{\text{distance}}{\text{time}} \equiv \frac{L}{T}$$

$$\text{Acceleration} = \frac{\text{velocity}}{\text{time}} \equiv \frac{L}{T^2}$$

In addition, the use of Newton's second law permits further simplification by reducing the number of fundamental dimensions to three, since

$$\text{Force} = \text{mass} \times \text{acceleration}$$

and, therefore,

$$F = \frac{ML}{T^2} \tag{3.1}$$

Equation (3.1) can be used to express F in terms of the other three dimension (M,L,T) leaving mass, length, and time as the *fundamental* dimensions. These are the fundamental dimensions that are generally chosen although a rearrangement of Eq. (3.1) would permit expressing either M, L, or T in terms of the other dimensions. In this way force, length, and time (F,L,T) systems are sometimes employed.

Adopting the M, L, T system, the dimensional expressions for pressure and viscosity may now be written:

$$\text{Pressure} = \frac{\text{force}}{\text{area}} = \frac{\frac{ML}{T^2}}{L^2} = \frac{M}{LT^2}$$

$$\text{Absolute viscosity} = \mu = \frac{\frac{F}{A}}{\frac{dV}{dy}} = \frac{\frac{ML}{T^2L^2}}{\frac{L}{TL}} = \frac{M}{LT} \tag{3.2}$$

The units of absolute viscosity in the M, L, T system are in this manner made evident by its dimensional formula. Thus,

$$\frac{M}{LT} = \frac{\text{mass}}{\text{length} \times \text{time}} = \frac{\text{slugs}}{\text{ft.-sec.}}$$

Dimensional expressions for all the common aeronautical quantities are tabulated for later reference in Table II.

Application of Dimensional Analysis.—The quantities on one side of any true equation must be exactly balanced by those on the other. This implies that every L, M, and T

TABLE II

Quantity	Symbol	Dimensional formula in M, L, T system	Engineering units in M, L, T or F, L, T systems
Length	L, l	L	Ft.
Mass	m	M	Slug
Time	t	T	Sec.
Area	A	L^2	Sq. ft.
Volume	V	L^3	Cu. ft.
Velocity	V, v	L/T	Ft./sec.
Acceleration	A, a	L/T^2	Ft./sec.^{2}
Force	F	ML/T^2	Lb.
Weight	W	ML/T^2	Lb.
Work, energy	W, E	ML^2/T^2	Ft.-lb.
Specific weight	w	M/L^2T^2	Lb./cu. ft.
Density	ρ	M/L^3	Slugs/cu. ft.
Pressure	p	M/LT^2	Lb./sq. ft.
Absolute viscosity	μ	M/LT	Slugs/ft.-sec.

dimension on one side of an equation must be offset by a corresponding dimension *raised to the same power* on the other, since a length, for instance, could not conceivably be balanced by any amount of mass or time. In other words, a true physical equation must be *dimensionally homogeneous.* This principle is commonly used in the checking of units. In Eq. (3.2), for example, the units of μ were taken as the units of its equal $(F/A)/(dv/dy)$.

The methods of dimensional analysis are often advantageously employed in the derivation of physical formulas. This application requires that the variables involved be known and to this extent relies upon the judgment and experience of the investigator. As an illustrative problem, the equation for the speed of sound in a gas C will be determined, based on the knowledge that C depends upon the mass density ρ and the pressure p. Expressed mathematically, C is a function of ρ and p or

$$C = f(\rho,p)$$

and, therefore,

$$C = k\rho^a p^b \tag{3.3}$$

where k, a, and b are unknown constants. Writing Eq. (3.2) dimensionally,

$$\frac{L}{T} = \left(\frac{M}{L^3}\right)^a \left(\frac{M}{LT^2}\right)^b$$

According to the principle of dimensional homogeneity, the exponents of L, M, and T on the two sides of this equation must balance.
Equating exponents,
Of L,

$$1 = -3a - b$$

Of M,

$$0 = a + b$$

Of T,

$$-1 = -2b$$

Thus $a = -\frac{1}{2}$ and $b = \frac{1}{2}$.
Substituting in the original Eq. (3.3),

$$C = k\rho^{-\frac{1}{2}}p^{\frac{1}{2}} = k\sqrt{\frac{p}{\rho}} \tag{3.4}$$

The value of k cannot be determined by dimensional analysis but can easily be found in the laboratory by measuring corresponding values of ρ and p and substituting these values into Eq. (3.4). In this case, $k = \sqrt{1.4}$ and Eq. (3.4) becomes

$$C = \sqrt{\frac{1.4p}{\rho}} \tag{3.5}$$

This relation will be useful in a later discussion of the effects of compressibility.

Dynamic Similarity.—The design of a new airplane is based to a large extent on data from wind-tunnel tests and on the actual performance of similar airplanes. Dimensional analysis proves very valuable in this connection by

indicating the conditions for accurate transference of experimental results to the new design.

For complete correspondence between a model and its full-scale prototype there must be geometrical similarity between the two, and each must be oriented in the same way to the fluid flow. Thus in Fig. 3.1, the model and prototype are of the same shape and are inclined at the same angle α (alpha) to the direction of flow. In addition to this condition, moreover, the flow patterns must be similar; that is, the velocities at *any* two corresponding points, such as M and P of Fig. 3.1, must be in the same

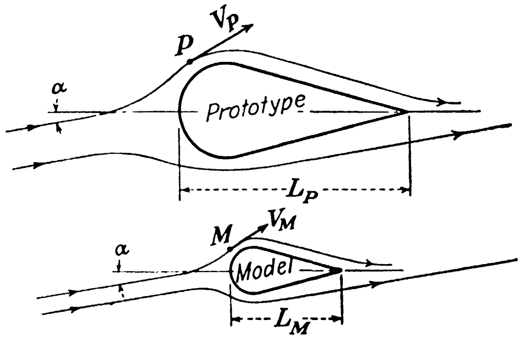

FIG. 3.1.—Similarity of fluid flows.

direction and in a constant ratio—the necessary conditions for *dynamic similarity* between the flow patterns.

The direction and magnitude of the velocity at any point in a fluid depend upon the resultant of the forces acting upon a fluid particle at that point. The principal forces acting upon such a particle are those due to inertia and to viscosity (for all but very high velocities of flow). If the resultants of the inertia forces and the viscous forces for any two corresponding points, such as M and P of Fig. 3.1, are to extend in the same direction, then

$$\left(\frac{\text{Inertia force}}{\text{Viscous force}}\right)_M = \left(\frac{\text{inertia force}}{\text{viscous force}}\right)_P \qquad (3.6)$$

These ratios are dimensionless since the dimensions of the numerator ML/T^2 cancel those of the denominator.

This fact will be used in their evaluation. To this end, the physical quantities upon which the viscous and inertia forces depend must be selected.
These are

1. The mass density of the fluid ρ
2. The velocity of flow of the fluid V
3. The length of the body L
4. The viscosity of the fluid μ

Therefore

$$\frac{\text{Inertia force}}{\text{Viscous force}} = \text{dimensionless ratio} = F(\rho, V, L, \mu)$$

and

$$\text{Dimensionless ratio} = \rho^w V^x L^y \mu^z$$

Raising each side to the $1/w$ power,

$$(\text{Dimensionless ratio})^{1/w}$$
$$= \text{another dimensionless ratio} = \rho V^{x/w} L^{y/w} \mu^{z/w}$$

Making the substitutions $x/w = a$, $y/w = b$, $z/w = c$,

$$\text{Dimensionless ratio} = \rho V^a L^b \mu^c \tag{3.7}$$

Substituting in terms of L, M, and T,

$$L^0 M^0 T^0 = \frac{M}{L^3}\left(\frac{L}{T}\right)^a L^b \left(\frac{M}{LT}\right)^c$$

Equating exponents,
Of M,

$$0 = 1 + c$$

Of L,

$$0 = -3 + a + b - c$$

Of T,

$$0 = -a - c$$

and

$$c = -1, \qquad a = 1, \qquad b = 1$$

Substituting in Eq. (3.7),

$$\text{Dimensionless ratio} = \rho V L \mu^{-1} = \frac{\rho V L}{\mu} = \frac{\text{inertia force}}{\text{viscous force}}$$

so that, in accordance with Eq. (3.6), the requirement for dynamic similarity of two fluid flows may be written

$$\left(\frac{\rho VL}{\mu}\right)_M = \left(\frac{\rho VL}{\mu}\right)_P \tag{3.8}$$

The ratio $\rho VL/\mu$ is termed "Reynolds number" and will be designated by the symbol R. The results of this analysis can now be summarized: *if two flows are dynamically similar, their Reynolds numbers must be equal.*

Further Significance of Reynolds Number.—In addition to serving as the criterion for dynamic similarity, the value of R furnishes additional information regarding the nature

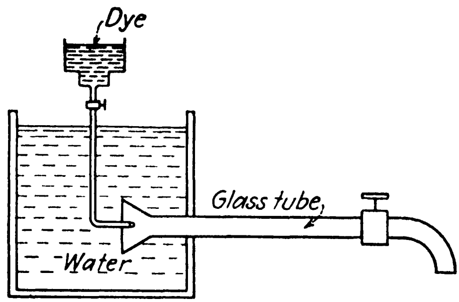

FIG. 3.2.—Reynold's apparatus.

of the flow around an immersed body. This can be effectively demonstrated by considering the original investigation of Sir Osborne Reynolds (from whom R received its name).

In Reynolds apparatus (Fig. 3.2) the flow of water through a glass pipe was made visible by injecting dye into the stream near the bell-mouthed entrance of the pipe. A systematic investigation with this apparatus covering a wide range of velocities and pipe diameters with practically constant fluid density and viscosity yielded the following results and conclusions:

1. At low values of the product of velocity and pipe diameter—and therefore low values of R (less than 2,000)—the dyed water formed a sharply defined line down the center of the pipe. The particles of water were conse-

quently moving parallel to the pipe wall in laminar flow. This was attributed to the predominant effect of the viscous forces in the fluid over the inertia forces.

2. At comparatively high values of R (greater than 12,000), the dye diffused uniformly across the stream a short distance downstream of its point of introduction. Individual particles were in this case following very irregular paths, a phenomenon ascribed to the predominance of the inertia forces in determining the turbulent flow (sometimes called "eddying" flow).

3. At intermediate values of R (2,000 to 12,000), the flow was found to be very unstable, becoming either laminar or turbulent according to the amount of initial turbulence in the water at the entrance to the pipe; later investigators have maintained laminar flow up to a value of R as high as 40,000 by exercising great care in eliminating initial disturbances in the supply tank.

These results have a direct bearing on the behavior of air flow in the region close to the surface of an immersed object —the *boundary* layer. Here the flow is either laminar or turbulent depending to a large extent on the value of R and upon the initial turbulence in the air stream. Chapter 6 will consider this subject in more detail.

The Airfoil.—Dimensional analysis finds important application to the fundamental problem of aerodynamics—that of determining the resultant force on an immersed body in an air stream. As a preparation for this analysis, the necessary terminology will be reviewed.

For convenience in later developments, this analysis will be applied to an airfoil (Fig. 3.3). In this case the air stream is represented as moving to the right with a velocity V with respect to the stationary airfoil. Exactly the same forces would result if the airfoil were moving to the left through still air with an equal and opposity velocity $-V$; in other words only the relative motion is of importance. In order to include both of these cases the *relative wind* is defined as the velocity of the air with reference to the airfoil.

The resultant force exerted on the airfoil by the relative wind is usually resolved into two components for convenience in aeronautical calculations:

The *lift* is the component of the resultant force in a direction perpendicular to the relative wind.

The *drag* is the component taken parallel to the relative wind.

In addition, the resultant force exerts a *pitching moment* tending to rotate the airfoil about an axis drawn perpendicular to the lift and drag forces. Obviously the magnitude

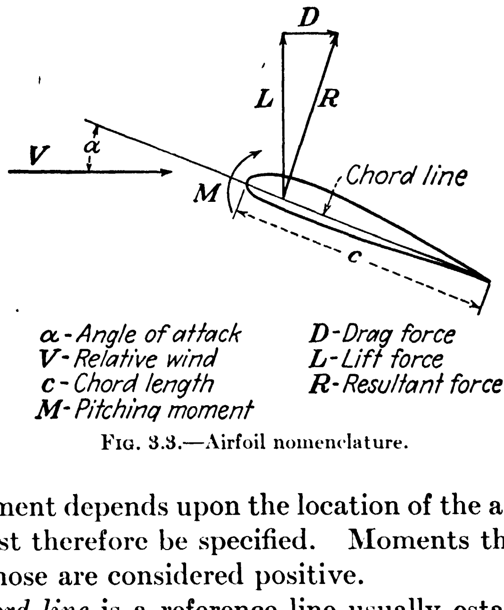

FIG. 3.3.—Airfoil nomenclature.

of the moment depends upon the location of the axis chosen, which must therefore be specified. Moments that tend to raise the nose are considered positive.

The *chord line* is a reference line usually established by the designer of any particular airfoil. It is often taken as the line joining the trailing edge with the center of curvature of the nose section.

The *chord* c of an airfoil is the length of the projection of the airfoil on its chord line. This is usually the same as the over-all length of the airfoil.

The *angle of attack* α is the acute angle between the chord line and the direction of the relative wind.

Dimensional Analysis of the Force on an Airfoil.—As a first step in determining the force on an airfoil exerted by a relative wind, the factors influencing this force must be selected. A careful consideration of the problem would indicate that the following are of importance:

1. The shape of the airfoil
2. The angle of attack α
3. The size of the airfoil as determined by any characteristic length l
4. The magnitude of the relative wind V
5. The density of the fluid ρ
6. The viscosity of the fluid μ

The first two items, the shape of the airfoil and its orientation to the air stream, do not lend themselves to mathematical expression. It therefore becomes necessary to leave the evaluation of the effects of shape and angle of attack to the laboratory and confine our attack by dimensional analysis to the other four variables. That is,

$$F = f(l, V, \rho, \mu)$$

or

$$F = Kl^a V^b \rho^c \mu^d \tag{3.9}$$

Substituting dimensionally,

$$\frac{ML}{T^2} = L^a \left(\frac{L}{T}\right)^b \left(\frac{M}{L^3}\right)^c \left(\frac{M}{LT}\right)^d$$

Equating exponents,
Of M,

$$1 = c + d$$

Of L,

$$1 = a + b - 3c - d$$

Of T,

$$-2 = -b - d$$

We now have three equations and four unknowns and will therefore express a, b, and c in terms of d.

$$c = 1 - d$$
$$b = 2 - d$$
$$a = 2 - d$$

Substituting these exponents in Eq. (3.9),

$$F = Kl^{2-d}V^{2-d}\rho^{1-d}\mu^{d}$$

and

$$F = K\left(\frac{\rho V l}{\mu}\right)^{-d}\rho l^2 V^2$$

The ratio $\rho Vl/\mu$ will be recognized as Reynolds number. Letting the *force coefficient* $C = 2K\left(\frac{\rho V l}{\mu}\right)^{-d}$ and noting that l^2 has the dimensions of an area which will be designated by S, there results

$$F = C\frac{\rho}{2}SV^2 \tag{3.10}$$

The factor $\frac{1}{2}$ is introduced to bring in the dynamic pressure of the flow $q = \frac{\rho}{2}V^2$, thereby doubling the value of the undetermined constant C.

Equations of Lift, Drag, and Moment.—As previously stated, the lift and drag components of the resultant force acting on an airfoil are more useful than the resultant force itself. If dimensional analysis were again employed for the lift and drag of an airfoil, expressions identical to Eq. (3.10) would be obtained, except for the value of the force coefficient. In deriving an expression for the moment, however, the right-hand side of Eq. (3.10) would have to be multiplied by a length dimension to secure dimensional homogeneity, since moment = force × length. This length dimension is commonly taken as the chord length of the airfoil. The resultant equations would then become

$$L = C_L\frac{\rho}{2}SV^2 \tag{3.11}$$

$$D = C_D\frac{\rho}{2}SV^2 \tag{3.12}$$

$$M = C_M\frac{\rho}{2}SV^2c \tag{3.13}$$

where L = lift force, lb.

C_L = coefficient of lift, dimensionless

ρ = mass density, slugs per cu. ft.

c = chord length, ft.

S = wing surface defined by the area of the projection of the wing on the plane of its chord, sq. ft.

V = relative wind, ft. per sec.

D = drag force, lb.

C_D = coefficient of drag, dimensionless

M = moment of wing about specified axis, ft.-lb.

C_M = coefficient of moment, dimensionless

In considering the application of Eqs. (3.11) to (3.13) to practical problems, it will be helpful to review the assumptions and limitations involved in their derivation. In the first place, the value of the coefficients for any given airfoil must be determined by actual measurement on a geometrically similar airfoil at the same angle of attack; moreover, the value of R must be the same for the two airfoils for accurate application of the measured value of the coefficients to the given airfoil; in other words there must be both geometric and dynamic similarity between two airfoils for accurate correspondence of the force and moment coefficients.

In practice both of these requirements are not usually fulfilled since test data for each commonly used airfoil shape are generally obtainable at only *one* value of R, which, of course, does not, except in rare cases, agree with the required value of R for design work. For rough calculations, this difference in Reynolds numbers may be neglected since the variation of the coefficients with R, the so-called "scale effect," is rather small. For more accurate work, scale-effect curves like those of the next chapter may be used to correct, at least approximately, for this lack of dynamic similarity.

The *characteristic curves* of Fig. 3.4, for a particular airfoil and a particular R, illustrate the manner of presentation of experimental measurements of the force and

moment coefficients. The experimental methods employed in obtaining these measurements will be discussed in the next chapter.

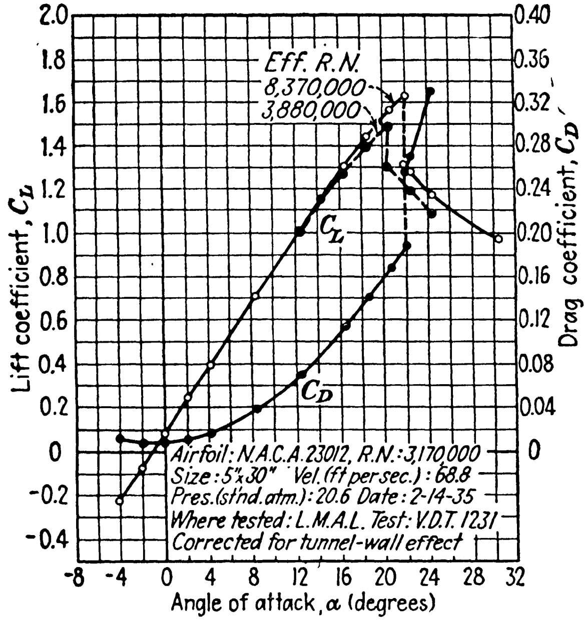

FIG. 3.4.—Typical characteristic curves of an airfoil. (*N.A.C.A. Technical Report* 610.)

PROBLEMS

1. An airplane of 100 ft. wing spread and 8 ft. average chord length cruises at 350 m.p.h. and lands at 100 m.p.h. Calculate the value of R corresponding to both cruising and landing speeds, assuming standard sea-level atmospheric conditions. (The characteristic length used in flight Reynolds number computations is the average wing chord.)

2. Show by dimensional analysis that centrifugal force $= KMV^2/r$.

3. Calculate the velocity of sound in "standard" air at sea level and at 30,000 ft. altitude.

4. The dimensionless coefficients for thrust T_c and power P_c are extensively used in propeller theory. Develop an expression for each of these coefficients of the form $T_c = f(T,\rho,N,D)$ and $P_c = f(P,\rho,N,D)$ where T = thrust force, ρ = mass density, N = speed of rotation, D = diameter of propeller, and P = power input to propeller.

5. An airplane weighing 2,000 lb. with an N.A.C.A. 23012 wing flies through standard sea-level air at a speed of 100 m.p.h. If the wing area of the airplane is 140 sq. ft., calculate the corresponding drag force. (For level flight the lift very closely equals the weight of the airplane.) The effects of the relative proportion of span to chord length (aspect ratio) and scale effect will not be considered in this problem.

CHAPTER 4

EXPERIMENTAL METHODS

The pioneers in aeronautics, as well as present-day designers, relied heavily on experimental results. Such well-known scientists as Otto Lilienthal, Samuel P. Langley, and the Wright brothers owed much of their success to research conducted with equipment that would seem crude today. Lilienthal's man-carrying gliders were designed on the basis of measurements made by supporting airfoil shapes on simple balances in natural winds. Professor Langley, a few years later, created an artificial "wind" by mounting models on the end of a whirling arm which was rotated in a horizontal plane by a steam engine. The Wright brothers conducted a remarkably thorough and far-reaching series of tests in a small wind tunnel which, in scientific importance, ranks with their epoch-making flight at Kitty Hawk in 1903. Later experimenters have towed models through the air with rail cars, automobiles, and airplanes. Others have dropped models and force-measuring equipment from high places, sometimes using guide wires or pendulum arms to stabilize the model during its fall.

Of all these methods, that of supporting a fixed model on force-measuring equipment and generating a movement of air past the model with fans or blowers in a *wind tunnel*, as the Wright brothers did, has proved the most practicable. Here the accuracy of test data is not affected by atmospheric disturbances, the force and moment-measuring balances may be made extremely sensitive, and changes in the model—often made with beeswax or modeling clay—can be accomplished very readily.

Atmospheric Wind Tunnels.—Wind tunnels that circulate air at or near atmospheric pressure, as do most present-day designs, are termed "atmospheric" wind tunnels. Many of the general features of atmospheric tunnels are illustrated in the early Eiffel tunnel of Fig. 4.1. The model under test is mounted in the throat section of a venturi-shaped passageway where the velocity is highest, with lower velocities and therefore lower frictional losses through the rest of the air circuit. Since atmospheric air enters the entrance cone, the pressure at the test section, according to Bernoulli's equation, falls below atmospheric pressure and

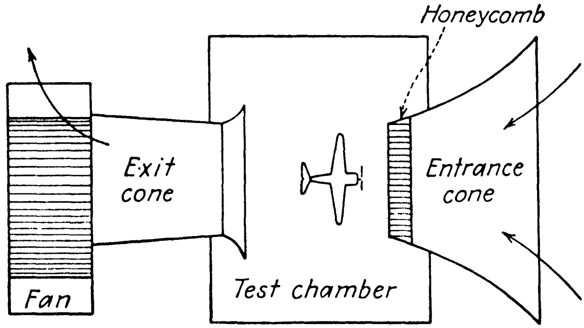

FIG. 4.1.—Eiffel wind tunnel.

an airtight test chamber is required. After passing through the test chamber, the diverging walls of the exit cone accomplish a partial restitution of the original pressure at the expense of the kinetic energy of the air stream to assist the fan in returning the air to the atmosphere. The *honeycomb* located just upstream of the test section consists of a large number of small parallel channels which improve the uniformity of the test jet in both direction and magnitude. The three components of lift, drag, and pitching moment are measured with a simple beam balance.

Despite its apparent simplicity, the Eiffel design is not very extensively used because of its two principal drawbacks: the difficulty in maintaining the reduced pressure in the test section, and the fluctuations in velocity of the air entering the entrance cone, particularly if it is exposed to

in Fig. 4.3 mounted on the three-point support system of the Full-scale Tunnel. The supports transmit the aerodynamic forces and moments acting on the model to the balance room below. With this arrangement, the drag of the complete airplane and of many of its parts and accessories may be investigated with a view toward making the airplane aerodynamically cleaner.

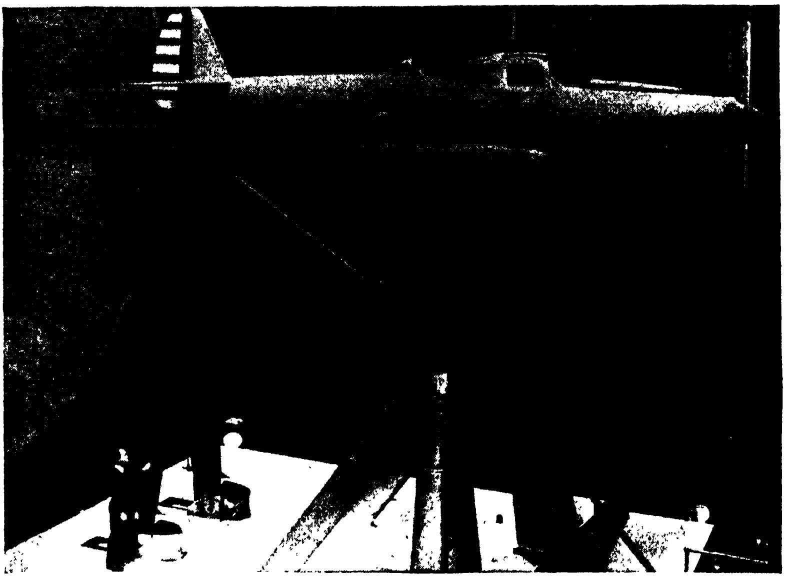

FIG. 4.3.—A military airplane mounted in the open test section of the Full-scale Wind Tunnel of the N.A.C.A. at Langley Field. (*Bell Aircraft Corporation.*)

In most recent tunnels the test sections have been enclosed with model supports extending through small openings to an exterior balance system. This *closed-throat* construction makes possible a higher efficiency and a slightly smoother air stream than does an open-throat tunnel.

Variable-density Tunnels.—It may be recalled that for a direct correspondence of the test results of a model to its full-sized prototype, a condition of dynamic similarity is necessary as defined by an equality of Reynolds numbers.

That is,

$$R_m = R_p$$

or

$$\left(\frac{\rho VL}{\mu}\right)_M = \left(\frac{\rho VL}{\mu}\right)_p$$

Since ρ and μ are practically the same for a model tested in an atmospheric tunnel and its prototype in normal flight,

$$VL_m = VL_p$$

and

$$V_m = \frac{L_p}{L_m} \times V_p \tag{4.1}$$

Thus for dynamic similarity the test velocity must equal the reciprocal of the model scale multiplied by the prototype air speed. Unfortunately this requirement generally leads to test velocities that are practically unattainable, since dynamic similarity to even a low prototype air speed of 100 m.p.h. with a $\frac{1}{10}$ model would require a test velocity of 1,000 m.p.h. Accordingly, it has become customary to run airplane tests in atmospheric tunnels at as high a wind speed as possible. Scale-effect corrections are then applied to the test data to "correct" for the lack of dynamic similarity.

Since a large R of the model to correspond with normal flight values of R (up to at least 30,000,000) is desired, in combination with a moderate velocity and a small-scale model, it is evident that the ratio ρ/μ for the model should be made as large as possible. This is accomplished in variable-density wind tunnels by compressing the circulating air. Compression of the air increases the density without affecting the viscosity, since the compressed air is maintained at atmospheric temperature. The variable-density tunnel (V.D.T.) of the N.A.C.A., designed by Dr. Max Munk, is one of the earliest tunnels of this type. As shown in Fig. 4.4, it consists essentially of a return-flow tunnel enclosed in a steel tank which is capable of with-

standing 20 atm. of pressure. Dynamic similarity can consequently be attained in this tunnel at a value of $(VL)_m$ equal to $\frac{1}{20}\,(VL)_p$. The variable-density tunnel has today been largely superseded by larger and more powerful tunnels employing the same principles.

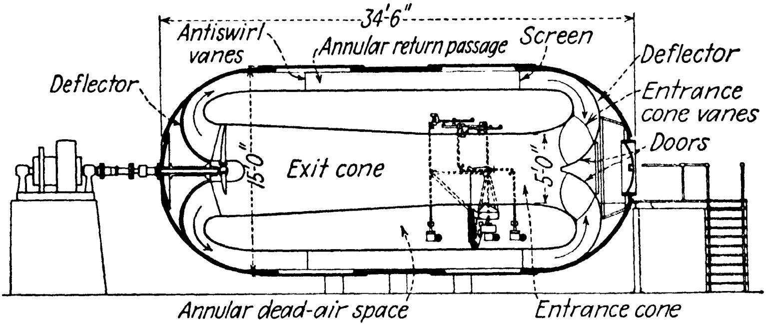

FIG. 4.4.—Diagrammatic longitudinal section of the variable-density wind tunnel.

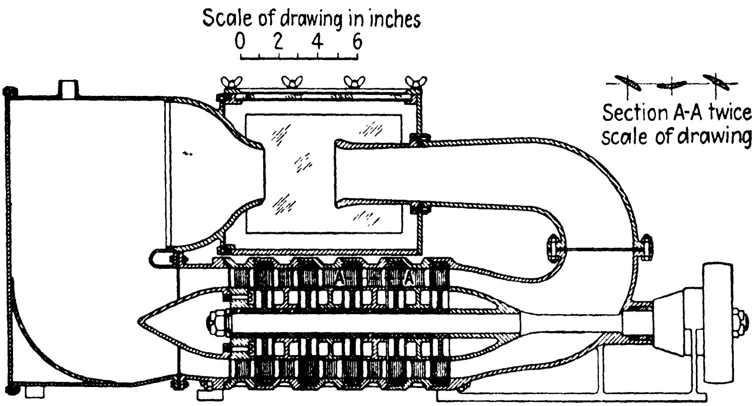

FIG. 4.5.

An interesting effort toward obtaining a higher value of R with low velocities and small models is reported by the N.A.C.A. in *Technical Note* 358.[1] Water, which has a ρ/μ value approximately 15 times that of atmospheric air,

[1] Experiments with a model water tunnel by Eastman N. Jacobs and Ira H Abbott in December, 1930.

was used as the circulating fluid of a tunnel as shown in Fig. 4.5. The water, in passing over the model, formed small bubbles of vapor which later collapsed so suddenly as to erode the surface of the model. This phenomenon, known as "cavitation," discouraged the further development of water tunnels by the N.A.C.A. Cavitation effects are also very detrimental to the economical operation of water pumps and turbines.

Modern Trends in Wind-tunnel Design.—High jet velocities, large test sections, and variable-density construction contribute to the large Reynolds numbers attained in tunnels of recent design. Offsetting the high construction and operating costs of these tunnels are their many advantages. These include closer correlation of model and full-scale flight results through a reduction of scale-effect corrections; capacity for testing full-sized motors, propellers, and control surfaces; direct evaluation of compressibility effects by means of test velocities approaching the speed of sound; and low turbulence to give comparable flow characteristics to those of the atmosphere.

A representative modern tunnel with some unusual design features is the 8- by 12-ft. wind tunnel of the Boeing Airplane Company's Edmund T. Allen Memorial Laboratory. In the cutaway drawing of Fig. 4.6, the air circuit may be readily followed. Starting at the 24-ft. 16-blade fan the air flows toward the right, passing through two sets of turning vanes and then into a sharply tapered entrance cone, thence through an octagonal test section merging into a diffuser of very gradual taper which conducts the air to another double set of turning vanes to return the air to the fan. Since the entire power input of 18,000 hp. is transformed through friction into heat energy, two methods of cooling the circulating air are provided: the corner turning vanes are hollow and are cooled by water sprays acting on their interior surfaces; an air interchanger, located above the corner immediately following the fan, serves to remove

11 per cent of the air during each circuit and to replace it with fresh, cool air from outside the tunnel. A photograph of the test section appears in Fig. 4.7 with a model of the

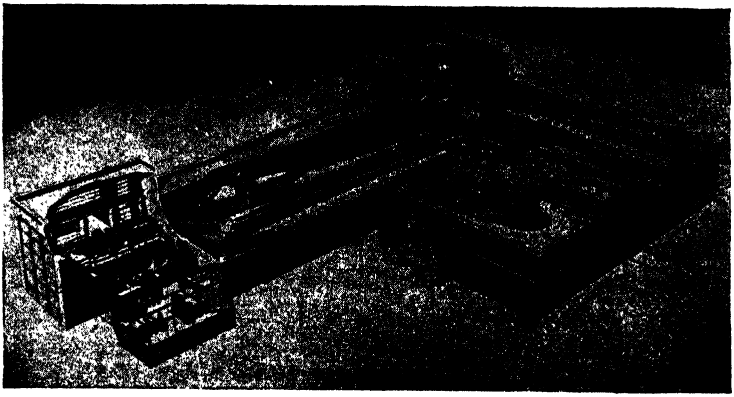

FIG. 4.6.—Cutaway view of the Edmund T. Allen Memorial Laboratory. (*Boeing Airplane Company.*)

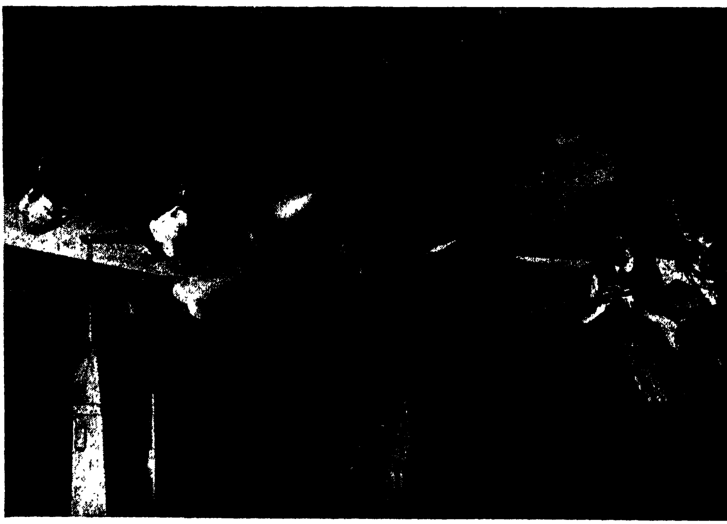

FIG. 4.7.—A model mounted in the octagonal test section of the Edmund T. Allen Memorial Wind Tunnel. (*Boeing Airplane Company.*)

Flying Fortress mounted on the tunnel supports. Test velocities in the 700-m.p.h. range may be obtained past the model.

One of the most powerful wind tunnels operating in this country is the 20-ft. Wright Field wind tunnel in which a 40,000-hp. induction motor drives two 40-ft. fans arranged in tandem on a single shaft. A plan view of the tunnel is shown in Fig. 4.8. An interesting feature of this design is the fresh-air intake system which utilizes the outer portion of the fan blades to draw air in from outside. Control is maintained by means of louvers which change the angle at which the fresh air meets the blades.

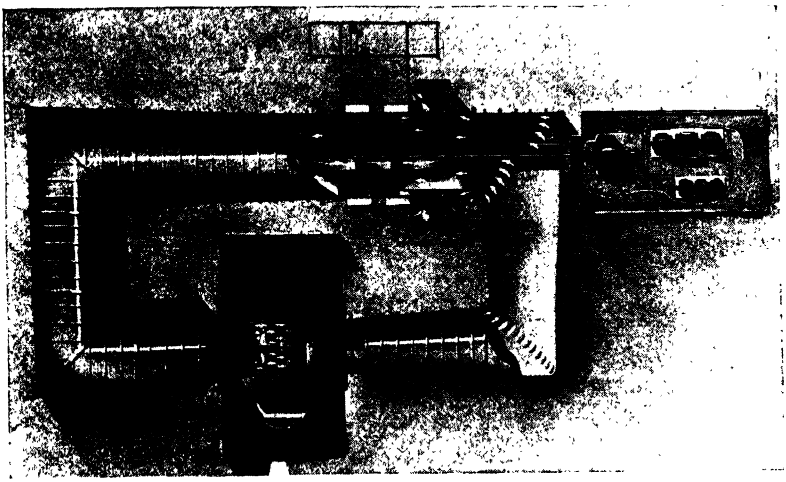

FIG. 4.8.—Cutaway view of the Wright Field 20-ft. Wind Tunnel. (*AAF Materiel Command Photograph.*)

From the standpoint of physical dimensions, the Ames Aeronautical Laboratory Full-scale Wind Tunnel is the largest wind tunnel in this country and probably in the world. Six 40-ft. fans arranged side by side in two rows of three each supply a moderately high test velocity through its 80- by 40-ft. throat.

High-velocity Tunnels.—At velocities of flow approaching the speed of sound, the characteristics of flow about an immersed body change very considerably. Since propeller tips and military planes frequently operate in this range, tunnels have been constructed to investigate these phenomena.

The arrangement of the 24-in. high-speed wind tunnel operated by the N.A.C.A. at Langley Field is illustrated in Fig. 4.9. Compressed air from the enclosing tank of the variable-density tunnel is expanded through the annular nozzle to a very high velocity and correspondingly low pressure, to draw air through the test section. This "ejector" principle of operation produces a smooth flow through the working section at velocities approaching the velocity of sound.

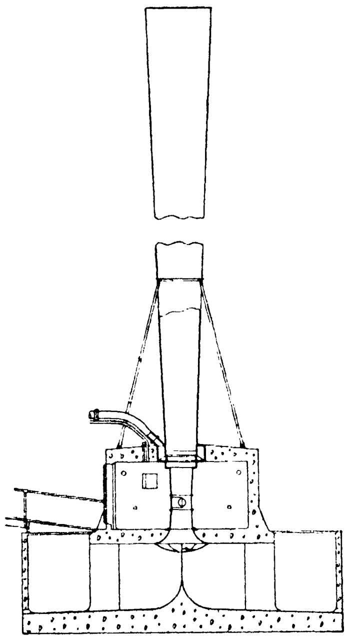

FIG. 4.9.—Diagrammatic cross section of the N.A.C.A. 24-in. High-speed Wind Tunnel. (*N.A.C.A. Technical Note* 543.)

Wind-tunnel Balances.—The requirements of a good wind-tunnel balance system are both diverse and exacting. The wires or struts supporting the model should be small enough for low drag and flow interference, and yet large enough for rigidity. The balances should be sensitive enough to measure small forces accurately, and yet accommodate large lift and drag forces. The system should be flexible for easy adaptation to models of various types and sizes, and simple in design and operation. In addition, some form of damping is generally desirable to minimize the effect of velocity fluctuations.

For the measurement of lift, drag, and pitching moment a *three-component wire balance*, as shown in Fig. 4.10, is often used, particularly in small tunnels. The wire supports for the model airfoil are attached to the wing tips and to the end of a streamlined outrigger, known as a "sting," at the rear of the model. The wires are stabilized with counter-

tures the action of the tufts at various angles of attack may be studied.

Since the phenomenon of stalling is subject to rather uncertain scale-effect variation, tests are usually run at as high a value of R as possible. One expedient, which is sometimes employed for increasing the maximum *effectice* Reynolds number for a given tunnel, is to create artificial turbulence by inserting a wire grillwork into the tunnel upstream from the model.

Wind-tunnel Tests on Control Surfaces.—Wind-tunnel models are usually fitted with movable control surfaces to provide information regarding stability and flying qualities. It is sometimes found, for instance, that the vertical tail

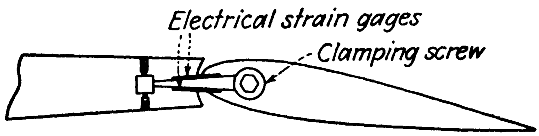

FIG. 4.19.—Measurement of the hinge moment of a control surface.

surfaces of the preliminary design are exposed to a lowered, fluctuating velocity produced by the wake of the wing fillets or by the nacelles, which makes advisable a change from single to twin tails or vice versa. In determining the final location of both horizontal and vertical tail surfaces, pitot-tube velocity surveys of possible locations are very helpful.

The forces and moments produced by the control surfaces at various angular displacements are generally measured on the wind-tunnel model and analyzed in terms of the stability and controllability of the full-sized airplane. These tests may indicate changes in the sizes, shapes, and locations of the surfaces for improving their effectiveness.

The stick or control forces are very important to the comfort and convenience of the pilot. These forces depend upon the moment produced by the air loads acting on the surfaces about their hinge lines, the *hinge moments*. For small-scale surfaces, hinge moments are very difficult to

measure accurately so that separate tests of full-sized or large-scale control surfaces may be run to secure hinge-moment data. A commonly used device for measuring hinge moments is shown in Fig. 4.19. The required hinge moment is resisted by a cantilever beam with previously calibrated *electrical strain gauges*[1] on its tension and compression sides. The control surface may be clamped at various angles with respect to the clamping screw for readings at various deflection angles of the control surface.

Powered Models.—The present-day use of high engine powers on relatively small airplanes has added another complicating factor to the problems of stability and control. A rotating propeller produces a slip stream with both axial and rotational components to combine with the normal air stream. In addition, the thrust and torque of the propeller must be balanced by appropriate aerodynamic forces acting on the airplane.

An aid to the solution of these problems which is being increasingly adopted by airplane manufacturers is to equip wind-tunnel models with propellers driven by small electric motors. This introduces a new set of problems: the models must be built large enough to accommodate the motors; the test Reynolds number must usually be lowered since the tunnel air speed must correspond to the relatively low output of the propeller motor; and the model propellers are usually of fixed pitch to make full correspondence with the full-scale propeller impossible, except at one tunnel speed. However, on military and pursuit planes particularly, the stability and control problems of a new design cannot be worked out satisfactorily in any other way, except by relatively more costly and time-consuming experimentation on full-scale airplanes.

[1] This type of strain gauge consists essentially of a small wire looped back and forth several times and cemented to the test member. Under the action of an applied load, the strain of the test member is transmitted to the wire which changes in diameter as it changes in length, according to Poisson's ratio. This change of diameter changes the electrical resistance of the wire which may be measured by instruments calibrated to read strain directly.

These tests are generally run only for conditions that are considered critical for the airplane being designed. For example, a take-off with full power or, in the case of a carrier-based plane, a landing with the flaps down and partial power is representative.

Visual-flow Methods.—Various techniques of air-flow visualization have been employed in aeronautical research work. Chemical smoke injected into an air stream in fine filaments has proved very effective for streams of low

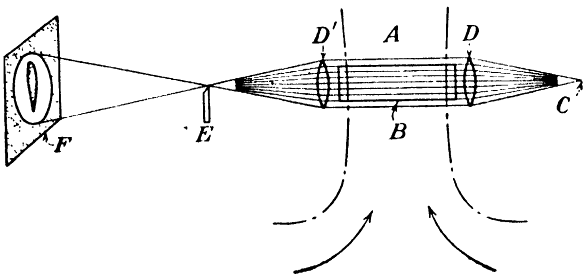

Light from a source located at C, the principal focus of lens D, emerges from lens D as a parallel beam, passes through the converging lens D', and is brought to focus at E, the principal focus of lens D'. At E a knife edge is located so as to cut off most of the light from the source C. The model B is placed in the parallel beam that crosses the test section A between the lenses so that its cross section is perpendicular to the light beam and an image is formed on the screen F. When air passes over the model, its density, and therefore its optical index of refraction, change. Thus, portions of the parallel beam of light are bent and some of the rays that were previously interrupted by the knife edge now pass over the knife edge at E to the screen F or, if desired, to a photographic plate. The illumination on the screen then shows regions of varying density.

FIG. 4.20.—Simplified diagram showing the schlieren method. (*N.A.C.A. Technical Report* 646.)

turbulence and velocity. Titanium tetrachloride produces a white dense smoke when exposed to normal atmospheric moisture and is often used for this purpose.

Another technique utilizes the principle underlying the illumination of dust particles by a stray sunbeam in a semi-darkened room. This principle has been adapted to wind-tunnel use by introducing aluminum dust into the air stream passing over a model in a darkened tunnel. The paths of individual particles are made visible by reflection from a narrow slit of intense light projected normal to the direction of viewing.

A very ingenious system of flow visualization known as the "schlieren method" requires no admixture of smoke or

powder to the air stream. As explained in detail in Fig. 4.20, this method makes visible changes in density of the air flowing around a model. For high-velocity flows where

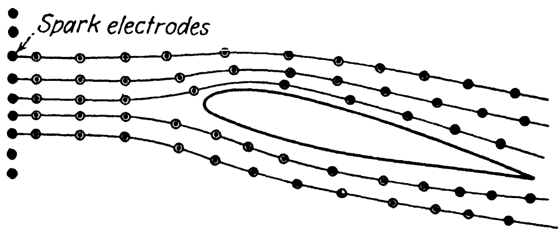

FIG. 4.21.—Schlieren visualization of localized masses of heated air.

the change in density is quite large, photographs like that of Fig. 8.4 may be made. For lower air speeds, variations of density may be artificially produced by heating small quantities of the air passing over a model with electric

FIG. 4.22.—Flow pattern about an airfoil as determined by the lampblack and kerosene method of flow visualization. (*The David Taylor Model Basin.*)

sparks, as indicated in Fig. 4.21. If the sparks are regulated to discharge at uniform time intervals, the spacing of the density discontinuities at any point in a streamline will be proportional to the velocity of flow at that point.

One of the simplest methods for obtaining the flow pattern about a model is the *lampblack and kerosene* method. Here the model is upended against a flat plate which is supported horizontally in an air stream and covered with a suspension of lampblack in kerosene and turpentine. The air flow, in passing around the model, cuts channels through the lampblack preparation and thereby exposes the lighter colored plate below. In a short time the mixture hardens, owing to the evaporation of the kerosene and turpentine, and leaves a clear record of the flow pattern. This record, however, represents conditions of flow in the vicinity of the plate and does not necessarily indicate the true undisturbed flow pattern about the model.

The flow pattern of Fig. 4.22 was determined by the lampblack and kerosene method.

PROBLEMS

1. A one-tenth scale model of a transport plane is to be tested in a variable-density tunnel at an air speed of 150 m.p.h. What density is necessary for dynamic similarity corresponding to a cruising speed of 250 m.p.h.? What speed would be required in a water tunnel operating at a temperature of 50°F.? (μ = 0.0000273 lb.-sec. per sq. ft. for water at 50°F.)

2. An N.A.C.A. 0015 airfoil of 24-in. span and 4-in. chord is tested in a 3-ft. diameter open-jet wind tunnel at an air speed of 100 m.p.h. A maximum lift force of 15.2 lb. is obtained at an angle of attack of 14 deg. corresponding to a drag force of 3 lb. (after correction for tare and interference). (*a*) Calculate the values of $C_{L_{max.}}$ and C_D *after* correction for tunnel-wall effect. (*b*) If the turbulence factor of the tunnel is 1.3, check the value obtained for $C_{L_{max.}}$ against the N.A.C.A. results shown in Fig. 4.16.

CHAPTER 5

THEORY OF LIFT

The lift and drag forces exerted on an airfoil by the relative motion of an ideal fluid represent the integrated effect of the varying pressures acting normal to its exposed surface. Generally, the negative pressures on the upper surface of an airfoil contribute in much greater measure to lift and drag than the pressures on its underside, as indicated in the pressure-distribution diagram of Fig. 5.1. The location of the greatest negative pressure near the leading edge of the airfoil confirms one of the conclusions drawn

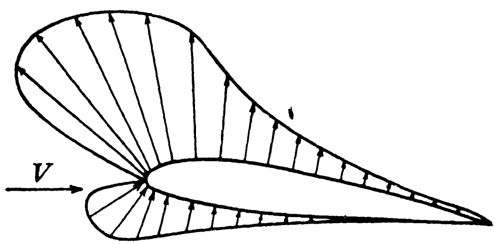

FIG. 5.1.—Pressure distribution for a typical airfoil at a moderate angle of attack.

from the analysis of the airfoil streamline flow pattern of Chap. 2.

To simplify the theoretical analysis of lift, an ideal fluid flowing over a wing with no endwise components of velocity will be assumed so that all planes passed perpendicular to the wing span would show identical flow patterns. In other words, two-dimensional flow will be considered with no frictional losses.

As might be expected, the lift of an airfoil is closely related to the streamline flow pattern of the fluid passing over it; for the lift force is due to the concerted action of the fluid pressure forces, the pressures are related through

Bernoulli's equation to the velocities in the fluid, and the velocities are inversely proportional to the streamline spacing. If, therefore, the flow pattern about an airfoil at any angle of attack could be derived theoretically, the corresponding lift force could be deduced. This is not a simple process, but a start may be made by studying the characteristics of several simple types of flow with the object in view of later combining them to produce flows of practical interest.

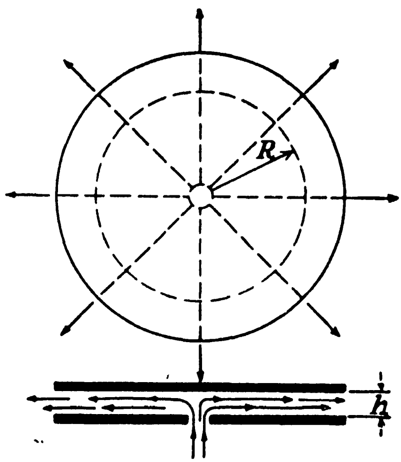

FIG. 5.2.—Flow from a source.

Source and Sink Flows.—If fluid is pumped through a hole in the lower of two parallel plates, as shown in Fig. 5.2, it will flow radially outward between the plates in all directions. If the quantity of flow Q is made constant, the velocity of flow at any radius R can easily be calculated since

$$V = \frac{Q}{\text{area}} = \frac{Q}{2\pi R h} = \frac{\text{constant}}{R} \tag{5.1}$$

where h is the distance between the plates. Hence, the flow proceeds radially outward with a velocity that varies inversely with its distance from the central hole or source. This type of flow is appropriately termed "source flow."

If the direction of flow is reversed, the hole will act as a drain or sink and the flow then becomes a "sink flow."

Vortex Flow.—The circulation of the particles of a fluid of uniform energy content in circular paths about a common center is known as "vortex flow." In such a flow, the pressure of the fluid drops off as the center is approached, as may be deduced through a consideration of the forces acting on a typical particle of the fluid as at A in Fig. 5.3. For equilibrium of such a particle in a radial direction, the outer pressure force must be large enough to counteract *both* the inner pressure force and the centrifugal force acting on the mass of the particle. The pressure in the fluid must therefore decrease as the center of the vortex flow is approached. To maintain the total energy constant, the kinetic energy must increase as the pressure energy falls off, so in vortex flow the velocity increases as the center is approached. A more detailed analysis would, in fact, show that this variation can be expressed by

$$V = \frac{\text{constant}}{R} = \frac{K}{R} \tag{5.2}$$

The effect of this inverse relation between velocity and radius is made evident in Fig. 5.3 by the lesser streamline spacings at the shorter radii.

Tornadoes and whirlpools are familiar examples of vortex flows in nature. The velocities of these natural vortexes do not, however, approach infinity at their centers as Eq. (5.2) would indicate. Instead, observations show that a central core of small radius exists which rotates like a solid flywheel with the velocity *directly* proportional to the radius; the rest of the flow conforms quite closely to that predicted by theory.

Circulation.—The strength of a vortex is commonly specified in terms of its *circulation*, Γ (gamma). In order to give an exact mathematical meaning to circulation, a closed curve containing a vortex center will be considered as in Fig. 5.4. If v is taken as the velocity at any point on

the curve, ds as an element of length at the point, and θ as the angle between ds and v, the circulation may be written

$$\Gamma = \oint^{C} v \cos \theta ds \tag{5.3}$$

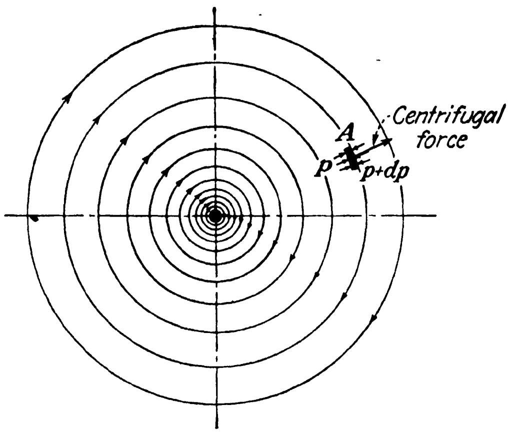

FIG. 5.3.—Vortex flow.

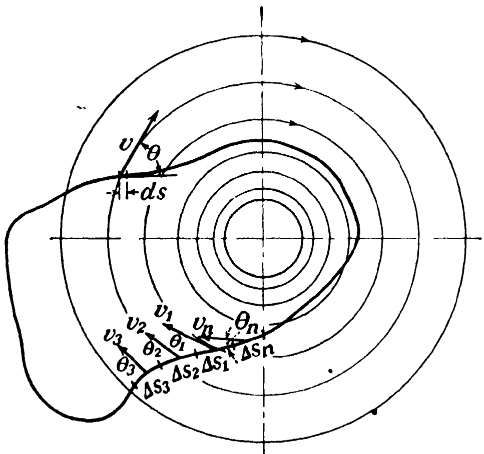

FIG. 5.4.—Circulation around an irregular curve.

The symbol $\oint^{C}$ is read "the line integral around the curve." Thus the circulation around any curve may be defined as the line integral of the tangential component of the velocity

around the curve. The meaning of circulation can best be understood by dividing the curve into many small subdivisions Δs_1, Δs_2, Δs_3, . . . Δs_n with velocities v_1, v_2, v_3, . . . v_n making angles of θ_1, θ_2, θ_3, . . . θ_n with these subdivisions. Then the circulation may be approximated by

$$\Gamma = v_1 \cos \theta_1 \Delta s_1 + v_2 \cos \theta_2 \Delta s_2 + v_3 \cos \theta_3 \Delta s_3 \ . \ . \ . \\ + v_n \cos \theta_n \Delta s_n$$

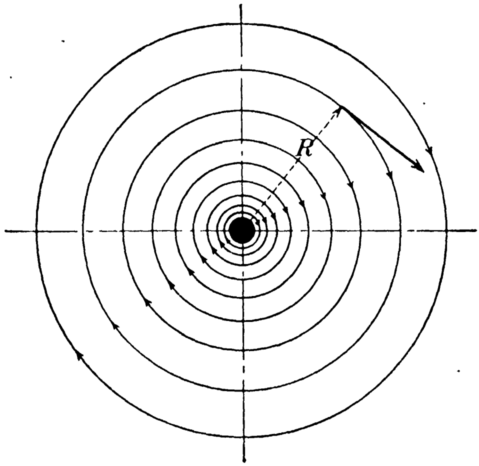

FIG. 5.5.—Circulation around a circular curve.

As the number of subdivisions approaches infinity, this summation becomes equivalent to the line integral of Eq. (5.3).

The circulation around a path formed by one of the circular streamlines of Fig. 5.5 may be easily calculated since the velocity remains constant in magnitude and is everywhere tangent to the curve. Choosing the streamline of radius R,

$$\Gamma = \oint^C v \cos \theta ds$$

But, $\theta = 0$ deg., making $\cos \theta = 1$, and $v = K/R$ so

$$\Gamma = \frac{K}{R} \oint^C ds = \frac{K}{R} \times 2\pi R = 2\pi K$$

This expression for the circulation around a circular streamline obviously does not contain the radius and so would have been the same for any of the circular streamlines of Fig. 5.5. Through a somewhat more involved analysis, it might also have been proved that the circulation is independent not only of the radius but of the shape of the path as well. The circulation of a vortex may therefore be computed around any convenient path as long as it loops around the vortex center once and only once.

Superposition of Flows.—The vectorial combination of two or more flows to produce a resultant flow pattern is

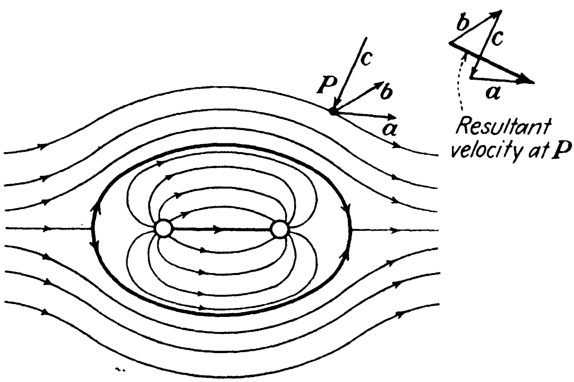

FIG. 5.6.—Superposition of a rectilinear flow with equal-strength source and sink flows.

termed the "superposition" of flows. The superposition of a rectilinear flow with source and sink flows of equal strength is illustrated in Fig. 5.6. The direction of the velocity, and therefore of the streamline, at any point in the pattern is found by adding the velocity vectors of each of the constituent flows as indicated for the point P. In this way the complete flow pattern could be developed.

All of the fluid emanating from the source is seen to flow into the sink within the oval boundary formed by the heavy closed streamline (Fig. 5.6). The rectilinear stream divides and remains on the outside of this boundary streamline. Since streamlines cannot intersect, there can be no flow across this boundary and the exterior flow would remain

2. If the circulation of a vortex is 30 sq. ft. per sec., what is the tangential velocity of flow at a radius of 2 ft.?

3. In a flow similar to that of Fig. 5.6, the source and sink have equal strengths based on a Q of 1 cu. ft. per sec. and a 1-in. separation of the guiding plates. With a rectilinear velocity of 20 ft. per sec., determine graphically the magnitude and direction of the resultant velocity of the fluid at a point 6 in. from the source and 8 in. from the sink. The distance between source and sink is 10 in.

4. An air stream under atmospheric pressure with a velocity of 60 m.p.h. passes over a 10-in. diameter circular cylinder. If the cylinder is rotated so as to produce a circulation of 300 sq. ft. per sec., what is the lift per unit length of the cylinder?

5. An airplane weighing 5,000 lb. has a wing area of 250 sq. ft. The airfoil efficiency factor is 0.90, and the value of α_{L_0} for the wing equals -1 deg. Calculate the angle of attack of this airplane corresponding to an air speed of 200 m.p.h. (The lift very closely equals the weight of the airplane for level flight.)

6. An airplane weighing 2,000 lb. is supported by a wing of 30 ft. span. Assuming a uniform spanwise lift distribution, what is the circulation about the wing corresponding to an air speed of 100 m.p.h.?

7. The lift per foot of span of a symmetrical airfoil ($\alpha_{L_0} = 0$) at an air speed of 60 m.p.h. and an angle of attack of 5 deg. is 20 lb. If the airfoil efficiency factor is 0.90, what is the necessary chord length of the airfoil?

CHAPTER 6

MONOPLANE WING THEORY

The airflow over an airplane wing has marked spanwise components of velocity, particularly near the wing tips, which make the flow essentially three-dimensional in character. The two-dimensional theory of the preceding chapter must consequently be modified and expanded for direct application to practical problems.

Vortex Flow in Three Dimensions.—Vortex flow, which circulates around a point known as a "vortex center" in two-dimensional flow, circulates around a line known as a "vortex filament" in three-dimensional flow. A vortex filament may be either straight or curved. The familiar smoke ring is made up of air and smoke particles in vortex flow about a circular vortex filament.

Several theorems pertaining to vortexes and vortex filaments are employed in aeronautical theory. The following three theorems, which were first developed by Helmholtz in 1858 for an ideal fluid, are of particular importance:

1. Vortex filaments either form closed curves or extend to the boundaries of the fluid.
2. The circulation about a vortex filament remains constant throughout its length for all time.
3. The particles of a fluid composing a vortex remain identified with that vortex indefinitely.

Idealization of a Wing by Means of a Vortex System.—The development of the two-dimensional flow about an airfoil as presented in the preceding chapter proved so complicated that only the principal steps were described. It may be recalled that the flow pattern about a circular cylinder in a rectilinear flow was obtained first of all

through the superposition of three simpler flows; then a vortex flow was superposed to provide circulation about the cylinder; and finally the flow pattern of the circular cylinder was transformed into the flow pattern about an airfoil through the use of conformal transformation. The possibility of adding flow in a third dimension to this analysis without extreme mathematical complication does not look very promising.

In meeting these difficulties, the aeronautical scientist employs a familiar technique, that of idealizing and simplifying the actual situation until it becomes practicable to use theoretical methods. To some extent this technique has already been practiced in the neglect of viscosity in most of our earlier fluid-flow developments.

In this case it proves expedient to replace the wing with a three-dimensional vortex flow. The vortex flow may be given the same circulation as the wing so that the vortex will have the same lift as the wing, according to the Kutta-Joukowsky equation, $L^1 = \rho V\Gamma$; the position of the lift force may be made the same on the vortex as on the wing by passing the vortex filament through the center of pressure of the wing. Such a vortex filament is appropriately termed the "lifting line."

Conditions at the wing tips also favor the selection of a vortex system to simulate actual flow conditions. It is well known from both observation and experiment that a vortex-like flow extends backward from the wing tips of an airplane in flight. Tufts or smoke may be readily used in the wind tunnel to make visible the spiraling flow leaving the wing tips; and under proper atmospheric conditions airplanes leave vapor trails of condensed droplets of moisture behind their wing tips. These so-called "trailing vortexes" are maintained by the flow of air around the wing tips from the relatively high-pressure region below the wing to the low-pressure region above. Thus vortex theorem 1, which does not permit vortex filaments to end within the fluid, may be easily satisfied by joining the two

ends of the lifting line with the trailing vortexes to form a U-shaped vortex filament (Fig. 6.1). Likewise, theorem 2 may be satisfied by making the circulation about the trailing vortexes equal to the circulation about the lifting line. Theorem 3, which requires that the particles composing a vortex flow remain identified with that vortex, is only partly satisfied. Although the trailing vortexes *do* remain identified with the same particles, the lifting line vortex must continually take up new particles and reject old ones to parallel the operation of an actual wing. Because of this violation of vortex laws, the vortex that circulates around the lifting line is known as a "bound vortex."

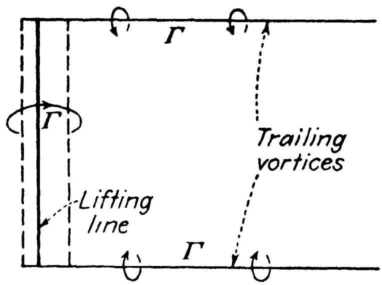

FIG. 6.1.—U-shaped vortex filament.

To comply with theorem 1, the U-shaped vortex filament must be continued past its open end to form a closed path. This is accomplished by a *starting vortex* which is shed off

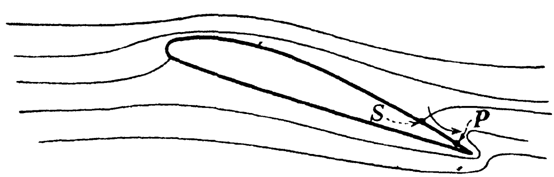

FIG. 6.2.—Development of a starting vortex.

the trailing edge of an airfoil at the beginning of its flight, as shown in Fig. 6.2. Successive flow observations made from the instant that relative motion begins between an airfoil and a fluid medium have indicated that initially the flow takes place without circulation with a stagnation point on its upper surface as shown at S in Fig. 6.2; the velocity of flow then becomes extremely large around the trailing edge and the pressure correspondingly low. Viscous effects absorb some of the forward velocity of flow on

the upper surface, and the unfavorable pressure gradient absorbs the rest, bringing the flow to a halt at some point P short of the original stagnation point S. A backflow develops from S toward P (Fig. 6.2) which induces the counterclockwise circulation of the starting vortex and moves the stagnation point back to the trailing edge where it remains until the angle of attack of the wing or the air speed is again changed.

After a wing has progressed a few chord lengths, the effect of the starting vortex in influencing the flow about a wing becomes negligibly small, so, except for starting conditions

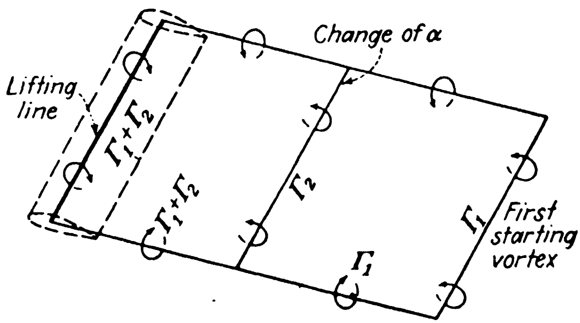

FIG. 6.3.—Vortex system of a wing after an increase in angle of attack.

or for wings undergoing a change in angle of attack, the effect of the starting vortex need not be considered. A complete vortex system for a wing that started from rest and effected one change of angle of attack is illustrated in Fig. 6.3.

Vortex Systems for Various Spanwise Lift Distributions. The variation of the downward velocities produced by the wing-tip vortexes along the lifting line of a constant circulation wing is shown in Fig. 6.4. The resultant velocity, termed the "down-wash velocity" (w), at any point along the lifting line is found by adding the downward velocities produced by each of the wing-tip vortexes. Since w varies inversely with the distance from the wing tips, the down-wash becomes infinitely large at each wing tip.

As might be expected, down-wash velocities of infinite magnitude are not present at the wing tips of actual airplanes. In addition, the lift distribution of an airplane wing is not constant across the span but rather rises to a

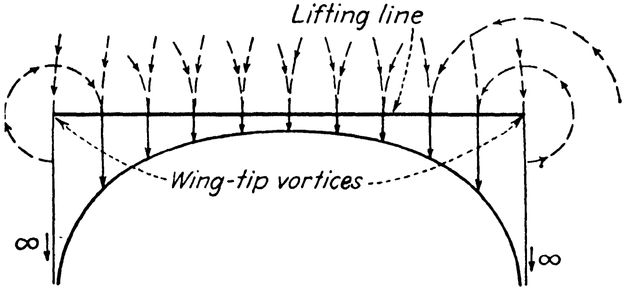

FIG. 6.4.—Spanwise distribution of down-wash for a wing of constant circulation.

maximum in the center of the span and gradually falls off to zero at the wing tips. It becomes evident that the simple vortex system of a wing of constant circulation (Fig. 6.4) must be modified to correspond with observed conditions..

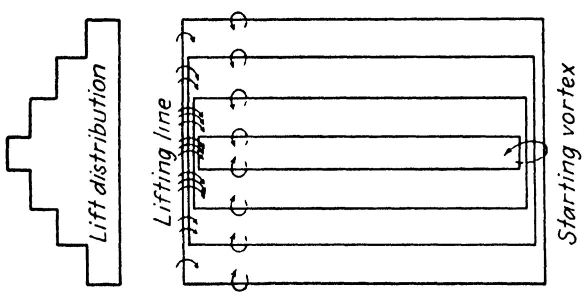

FIG. 6.5.—Superposition of vortexes. (To clarify the illustration, the vortex filaments along the lifting line and the starting vortex are individually shown, although they actually coincide.)

Any spanwise distribution of circulation—and therefore any lift distribution—can be obtained by a superposition of U-shaped vortexes, as shown in Fig. 6.5. The circulations add where the vortex filaments coincide to give a distribution of circulation—and therefore of lift—as illustrated.

In order to obtain a smooth lift curve the trailing vortexes are assumed to leave the wing continuously in a *vortex sheet*, as shown in Fig. 6.6. The difference in the circulation between any two points 1 and 2 along the lifting line is then equal to the mathematical summation—that is, the

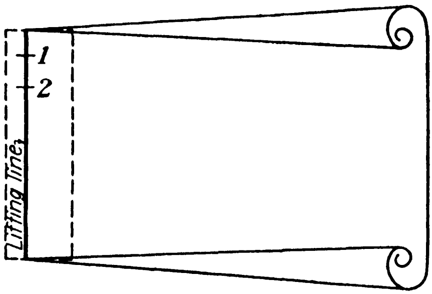

FIG. 6.6.—Vortex sheet behind a wing. (*N.A.C.A. Technical Report* 116.)

integration—of the strengths of the trailing vortexes between these two points.

Now that the system has been made flexible enough to accommodate any desired lift distribution, the next step is to choose a lift distribution which conforms reasonably well to practical distributions and which can be handled by

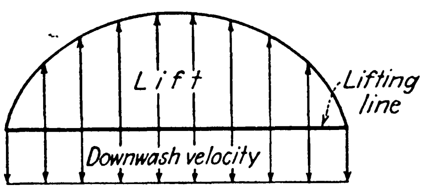

FIG. 6.7.—Variation of lift and down-wash velocity across the span of a wing with elliptical lift distribution.

mathematical theory. An elliptical lift distribution, as shown in Fig. 6.7, fulfills these two requirements. The down-wash is constant across the span (Fig. 6.7) for elliptical lift distribution which promotes the operation of a wing at its highest efficiency.

Effect of Down-wash on the Characteristics of a Wing.—The down-wash velocity produced by the wing-tip vortexes tends to deflect an approaching air stream downward to

reduce the effective angle of attack of an airplane wing. A typical airfoil section of a wing with elliptical lift distribution is shown in Fig. 6.8. The undisturbed velocity of flow V is shown intersecting the chord line at an angle of attack α. The true or *resultant velocity* of the airstream at the lifting line $V_{\text{resultant}}$ is found by adding vectorially the down-wash velocity w to the undisturbed velocity V. This resultant velocity makes an angle, α_0, with the chord line called the "effective angle of attack."

The resultant lift force produced on the wing must act in a direction normal to the resultant velocity and have a magnitude determined by the Kutta-Joukowsky formula

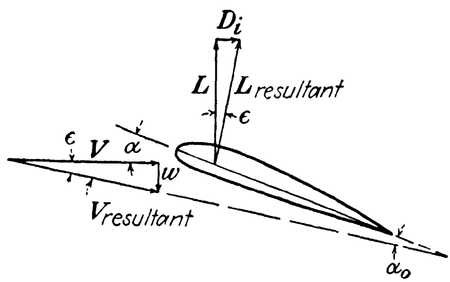

FIG. 6.8.—Effect of down-wash on the flow over an airfoil.

$L_{\text{resultant}} = \rho V_{\text{resultant}}\Gamma$. The conventional lift force L acts normal to the undisturbed velocity V.

From the foregoing it may be seen that the *resultant* velocity and the *effective* angle of attack are the governing factors in determining the *resultant lift* of an airfoil with down-wash. On the other hand, the undisturbed velocity V, the angle of attack α, and the ordinary lift force L are the quantities that are of the most value in aeronautical considerations. L, V, and α will consequently be expressed in terms of $L_{\text{resultant}}$, $V_{\text{resultant}}$, and α_0.

Referring to Fig. 6.8, the angle between the undisturbed and resultant velocities has been designated ϵ (epsilon), the *angle of down-wash.* The angle between the lift vectors must also equal ϵ since the lifts are respectively perpendicu-

lar to the velocities. If ϵ is considered a small angle, as is generally the case in practice, then

$$\epsilon_{\text{radians}} \doteq \tan \epsilon \doteq \sin \epsilon$$

and

$$\cos \epsilon \doteq 1$$

From Fig. 6.8

$$L = L_{\text{resultant}} \cos \epsilon \doteq L_{\text{resultant}}$$

and

$$V = V_{\text{resultant}} \cos \epsilon \doteq V_{\text{resultant}}$$

The component of $L_{\text{resultant}}$ in the drag direction will be designated as D_i, the *induced drag.* From the force triangle of Fig. 6.8,

$$D_i = L \sin \epsilon \doteq L\epsilon \tag{6.1}$$

From the velocity triangle of Fig. 6.8,

$$\frac{w}{V} = \tan \epsilon \doteq \epsilon \tag{6.2}$$

Substituting in Eq. (6.1),

$$D_i = L \tan \epsilon \doteq \frac{Lw}{V} \tag{6.3}$$

Again referring to Fig. 6.9,

$$\alpha = \alpha_0 + \epsilon = \alpha_0 + \frac{w}{V} \tag{6.4}$$

since an exterior angle of a triangle is equal to the sum of the alternate interior angles.

The application of Eqs. (6.3) and (6.4) to practical problems requires that the ratio w/V be evaluated. This may be accomplished by equating the lift force of the wing to the change in momentum per unit time of the air passing over the wing. Applying Eq. (2.13) to the problem,

$$F = L = M\Delta V \tag{6.5}$$

The change in velocity ΔV experienced by the air in passing over the wing is due to the effect of the trailing

vortexes in producing a downward velocity at points *far behind the wing.* Since the trailing vortexes that produce this velocity extend on *each* side of points behind the wing, the resultant velocities are twice as large as the down-wash at the lifting line where the trailing vortexes extend in the downstream direction only. ΔV therefore equals twice the down-wash velocity, $2w$.

The value of the mass of air deflected is more difficult to determine since only particles of air in the vortex sheet

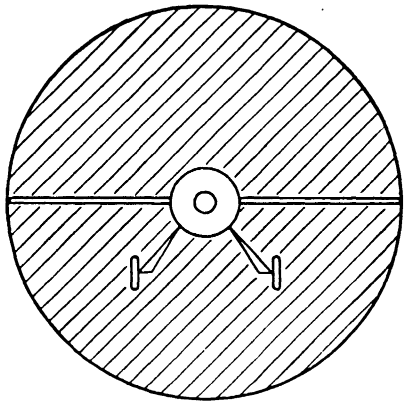

FIG. 6.9.—Volume of air deflected by a monoplane wing according to Prandtl's assumption.

experience a change in down-wash velocity of $2w$ whereas particles on either side are deflected by varying amounts. Prandtl[1] has shown that correct results can be obtained by momentum methods if the mass of air flowing through a circle of diameter equal to the wing span (Fig. 6.9) is assumed to experience the full deflection, $2w$.

Substituting in Eq. (6.5),

$$L = M2w = AV\rho 2w = \frac{\pi b^2}{2} V\rho w \tag{6.6}$$

but

$$L = C_L \frac{\rho}{2} SV^2$$

[1] L. PRANDTL, Applications of Modern Hydrodynamics to Aeronautics, *N.A.C.A. Technical Report* 116.

Substituting in Eq. (6.6) and solving for w/V ($= \epsilon$),

$$\frac{w}{V} = \frac{C_L S}{\pi b^2} \tag{6.7}$$

The ratio $\frac{b^2}{S} = \frac{(\text{wing span})^2}{\text{wing surface}}$ is customarily defined as the *aspect ratio* (A.R.) of the wing. (For a *rectangular* wing,

$$A.R. = \frac{b^2}{S} = \frac{(\text{span})^2}{\text{span} \times \text{chord length}} = \frac{\text{span}}{\text{chord length}}\Big)$$

Using this definition in Eq. (6.7),

$$\frac{w}{V} = \frac{C_L}{\pi A.R.}$$

The induced drag D_i then becomes

$$D_i = L\epsilon = \frac{Lw}{V} = \frac{LC_L}{\pi A.R.} \tag{6.8}$$

and, in coefficient form,

$$C_{D_i} = \frac{C_L^2}{\pi A.R.} \tag{6.9}$$

The angle of attack of a wing as expressed in Eq. (6.4) may now be written

$$\alpha = \alpha_0 + \frac{w}{V} = \alpha_0 + \frac{C_L}{\pi A.R.} \tag{6.10}$$

The foregoing discussion does not constitute a complete derivation of Eqs. (6.9) and (6.10) since it is predicated on the acceptance of Prandtl's suggestion regarding the mass of air deflected. This analysis has the advantage of simplicity, however, and affords a general physical picture of the production of down-wash, whereas a rigorous analysis would be considerably more involved.

Aspect-ratio Corrections.—Experiments have confirmed the validity of the expressions for induced drag and angle of down-wash [Eqs. (6.7) and (6.9)] to most conventional wing shapes and aspect ratios within reasonable limits of

accuracy. The expressions take into account the effect of varying the relative dimensions of the span and chord of a wing, that is, the top view or *plan form* so that wind-tunnel tests need be resorted to only for determining the effect of the wing profile and the scale effect.

In general, the aerodynamicist has available characteristic curves of a given profile for one aspect ratio A.R.$_1$, and desires corresponding values of the angle of attack, the coefficient of drag, and the coefficient of lift for the same profile but a different aspect ratio A.R.$_2$. This problem is illustrated in Fig. 6.10 where A.R.$_2$ has been arbitrarily chosen as the greater. If the two wings are compared with

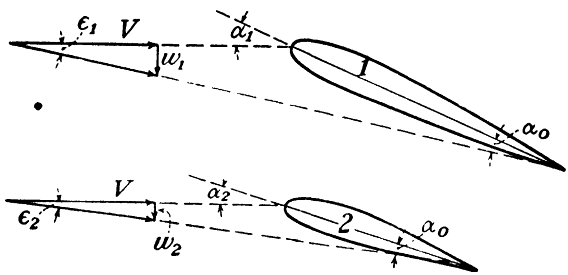

FIG. 6.10.—Velocity relations for two airfoils of the same profile but different aspect ratios.

equal undisturbed velocities, then the *effective* angles of attack must be equal *for equal lift coefficients;* that is,

$$\alpha_{0_1} = \alpha_{0_2}$$

But

$$\alpha_{0_1} = \alpha_1 - \epsilon_1 = \alpha_1 - \frac{C_L}{\pi A.R._1}$$

and

$$\alpha_{0_2} = \alpha_2 - \epsilon_2 = \alpha_2 - \frac{C_L}{\pi A.R._2}$$

Equating, solving for α_2, and changing from radians to degrees,

$$\alpha_2 = \alpha_1 - \frac{57.3C_L}{\pi}\left(\frac{1}{A.R._1} - \frac{1}{A.R._2}\right) \qquad (6.11)$$

The total drag of an airfoil D_t can be separated into two parts: the *profile drag* D_p due to viscous effects in the air stream which depends on the profile and on its effective angle of attack α_0; and the *induced drag* D_i which depends on the lift coefficient and the aspect ratio. Stated mathematically,

$$D_t = D_p + D_i$$

and, therefore,

$$C_{D_t} \frac{\rho}{2} SV^2 = C_{D_p} \frac{\rho}{2} SV^2 + C_{D_i} \frac{\rho}{2} SV^2$$

so that

$$C_{D_t} = C_{D_p} + C_{D_i} \tag{6.12}$$

For the two wings of Fig. 6.10 of different aspect ratios but *identical profiles*,

$$C_{D_{p_1}} = C_{D_{p_2}}$$

But from a rearrangement of Eq. (6.12),

$$C_{D_{p_1}} = C_{D_{t_1}} - C_{D_{i_1}} = C_{D_{t_1}} - \frac{C_L^2}{\pi A.R._1}$$

and

$$C_{D_{p_2}} = C_{D_{t_2}} - \frac{C_L'^2}{\pi A.R._2}$$

Equating and solving for $C_{D_{t_2}}$,

$$C_{D_{t_2}} = C_{D_{t_1}} - \frac{C_L'^2}{\pi} \left(\frac{1}{A.R._1} - \frac{1}{A.R._2} \right) \tag{6.13}$$

Since Eqs. (6.11) and (6.13) are used for transforming values of the angle of attack and drag coefficient *corresponding to a given lift coefficient* from a wing of one aspect ratio to another, these relations are known as the "transformation equations."

ILLUSTRATIVE PROBLEM

An airplane weighing 6,000 lb. flies at an air speed of 100 m.p.h. through air of standard sea-level density. If it is equipped with an

N.A.C.A. 23012 wing of 200 sq. ft. area and has an aspect ratio of 10, calculate for this air speed (neglect scale effect): (*a*) the angle of attack, (*b*) the induced drag, (*c*) the total drag.

Solution: a. For level flight and for moderate rates of climb or descent, the weight of an airplane very closely equals the lift of its wings,

$$W = L = C_L \frac{\rho}{2} SV^2$$

and, solving for C_L,

$$C_L = \frac{2W}{\rho SV^2} = \frac{2 \times 6{,}000}{0.002378 \times 200 \times (100)^2} \left(\frac{60}{88}\right)^2 = 1.17$$

Referring to Fig. 3.4 for the characteristic curves for the N.A.C.A. 23012 airfoil *with aspect ratio* $= 30/5 = 6$.

$$\alpha = 14.6 \text{ deg. and } C_D = 0.09 \text{ corresponding to } C_L = 1.17$$

From Eq. (6.11),

$$\alpha_2 = \alpha_1 - \frac{57.3 C_L}{\pi}\left(\frac{1}{A.R._1} - \frac{1}{A.R._2}\right)$$

$$= 14.6 - \frac{57.3 \times 1.17}{3.14}\left(\frac{1}{6} - \frac{1}{10}\right) = 13.2 \text{ deg.}$$

b. $$D_i = L\epsilon = \frac{LC_L}{\pi A.R.} = \frac{6{,}000 \times 1.17}{3.14 \times 10} = 223.5 \text{ lb.}$$

c. $$C_{D_2} = C_{D_1} - \frac{C_L^2}{\pi}\left(\frac{1}{A.R._1} - \frac{1}{A.R._2}\right)$$

$$C_{D_2} = 0.09 - \frac{(1.17)^2}{3.14}\left(\frac{1}{6} - \frac{1}{10}\right) = 0.061$$

$$D_t = 0.061 \times \frac{0.002378}{2} \times 200 \times (100)^2 \left(\frac{88}{60}\right)^2 = 313 \text{ lb.}$$

or, alternatively,

$$\frac{D}{L} = \frac{C_D}{C_L}$$

Therefore,

$$D = L \times \frac{C_D}{C_L} = \frac{6{,}000 \times 0.061}{1.17} = 313 \text{ lb.}$$

Effect of Wing Plan Form on Aspect-ratio Corrections.—The aspect-ratio transformation Eqs. (6.11) and (6.13) theoretically apply only to elliptical lift distribution corresponding to an untwisted wing of elliptical plan form. As observed in Fig. 6.11, the lift distributions of rectangular

and highly tapered wings differ substantially from the elliptic distribution. This difference is taken into account

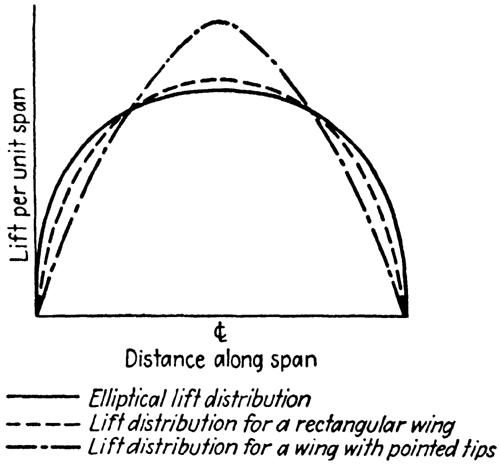

FIG. 6.11.—Lift distributions for wings of different plan forms.

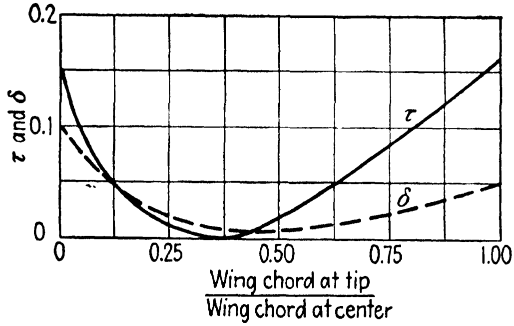

FIG. 6.12.—Glauert correction factors for tapered airfoils.

by Glauert who modified the transformation equations as follows:

$$\alpha_2 = \alpha_1 - 57.3\,\frac{C_L}{\pi}\left(\frac{1+\tau_1}{A.R._1} - \frac{1+\tau_2}{A.R._2}\right) \tag{6.14}$$

and

$$C_{D_2} = C_{D_1} - \frac{C_L^2}{\pi}\left(\frac{1+\delta_1}{A.R._1} - \frac{1+\delta_2}{A.R._2}\right) \tag{6.15}$$

The symbols τ (tau) and δ (delta) represent quantities that depend upon the shape or plan form of the wings. For

tapered airfoils, the values of these factors are given in Fig. 6.12. It may be noted that values are given for a ratio of $\frac{\text{tip chord}}{\text{central chord}} = 1$ which refers to a rectangular airfoil.

Wings in Combination.—A biplane will have a greater induced drag than a monoplane *of the same aspect ratio and weight,* owing to mutual interference effects between its two wings. The vortex system of one wing will produce a down-wash component at the other which will add to the down-wash velocity of the other wing's own vortex system,

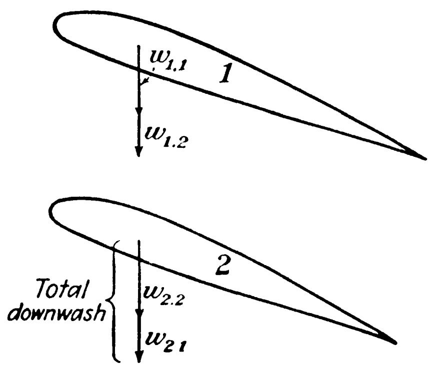

FIG. 6.13.—Increase in downwash owing to the interaction of the wings of a biplane.

as indicated in Fig. 6.13. The magnitude of this interaction depends upon the ratio of the spans of the two wings, the ratio of their lifts, and the gap between the wings.

In spite of these mutual interference effects, the biplane has considerably less induced drag than a monoplane of equal weight, *span,* and wing surface since, in this case, the chord length of the monoplane would be twice that of the biplane. Although the biplane has been used on aircraft carriers where space is at a premium, monoplanes with folding wings are now extensively employed for this purpose.

When wings are disposed in a side-by-side relationship, the trailing vortexes of one wing produce an upward velocity at the other which tends to reduce the down-wash

and therefore the induced drag of each wing. Thus an airplane in close military formation may perform more efficiently than when flying alone.

Ground Effect.—As an airplane approaches the ground, its down-wash velocity is increasingly reduced since there can be no vertical component of air velocity at the surface of the ground. To reproduce this situation in a manner

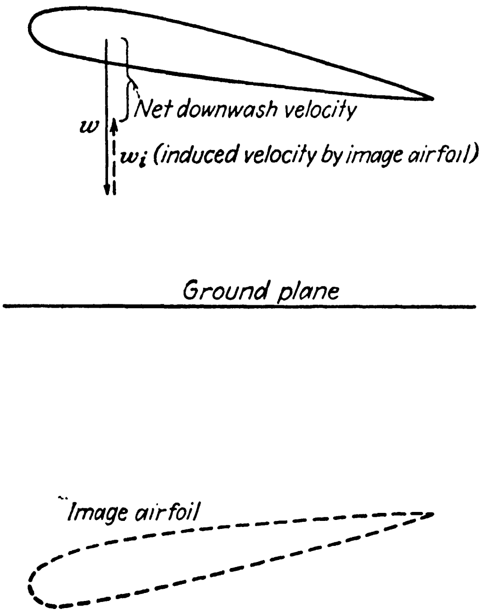

FIG. 6.14.—Evaluation of ground effect.

that can be handled mathematically, a so-called "image system" may be employed in which the ground plane is assumed to be replaced by an equal and inverted hypothetical wing located as far below the ground plane as the actual wing is above, as shown in Fig. 6.14. Any downward velocity components at the ground plane are then offset by equal upward components from the image wing to establish the necessary condition of zero normal velocity to the ground plane. Using this system, the down-wash of the image airfoil becomes an upwash velocity at the

actual wing which must be subtracted from the normal down-wash of the regular wing to give its net down-wash velocity in the presence of the ground.

Ground effects begin to assume practical importance at an altitude approximately equal to the wing span of an airplane. The reduction in down-wash near the ground is reflected in a lowering of the induced drag, a decrease in the angle of attack, and a change in the elevator effectiveness. When an airplane descends until its landing gear barely clears the ground, the reduction in the induced drag may amount to as much as 50 per cent. This makes possible the usual flattening of the glide path of an airplane during landing.

Wind-tunnel tests are often conducted to investigate ground effect. A flat ground board may be supported beneath the model, or less frequently a second inverted image model may be used to simulate the effect of a ground plane located halfway between.

PROBLEMS

1. An airplane weighing 2,000 lb. cruises at a speed of 100 m.p.h. If the down-wash velocity induced by its wing has a constant value of 4 ft. per sec. along the span, determine for the cruising condition (*a*) the angle of down-wash, (*b*) the induced drag.

2. If the airplane of Prob. 1 has a wing aspect ratio of 6, what is the value of C_L corresponding to the cruising speed down-wash velocity of 4 ft. per sec.?

3. Partial specification and performance figures for a private airplane are as follows:

Span................	35 ft.	Gross weight..............	1,160 lb.
Wing area...........	173 sq. ft.	Cruising speed............	75 m.p.h.
Wing section.........	N.A.C.A.23012	Landing speed.............	42 m.p.h.

(*a*) Calculate the angle of down-wash and the induced drag for this airplane corresponding to its cruising speed. (*b*) Calculate the angle of attack and the total drag of this airplane for the cruising condition. (*c*) What percentage of the total drag is the induced drag?

4. Repeat Prob. 3 for the landing condition.

5. What would be the saving in drag at the cruising speed of the airplane of Prob. 3 resulting from an increase of wing aspect ratio to

12 with all other specifications remaining the same? the saving in horsepower?

6. An airplane, having linearly tapered wings with a taper ratio of 2:1 of N.A.C.A. 23012 section has a gross weight of 3,000 lb., an aspect ratio of 10, and a span of 40 ft. Determine its total drag corresponding to a coefficient of lift of 0.5. Assume nonelliptical lift distribution.

CHAPTER 7

THE BOUNDARY LAYER

The theory of lift of an airfoil has been developed without reference to viscosity effects, except in the formation of the starting vortex and in the limitation of the maximum lift at the burble point. The drag force, on the other hand, depends entirely (except for the *induced* drag) on the action of viscous forces within the fluid. The viscous forces, it will be recalled, are directly proportional to both the absolute viscosity μ of the fluid and the velocity gradient dV/dy within the flow pattern. The study of drag is therefore closely linked to the regions in the flow about an immersed body where the velocity gradient is comparatively high. In general, this condition exists only in a very thin boundary layer of fluid close to the surface of the body and in the usually narrow turbulent wake behind the body.

The Laminar Boundary Layer of a Flat Plate.—A thin, flat plate placed parallel to the direction of flow of an air stream, as in Fig. 7.1, will experience a drag force due to viscous action in the boundary layers of its upper and undersides. The velocity of flow over the plate varies from zero to the undisturbed velocity within a very short distance from the surface. The distance from the surface to the point where the velocity differs only a negligible amount from the undisturbed velocity is defined as the thickness of the boundary layer δ.

As illustrated in Fig. 7.1, the thickness of the boundary layer increases in the direction of flow. This is a consequence of the action of the viscous forces in the boundary layer in overcoming the inertia force of the air stream at increasing distances from the plate as the flow proceeds

away from the leading edge. This reasoning suggests that the distance from the leading edge and the Reynolds number of the flow are two important factors in determining boundary layer thickness—a conclusion borne out by the

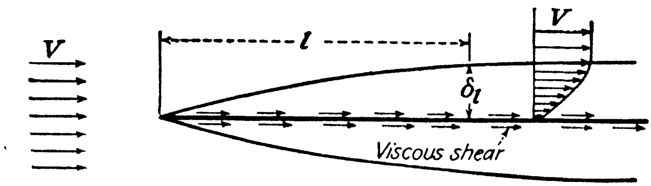

FIG. 7.1.—Laminar boundary layer (thickness greatly exaggerated).

mathematical treatment of Prandtl who obtained the following result:

$$\delta \text{ is proportional to } \frac{l}{\sqrt{R_l}} \tag{7.1}$$

where δ = thickness of the boundary layer
l = distance from leading edge to point where δ is desired
$R_l = \frac{\rho V l}{\mu}$ local Reynolds number

An expression for the drag force resulting from laminar boundary layer flow was determined by Blasius in 1907 and has been closely confirmed by actual measurements. His results can be conveniently presented by means of a skin friction coefficient C_F, such that

$$D_F = C_F \frac{\rho}{2} A_w V^2 \tag{7.2}$$

where $C_F = \frac{1.328}{\sqrt{R_l}}$ for laminar flow (plotted in Fig. 7.3) (7.3)
A_w = total wetted area, sq. ft.

The Turbulent Boundary Layer of a Flat Plate.—In Reynolds' original experiments, as described in Chap. 3, the flow of water through a glass pipe changed from laminar to turbulent as R was increased. The onset of turbulent

flow occurred first at the exit end of the pipe and then progressed toward the inlet as R was increased. The initial turbulence in the water entering the pipe was an important factor in influencing the value of R at which the flow changed from laminar to turbulent—the "critical Reynolds number."

These same characteristics are observed in the boundary layer. As illustrated in Fig. 7.2, an initially laminar flow may pass through a short transition region to become turbulent. The condition of turbulent flow in the boundary layer is characterized by particles of the air moving in an irregular fashion with velocity components normal to

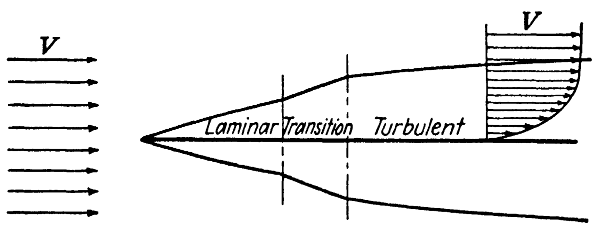

FIG. 7.2.—Transition from laminar flow to turbulent flow in the boundary layer. (Thickness greatly exaggerated.)

the plate as well as parallel to it. These normal components cause high-speed particles from the outer layers to exchange momentum with slower particles near the plate and vice versa. This interchange of momentum tends to move the film of air in contact with the plate—and therefore the plate itself—in the direction of flow, producing the external drag force.

Since drag is produced in laminar flow by movement of the air particles normal to the plate owing to *molecular* vibration, the causes of drag for laminar and turbulent boundary layers are basically the same. The effects are much greater for turbulent boundary layers, however, because the normal components of velocity of particles in turbulent flow produce more thorough mixing than the molecular vibration of particles in laminar flow; consequently the velocity profile of turbulent flow is "fuller"

and the value of the skin-friction coefficient is much higher for the turbulent condition.

The drag of a flat plate can be determined with reasonable accuracy by means of Eq. (7.2) using a value of C_F from Fig. 7.3, provided the flow in the boundary layer is either laminar or turbulent. In the general case, however, the initially laminar boundary layer passes through a short transition region and then becomes turbulent with the value of C_F increasing during transition along some path

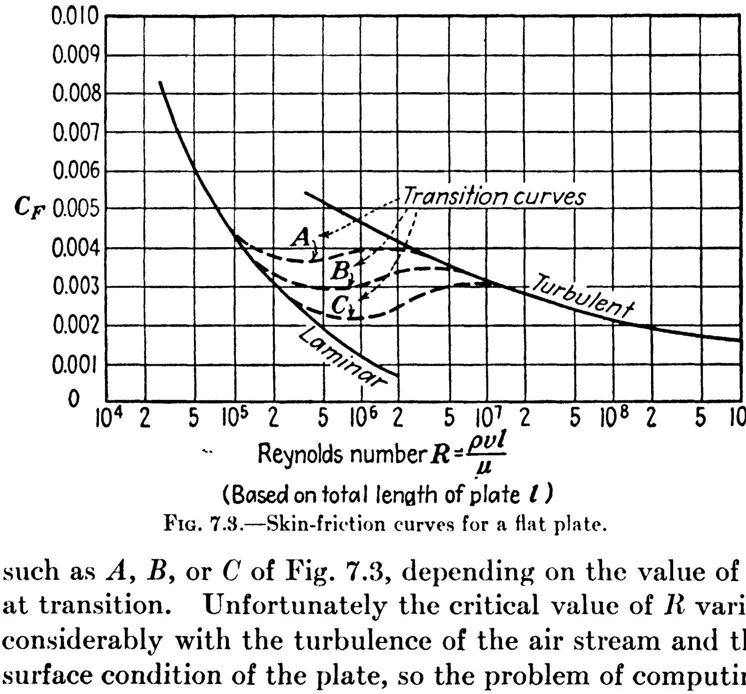

FIG. 7.3.—Skin-friction curves for a flat plate.

such as A, B, or C of Fig. 7.3, depending on the value of R at transition. Unfortunately the critical value of R varies considerably with the turbulence of the air stream and the surface condition of the plate, so the problem of computing the friction drag of a plate cannot usually be solved without experimental information regarding the position of the transition point. For minimum skin friction, transition should be delayed as long as possible, which may be promoted by low values of R, low turbulence, and smooth exposed surfaces.

Flow around a Sphere.—The flow of an *ideal* fluid around a sphere, as developed in Chap. 5, results in the formation

of velocities and pressures on the front surface of the sphere identical with those at corresponding points on its rear surface, leaving no resultant force in the drag direction. But spheres and all other bodies experience drag when exposed to an air stream, so ideal fluid theory, which proved so valuable in connection with lift, must omit some factor of importance in the treatment of drag. This factor is the influence of viscosity both in boundary layer skin-frictional effects and in controlling the size of the wake behind the sphere. To study these actions in detail, the history of a particle of ideal fluid moving through the flow pattern of a sphere will be contrasted with that of an air

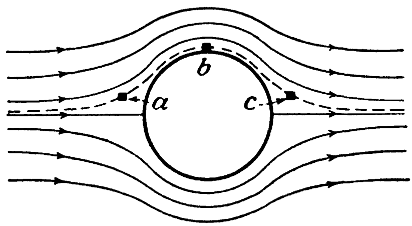

FIG. 7.4.—Flow of an ideal fluid about a sphere.

particle moving through the boundary layer of an actual sphere flow pattern.

The flow pattern of an ideal fluid past a sphere is shown in Fig. 7.4. The spacing of the streamlines indicates low velocities directly in front and behind the sphere with maximum velocities at the sides. The corresponding pressures, as a consequence of Bernoulli's equation, are high in front and behind and lowest at the sides. A representative particle moving along the dotted streamline (Fig. 7.4) would accordingly slow down at a in the relatively high-pressure area in front of the sphere, proceed at an accelerating rate to the point of minimum pressure and maximum velocity at b, and then continue with decreasing speed and increasing pressure to regain its original pressure and velocity at c. The process therefore involves an interchange of pressure and kinetic energies in such a way as to keep the total energy constant.

In charting the course of a comparative air particle in an actual flow pattern, points a, b, and c of the ideal flow will have as their counterparts a', b', and c' of the actual flow, as illustrated in Fig. 7.5.

A particle at a' in the actual flow will again be accelerated to position b' by the decreasing *pressure gradient* (that is, the change of pressure with distance) between a' and b'. The sum of the kinetic and pressure energies at b' will, however, be less than the initial total energy at a' by the amount of the thermal energy produced by viscous action in the boundary layer between a' and b'. Hence, the particle in proceeding toward c' must overcome a retarding pressure gradient and the action of viscous forces, with smaller initial total energy than in the ideal case. Consequently, the particle never reaches c' but instead its kinetic energy drops to zero at some intermediate point S, known as the "separation point," where the particle is carried away from the surface of the sphere by the exterior flow. The pressure at the separation point is low, corresponding to the pressure at a similarly situated point in the ideal flow. There is, moreover, a pressure gradient downstream of the separation point which promotes reversed flow, as indicated in Fig. 7.5. The region of reversed and discontinuous flow between the separation points forms the wake of the sphere. The pressure in the wake is low and produces a force on the sphere in the direction of flow which is commonly termed the "pressure drag." In the case of the sphere, the pressure drag forms a much larger part of the total drag than the skin-frictional drag. This predominance of the pressure drag holds true for most blunt (nonstreamline) bodies.

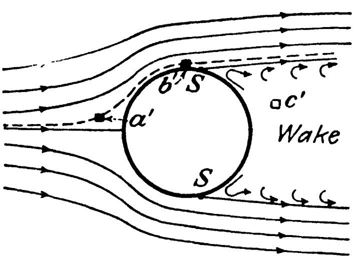

FIG. 7.5.—Flow of air about a sphere at a low Reynolds number.

If the velocity of flow over the sphere is increased, the

local Reynolds number R_l for any point in the boundary layer is proportionally increased, with a maximum value at the separation points (where the characteristic dimension l is greatest). With a continued increase, R_l at the separation points reaches the critical value necessary for transition to turbulent flow. With turbulent flow, the kinetic energy of the boundary layer is replenished by fluid particles of the outer flow. Consequently, the boundary layer flow progresses farther around the sphere to a new separation point, as at S' of Fig. 7.6. The resultant narrowing of the wake reduces the pressure drag of the sphere. The total drag is likewise reduced because the reduction of pressure drag more than offsets the increase of frictional drag which arises in the small portion of the

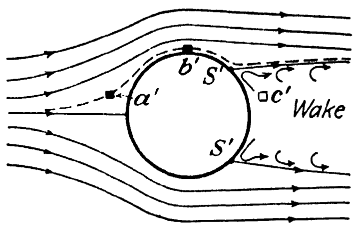

FIG. 7.6.—Flow of air about a sphere at a high Reynolds number.

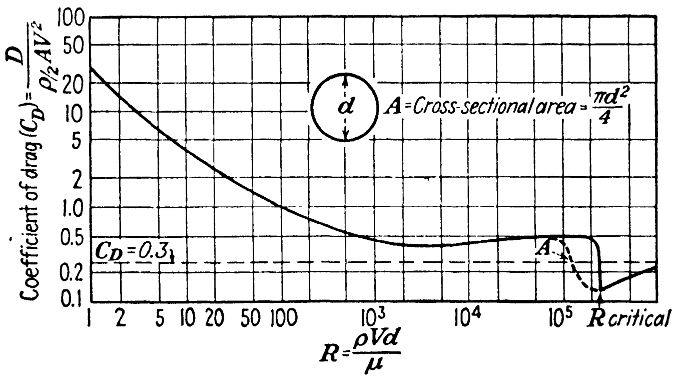

FIG. 7.7.—Typical variation of the drag coefficient of a sphere with Reynolds number.

boundary layer flow near the separation points where the flow changes from laminar to turbulent.

The rearward movement of the separation points at a critical value of R has been observed by several investigators using chemical smoke, tufts, and other methods of flow

visualization. The associated decrease in drag is illustrated in Fig. 7.7 which shows a typical variation of drag coefficient with Reynolds number for a sphere. The critical Reynolds number is clearly marked by the sharp drop in the drag coefficient at a value of R of approximately 2.5×10^5.

The Sphere as a Turbulence Meter.—The *turbulence* of an air stream consists of fluctuations in velocity which vary in frequency from about 5 to over 5,000 cycles per second. The direct measurement of turbulence therefore requires a very sensitive instrument of wide range. Obviously a pitot tube would be unsuited to this purpose since it would furnish only an average velocity reading.

A special hot-wire anemometer has been developed for the measurement of turbulence by Dr. Dryden[1] of the National Bureau of Standards. The sensitive element of this device is a short small-diameter platinum wire of low total-heat content which during operation is heated by electricity and exposed to the test air stream. The fluctuations in velocity of the air stream produce corresponding changes in the temperature of the wire; the changing temperature affects the resistance of the wire as measured by electrical instruments; and through suitable preliminary calibration in air streams of known velocity, the electrical measurements are converted into air velocities.

Since hot-wire anemometers of the required sensitivity are not available at the usual wind tunnel, the sphere has been calibrated as a secondary turbulence meter. The use of a sphere as a turbulence meter rests upon two facts that have already been discussed: the beginning of turbulent flow in the boundary layer of a sphere is marked by a sharp decrease in drag which is readily measurable in the average wind tunnel; and the beginning of turbulence in the boundary layer is very sensitive to the turbulence of the approaching air stream. The relationship between the

[1] Hugh Dryden, Reduction of Turbulence in Wind Tunnels, *N.A.C.A. Technical Report* 392.

turbulence of an air stream and the critical value of Reynolds number R_c, at which the drag coefficient suffered a marked drop, was determined accordingly by measurements of sphere drag and hot-wire anemometer turbulence in air streams of varying degrees of turbulence. In the resultant calibration curve of Fig. 7.8, it was found convenient to define R_c as the value of the Reynolds number corresponding to a value of C_D of 0.3 which locates a point at about the middle of the drop in drag coefficient, as may be seen in Fig. 7.7. With this curve it may be noted that the tur-

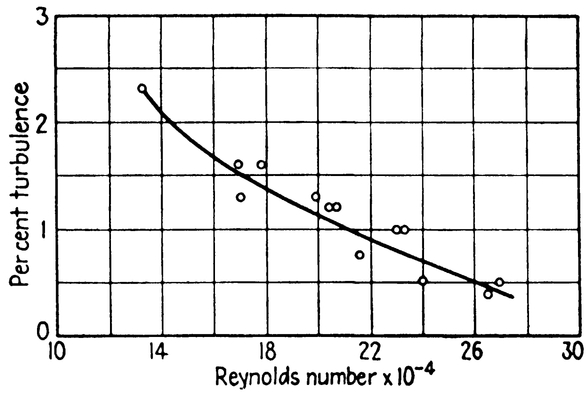

FIG. 7.8.—Reynolds number when C_D for sphere is 0.3 as a function of the turbulence. (*N.A.C.A. Technical Report* 392.)

bulence of the air stream corresponding to branch *A* is between 2 and 3 per cent, whereas the turbulence of the air stream giving the solid curve is about one-half of 1 per cent.

In more recent measurements of turbulence, it has been found more convenient to locate the value of R_c by means of pressure readings taken at certain positions on the front and the rear surfaces of the sphere. The value of the pressure readings corresponding to a drag coefficient of 0.3 has been established by wind-tunnel test.

Von Kármán Vortex Street.—A regular arrangement of vortexes known as the "von Kármán vortex street" has been observed in the wake of cylinders and other bodies when exposed to fluid flows of greater Reynolds number

than about 20. As illustrated in Fig. 7.9, the vortexes that compose the vortex street are arranged behind the cylinder at equal intervals in two parallel rows, which indicates that they were shed alternately from opposite sides of the cylinder at uniform time intervals. This periodic formation of eddies changes the pressure distribution behind the cylinder in a cyclical manner so that an alternating force is created which tends to vibrate the cylinder in a direction normal to the flow. The frequency, diameter, and velocity

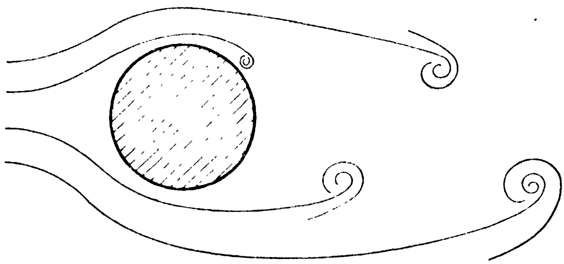

FIG. 7.9.—Von Kármán vortex street.

of flow have been interrelated experimentally to give the following approximation:

$$\frac{fD}{V} \doteq 0.22 \tag{7.4}$$

where f = frequency of vibration, cycles per second
D = diameter of cylinder, ft.
V = velocity of flow, ft. per sec.

Vibrations of this character are responsible for the "singing" of telephone wires in natural winds, sometimes causing mechanical failure. Gun turrets and other cylindrical protuberances on airplanes are susceptible to troublesome vibrations arising from this phenomenom.

A similar periodicity of vortex formation occurs in the wake of airfoils. At low angles of attack the wake behind an airfoil is small and the vortexes are weak so that no noticeable vibration is established. Near the stall, however, the vortexes set up a strong vibration of the wing

and severely buffet anything in the wing wake. The frequency of vibration may be approximated through the use of Eq. (7.4) with the projected length of the chord line on a plane normal to the flow as the length *D*.

TABLE III DRAG OF VARIOUS SHAPES			
Item No.	Shape	Coefficient of drag C_D	*R*
1	Curved plate	2.40	10,000
2.	Flat plate	1.90	4000 to 300,000
3	Square prism	1.82	10,000
4	60° Triangular prism	1.40	10,000
5	Curved plate	1.18	10,000
6	30° Triangular prism	1.05	100,000
7	Sphere	0.52	500
8	2:1 Elliptical cylinder	0.480	100,000
9	4:1 Elliptical cylinder	0.300	100,000
10	20° Sphere with conical tail	0.26	500
11	8:1 Elliptical cylinder	0.202	100,000

Drag of Various Shapes.—An understanding of boundary layer flow provides some insight into the effect of change of body form on both the drag coefficient and the scale effect. Adding a tail to a smooth sphere, for instance, should delay separation by providing a lower adverse pressure gradient behind the equatorial diameter and should thereby decrease the size of the wake and the pressure drag. The success of

this expedient is shown in Table III, items 7 and 10, which indicate that the addition of a 20-deg. conical tail to a sphere reduces the total drag of a sphere by about 50 per cent. On the other hand, if an effort were made to decrease

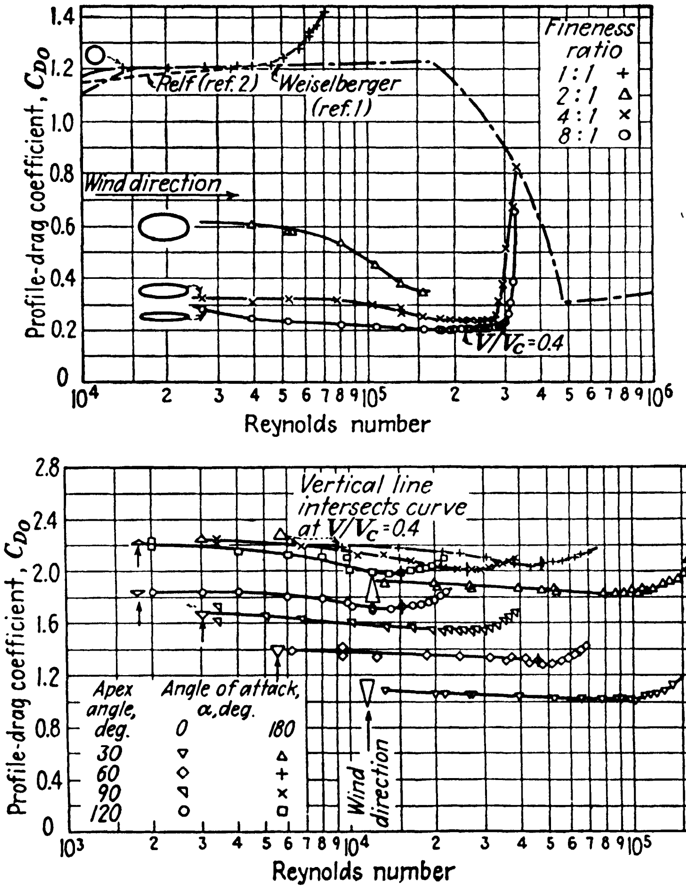

Fig. 7.10.—Scale-effect curves for various shapes. (The marked increase of drag at the higher Reynolds numbers is due to compressibility effects.) (*N.A.C.A. Technical Report* 619.)

the size of the wake still more by means of a very long tail, the increased frictional drag, due to the larger surface area, would offset the diminution in pressure drag. The most favorable proportions for minimum total drag as deter-

mined by experiment require a total length of about four times the sphere diameter.

An air stream would separate from the angular profiles of items 1 to 6 of Table III at the corners. One would therefore expect very little scale effect for these shapes. On the other hand, the elliptical cylinders, particularly the thicker ones, would be expected to have a scale-effect variation similar to that of the sphere. The curves of Fig. 7.10 are seen to be consistent with this reasoning.

Although a knowledge of the respective contributions of pressure and frictional drags is fundamental to an understanding of drag, these components are generally added together to form total or *parasite* drag for application to practical problems. Thus in Table III, only the parasite drag coefficient, C_D, is listed. The parasite drag force is related to C_D by

$$D = C_D \frac{\rho}{2} A V^2 \tag{7.5}$$

where D = parasite drag force, lb.

A = area of object projected on a plane *normal* to the flow, sq. ft.

The Drag of Airfoils.—An airfoil, like any other immersed body, is acted upon by both friction and pressure drags when exposed to an air stream. The sum of these two drag forces is, however, known as the "profile" drag instead of parasite drag as in other bodies. This distinction is necessary since the coefficient of profile drag C_D is associated with the wing surface (the projected area of the wing on the plane of its chord), while the parasite drag coefficient of other bodies is based on the projected area on a plane *normal* to the air flow. It would therefore have been misleading to include the profile drag coefficient of an airfoil in Table III. Figured on the same basis as the other items of Table III, the drag of a typical airfoil would fall slightly below that of the 8:1 ellipse.

For a modern high-performance airplane under cruising conditions, the drag contributed by the wing alone makes

up about 50 per cent of the total drag of the airplane. Any reduction in the induced drag, the pressure drag, or the frictional drag of an airplane wing would consequently prove of considerable value in adding to the efficiency and performance of the complete airplane.

The induced drag of a wing, as discussed in Chap. 6, depends upon the total lift (equal to the weight of the airplane), the aspect ratio, and the lift distribution. For a given airplane the induced drag will be a minimum for the highest practicable aspect ratio and for elliptical lift distribution, the latter usually being approached quite closely in practice.

Since the pressure drag of a wing operating at small angles of attack—corresponding to cruising or top speeds

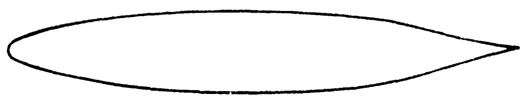

FIG. 7.11.—Profile of a typical laminar-flow airfoil.

is generally low especially for the thinner profiles, there is little opportunity for drag reduction here.

For a conventional wing profile the frictional drag shows more promise for total drag reduction. For minimum drag, it would be most advantageous to delay transition in the boundary layer to turbulent flow as long as possible. Conditions favorable to delayed transition are smooth surfaces, gentle curvatures, and small adverse pressure gradients. These are incorporated in the so-called "laminar-flow" (or low-drag) wing of Fig. 7.11 which has a minimum profile drag coefficient of less than half that of a conventional airfoil. The relatively sharp leading edge, the gradual increase in thickness with maximum thickness at about the center of the chord, and the slightly concave curvature near the tail are characteristic features. In addition to the low-drag advantage, the laminar-flow airfoil encounters compressibility effects at higher air speeds than conventional shapes. On the other hand, the maxi-

mum lift, the moment, and even the drag characteristics *at high angles of attack* are generally inferior. These shortcomings are gradually being overcome, however, and the low-drag and compressibility advantages have made it the logical choice for many high-performance airplanes.

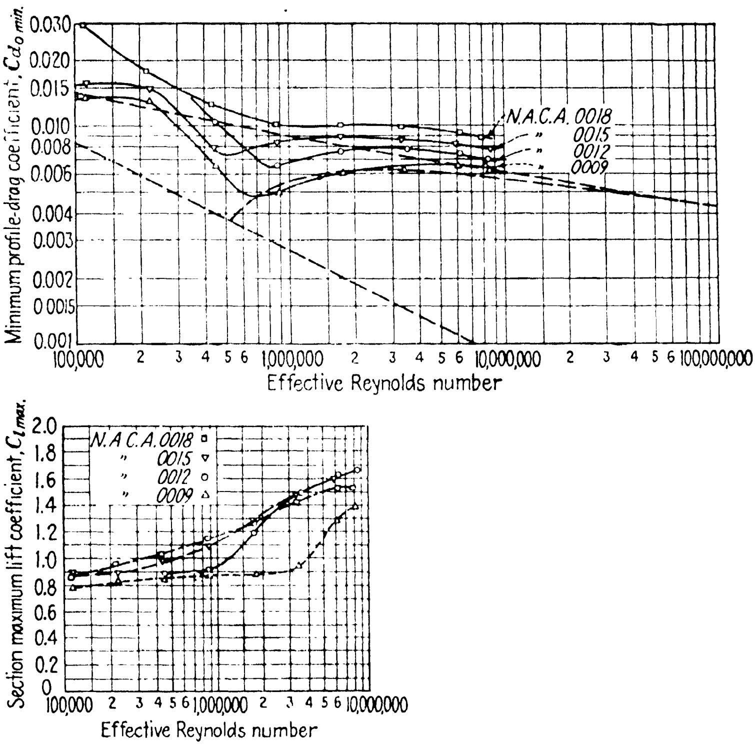

FIG. 7.12.—Scale-effect curves for symmetrical airfoils of varying thicknesses. (*N.A.C.A. Technical Report* 586.)

The scale effect on the force coefficients of conventional airfoils is closely related to boundary layer flow. The curves of Fig. 7.12 for symmetrical airfoils of various thicknesses show that the maximum lift coefficient is particularly sensitive to changes in the effective Reynolds number. The rather sharp increase of the maximum lift coefficient with Reynolds number is associated with earlier transition to turbulent flow in the boundary layer which delays

separation until a higher angle of attack is reached. In the same way the decrease in minimum profile-drag coefficient of the airfoils results primarily from the movement of the transition point with Reynolds number,[1] although it may be noted that the decrease in drag is not steeper and greater for the thicker airfoils as a strict analogy to the flow around the elliptical cylinders of Fig. 7.10 would indicate.

Of considerable importance in the reduction of wing drag is the need for making the surface of a wing as smooth and free of obstructions as possible. An irregularity near the leading edge of a wing, although having little parasite drag of its own, will cause the boundary layer flow to change to the turbulent condition in a fan-shaped area behind it and thus increase the wing drag substantially. Tests conducted by the N.A.C.A.[2] on a low-wing single-engine monoplane showed that 50 per cent of the profile drag of the wing could be eliminated by removing manufacturing irregularities in rivets, lap joints, and access doors.

The foregoing considerations do not hold true for wings operating at very low Reynolds numbers. For values of R less than 100,000, the boundary layer of a wing may remain completely laminar, which encourages early separation of flow with an associated increase of pressure drag and decrease of lift. Small wind-tunnel models tested at low speeds and some model airplanes fall into this category.

It may be seen that the effectiveness of wings operating in this "subcritical range" may be improved in quite the opposite way to that suggested for full-scale wings. Transition to turbulent flow should be encouraged so that rough wing surfaces and sharp leading edges are desirable whereas laminar flow sections are to be avoided. A thread cemented to the top surface of a wing in a position near to and parallel to the leading edge provides a simple means of

[1] EASTMAN N. JACOBS and ALBERT SHERMAN, Airfoil Section Characteristics as Affected by Variations in the Reynolds Number, *N.A.C.A. Technical Report* 586.

[2] JOSEPH BICKNELL, Determination of the Profile Drag of an Airplane Wing in Flight at High Reynolds Numbers, *N.A.C.A. Technical Report* 667.

artificially producing transition in the boundary layer of a wing operating in the subcritical range.

The Stalling of an Airfoil.—The process of stalling involves the separation of the flow near the leading edge

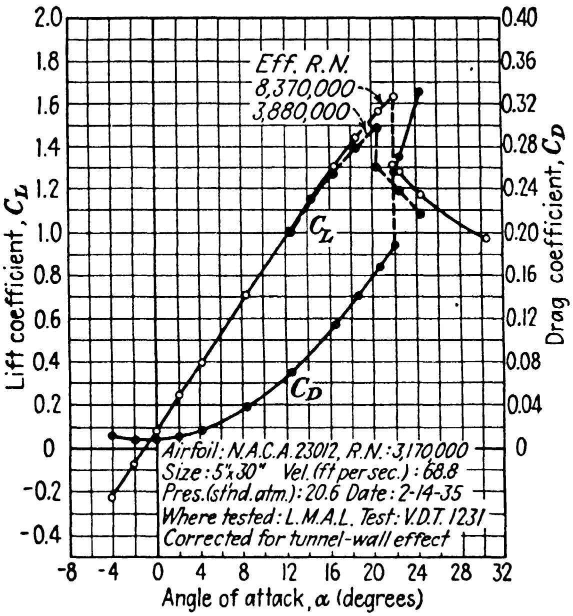

FIG. 7.13.—Characteristic curves of an N.A.C.A. 23012 airfoil. (*N.A.C.A. Technical Report* 610.)

of an airfoil with consequent loss of lift and increase of drag as shown in the characteristic curves of Fig. 7.13 (at $\alpha = 22$ deg.). Since separation results from the loss of kinetic energy of the flow in the boundary layer, it is evident that stalling might be eliminated or at least postponed if this energy were replenished.

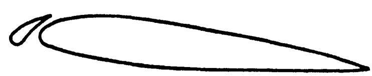

FIG. 7.14.—Wing with slot for postponing the stall.

A practical device for accelerating the upper boundary layer of a wing is the so-called "slot" which consists of a narrow channel extending along the wing just back of the leading edge. As shown in Fig. 7.14, the channel conducts a high-velocity jet of air from the relatively high-pressure

area below the wing and directs it against the retarded boundary layer on the upper side. The slot has proved successful in postponing the stall and thereby increasing the maximum lift coefficient of a wing. The performance of slots will be discussed more fully in a later article.

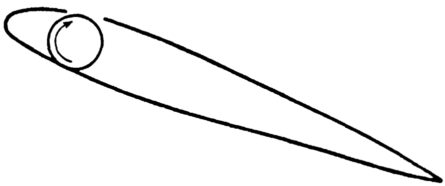

FIG. 7.15.—Rotating cylinder for the acceleration of the boundary layer. (*N.A.C.A. Technical Memorandum* 354.)

Two other methods of accelerating the boundary layer flow on the top surface of a wing are illustrated in Figs. 7.15 and 7.16. Both systems have proved effective in increasing the stalling angle and the maximum lift coefficient of a wing but suffer the disadvantage of requiring auxiliary equipment.

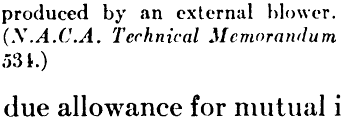

FIG. 7.16.—Removal of the boundary layer flow from the upper surface of a wing by suction produced by an external blower. (*N.A.C.A. Technical Memorandum* 534.)

Total Drag of an Airplane.—The drag of an airplane is equal to the sum of the drags of its components, the wing, fuselage, nacelles, and tail surfaces, with due allowance for mutual interference effects. These interference effects can be automatically taken into account by using a wind-tunnel model with removable wing, fuselage, nacelles, and tail surfaces. The *increase of drag* resulting from the addition of each part can then be measured. Average values of the drag coefficients *based upon the wing area S* for various components of a typical pursuit airplane are listed in Table IV.

The total drag of the wing of any airplane may be evaluated through reference to the appropriate characteristic curves for the section employed as discussed in Chap. 6. Values from the characteristic curves should be

corrected for aspect ratio and, if possible, for scale effect to permit accurate application to design problems. In using the characteristic curves of an airfoil for the determination of C_D, either the angle of attack or C_L must be known. For any given speed, the value of C_L can usually be calculated, since for level flight the total lift of the wings is very closely equal to the weight of the airplane. That is,

$$L = W = C_L \frac{\rho}{2} S V^2$$

and

$$C_L = \frac{2W}{\rho S V^2} \tag{7.6}$$

TABLE IV.—DRAG COEFFICIENTS OF THE COMPONENT PARTS OF A TYPICAL PURSUIT AIRPLANE*

Part	Description	C_D based on wing area, S
Fuselage.	Well-streamlined for liquid-cooled engine, without pilot's enclosure	0.0045
Pilot's canopy.	Low, well-rounded	0.0002
Cooling ducts.	For engine and oil cooling	0.0009
Tail.	Single vertical surface	0.0018

* *Courtesy of Bell Aircraft Corporation.*

PROBLEMS

1. The thickness of the laminar boundary layer of a flat plate exposed to an air stream of 120 m.p.h. is 0.10 in. at a distance of 3 ft. behind the leading edge. Calculate the boundary layer thickness at distances of 1, 2, 4, and 8 ft. from the leading edge.

2. A model wing of N.A.C.A. 23012 profile, 1-ft. chord length, and 6-ft. span is tested in a 100-m.p.h. air stream. Using the characteristic curves of Fig. 7.13, compare the minimum drag of the wing with (*a*) the drag of a flat plate of the same over-all dimensions and laminar boundary layer flow, that is, $A_w = 2S$; (*b*) the drag of a flat plate of the same dimensions and turbulent boundary layer flow. (Neglect the scale effect on the minimum drag coefficient of the airfoil.)

3. The coefficient of drag of a smooth 5-in. sphere reached a value of 0.3 at an air speed of 60 m.p.h. in a certain atmospheric wind tunnel. Determine the percentage of turbulence of this air stream.

4. A 5-in. sphere weighing 6 lb. is dropped from an airplane. Assuming a value of $C_D = 0.2$ and standard sea-level atmospheric conditions, what is the terminal (final) velocity of the sphere?

5. A directional antenna loop of 20 in. mean diameter has an elliptical section of ¼ in. (radially) by 2 in. Referring to the curves of Fig. 7.10, what is the drag of this loop at an air speed of 300 m.p.h.?

6. A pilot's windshield consists of a flat plate of glass 18 in. wide by 8 in. high. Calculate the drag and the horsepower consumed by this windshield at an air speed of 120 m.p.h. If a curved plate is used similar to item 5 of Table III for a windshield of the same projected area, what are the resultant drag and the horsepower?

7. In the design of a private airplane, a landing speed of 30 m.p.h. and a cruising speed of 120 m.p.h. are required. The designer desires an airfoil with a high $C_{L_{\text{max.}}}$ to meet the low landing speed and a low value of $C_{D_{\text{min.}}}$ to provide the high cruising speed. The ratio $C_{L_{\text{max.}}}/C_{D_{\text{min.}}}$ should therefore be as high as possible. Using the curves of Fig. 7.12 for an N.A.C.A. 0015 airfoil of 3.5-ft. chord, calculate the value of this ratio. If this ratio were obtained from characteristic curves corresponding to a test R of 8,000,000 without regard to scale-effect correction, what would be its percentage error?

8. A single-engined low-wing monoplane equipped with an N.A.C.A. 23012 wing of 30-ft. span and 5-ft. average chord weighs 2,000 lb. Using average drag values from Table IV, compute the total drag and the horsepower required corresponding to a cruising speed of 150 m.p.h. (Disregard scale effect.)

9. If the airplane of Prob. 8 were equipped with an N.A.C.A. 23012 wing of 35-ft. span and 4-ft. chord, calculate the total drag and the horsepower required at a cruising speed of 150 m.p.h. (Disregard scale effect.)

CHAPTER 8

COMPRESSIBILITY

As aircraft and propeller-tip speeds increase, the usual form of Bernoulli's equation falls increasingly into error, owing to its underlying assumption of constant air density. Especially is this true when the local velocity over an airplane or its propeller equals or exceeds the velocity of sound; in this event the formation of a shock wave is extremely likely, which invalidates Bernoulli's equation and seriously modifies the aerodynamic coefficients.

Modification of Bernoulli's Equation for Compressible Flow.—When air changes in velocity and pressure in passing over an immersed object, the mass density of the air also changes, although in most practical problems the error introduced by assuming constant density remains small. Only when high velocities are involved does a more complicated analysis become necessary to take into account the change of density with pressure.

Starting out with Bernoulli's equation for an incompressible fluid,

$$p + \frac{\rho}{2} V^2 = \text{constant} \tag{8.1}$$

or

$$\frac{p}{\rho} + \frac{V^2}{2} = \text{another constant} \tag{8.2}$$

Equation (8.1) or its equivalent, Eq. (8.2), was derived for a fluid of constant density (Chap. 2). Hence, Eq. (8.2) may be expressed in differential form by differentiation with ρ considered constant:

$$\frac{dp}{\rho} + V dV = 0 \tag{8.3}$$

This differential equation is directly applicable to a *compressible* fluid flowing through a stream tube provided that ρ is considered variable. Integration between any two sections of the stream tube may then be accomplished if the relation between ρ and one or both of the other variables is known. If the fluid in the stream tube does not gain or lose energy from outside influences, the adiabatic law may be used to establish this relation,

$$pv^k = \text{constant}$$

where v is the specific volume of the compressible fluid in cubic feet per pound and k is the ratio between the specific heats at constant pressure and constant volume ($k = 1.4$ for air). For any two sections of the stream tube

$$p_1 v_1^k = pv^k$$

and, since v is the reciprocal of the weight density w and $w = \rho g$,

$$\frac{p_1}{p} = \left(\frac{v}{v_1}\right)^k = \left(\frac{w_1}{w}\right)^k = \left(\frac{\rho_1 g}{\rho g}\right)^k = \left(\frac{\rho_1}{\rho}\right)^k$$

so that

$$\rho = \left(\frac{p}{p_1}\right)^{1/k} \rho_1$$

Substituting this expression for ρ in Eq. (8.3) and integrating between section 1 of the stream tube and any other section, section 2,

$$\int_{p_1}^{p_2} \frac{p_1^{1/k}}{\rho_1} p^{-1/k}\, dp + \int_{V_1}^{V_2} V dV = 0$$

As a consequence of the adiabatic law, it may readily be seen that the ratio $p_1^{1/k}/\rho_1$ is constant. The integration therefore becomes

$$\frac{p_1}{\rho_1}\left(\frac{k}{k-1}\right)\left[\left(\frac{p_2}{p_1}\right)^{\frac{k-1}{k}} - 1\right] + \frac{V_2^2 - V_1^2}{2} = 0$$

This equation corresponds to Bernoulli's equation for an adiabatic change of state. Solving for p_2,

$$p_2 = p_1\left[1 + \frac{\rho_1}{p_1}\left(\frac{V_1^2 - V_2^2}{2}\right)\left(\frac{k-1}{k}\right)\right]^{\frac{k}{k-1}} \tag{8.4}$$

Expanding the expression in brackets with the binomial theorem,

$$p_2 = p_1\left[1 + \frac{\rho_1}{p_1}\left(\frac{V_1^2 - V_2^2}{2}\right) + \frac{1}{2k}\left[\frac{\rho_1}{p_1}\left(\frac{V_1^2 - V_2^2}{2}\right)^2 + \cdots\right]\right.$$

and, therefore,

$$p_2 - p_1 = \frac{\rho_1}{2}(V_1^2 - V_2^2)\left(1 + \frac{\rho_1(V_1^2 - V_2^2)}{4kp_1}\cdots\right) \tag{8.5}$$

It may be noted that the first term of the series on the right side of Eq. (8.5) together with its left side represents the incompressible form of Bernoulli's equation. The effect of compressibility on the pressure difference can consequently be obtained very closely by evaluating the term $\rho_1 \frac{(V_1^2 - V_2^2)}{4kp_1}$. (Since the series converges rapidly, the remaining terms are relatively small.)

The application of Eq. (8.5) to a pitot-static tube results in some simplification since V_2, the velocity at the stagnation point, equals zero. Introducing the velocity of sound, $C = \sqrt{kp/\rho}$ (Chap. 3), letting p_t equal the pressure at the stagnation point, and dropping the subscripts of the pressure, velocity, and density of the free stream, Eq. (8.5) becomes

$$p_t - p = \frac{\rho V^2}{2}\left(1 + \frac{V^2}{4C^2}\cdots\right) \tag{8.6}$$

The ratio $\frac{V}{C} = \frac{\text{velocity of the undisturbed flow}}{\text{velocity of sound}}$ is of considerable significance in high-velocity flow since it is proportional to the ratio $\frac{\text{inertia force}}{\text{elastic force}}$ in the fluid. It therefore serves as a criterion of similarity for high-velocity

flow just as Reynolds number, $\frac{\text{inertia force}}{\text{viscous force}}$, serves for low-velocity flow. This ratio V/C is known as the "Mach number" and is commonly designated by the symbol M. In terms of M, Eq. (8.6) may be written

$$p_t - p = \rho \frac{V^2}{2}\left(1 + \frac{M^2}{4} \cdots\right)$$

Solving for the velocity of flow and neglecting the terms of the series beyond $M^2/4$

$$V = \frac{\sqrt{2(p_t - p)/\rho}}{\sqrt{1 + M^2/4}} \tag{8.7}$$

The numerator of the right side of this equation represents the velocity of flow as calculated for a pitot-static tube in an incompressible fluid (Chap. 2). Hence the "correction for compressibility" for a pitot-static tube in a compressible fluid is given by the expression $1/\sqrt{1 + M^2/4}$. The correction reaches 1 per cent at a speed of approximately 215 m.p.h.

Compressible Flow around an Immersed Body.—In the preceding discussion an expression for the flow of a compressible fluid through a stream tube was developed and then applied to a pitot-static tube. The general treatment of the three-dimensional flow of a compressible fluid around an immersed body may be approached in a similar manner. Bernoulli's equation and the continuity equation may be applied to a frictionless fluid in adiabatic flow to give a differential equation which relates the velocity components of the flow with position in the flow pattern and with Mach number. Some simplification of this equation is generally required in order to reach a satisfactory solution. Such a simplification is proposed in the Glauert-Prandtl approach wherein the immersed body is considered long and slender so that it produces only small deviations from the undisturbed flow. With this assumption, the equation for compressible flow may be placed in the same form as the

corresponding equation for incompressible flow to facilitate comparison.

The comparison shows that a body in compressible flow is equivalent to a thicker body in incompressible flow, the ratio between the two thicknesses being equal to the factor $\sqrt{1 - M^2}$. Thus the streamlines in compressible flow deviate farther from the surface of an immersed body than those of an incompressible flow, as shown in Fig. 8.1.

In the case of an airfoil in compressible flow the thickness, camber, and angle of attack each increase in the ratio $1:\sqrt{1 - M^2}$ for the equivalent incompressible flow. Hence the lift coefficient of an airfoil at a high Mach number C_{L_M}

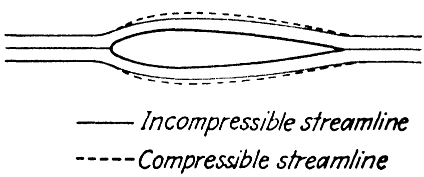

FIG. 8.1.—Streamlines in incompressible and compressible flow.

may be related to the incompressible lift coefficient, or for practical purposes the low-speed lift coefficient, C_{L_0}, by the equation

$$C_{L_M} = \frac{C_{L_0}}{\sqrt{1 - M^2}} \tag{8.8}$$

As discussed in the next article, serious difficulties may arise in the operation of an airplane whenever the maximum local velocity over any part of it equals or exceeds the speed of sound. For this reason the Mach number of the free stream corresponding to the attainment of the speed of sound by the maximum local velocity in the flow over an immersed body is known as the "critical Mach number." According to Bernoulli's equation, the maximum local velocity occurs where the pressure in the flow pattern reaches a minimum. The minimum pressure may conveniently be expressed in dimensionless form as a "pressure

coefficient" $P_{\text{min.}}$ such that

$$P_{\text{min.}} = \frac{p_l - p_0}{q_0}$$

where p_l = minimum local pressure in the flow pattern
p_0 = pressure of the undisturbed stream
q_0 = dynamic pressure $\frac{\rho V_0^2}{2}$ of the undisturbed stream

The maximum negative value of the pressure coefficient may be related to the critical Mach number by means of the Glauert-Prandtl approximation. However, von Kármán[1]

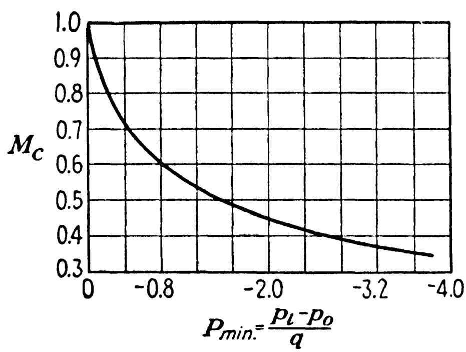

FIG. 8.2.—Variation of critical Mach number with low-speed pressure coefficient.

and Tsien have developed a relation which is shown to check experimental results more closely. The variation of critical Mach number with the maximum negative value of the pressure coefficient of Fig. 8.2 is based on this relation. The pressure coefficient for use with this curve may be obtained from pressure-distribution diagrams which are plotted from wind-tunnel tests run at low Mach numbers.

Such a pressure-distribution diagram for an airfoil at a moderately high angle of attack is shown in Fig. 8.3. The high suction peak on the upper surface near the leading edge is apparent. For higher angles of attack the pressure peak would rise still higher. For a typical airfoil near the

[1] THEODORE VON KÁRMÁN, Compressibility Effects in Aerodynamics, *Journal of the Aeronautical Sciences*, July, 1941.

stall, the critical Mach number may correspond to air speeds as low as 200 m.p.h. Difficulties due to shock waves are consequently not confined to high-speed flight.

Shock Waves.—The velocities at various points in the flow over the upper surface of an airfoil are not commonly greater than the speed of sound, although these local velocities greatly exceed the undisturbed approach velocity, particularly near the leading edge. Under these conditions, a change in pressure at any point is felt throughout the flow pattern; such a pressure change is propagated in all

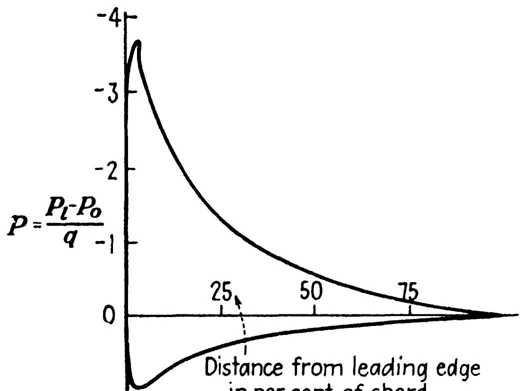

FIG. 8.3.—Pressure distribution of an N.A.C.A. 23012 airfoil at an angle of attack of 12 deg.

directions from its point of origin at the normal speed of travel of a pressure wave through air—the speed of sound.

If, however, the undisturbed velocity of flow is increased until the local velocity over a portion of the top surface equals the velocity of sound, a change in pressure near the trailing edge of the airfoil propagates a pressure wave forward only as far as the downstream boundary of the region of sonic velocity. Here the forward velocity of propagation remains in equilibrium with the backward velocity of flow. Such a wave front may then become a surface of separation between regions of different pressures and velocities so that the air stream passing through the front

experiences a sudden increase in pressure and drop in velocity. This is accompanied by shock and turbulence resulting in the transformation of a considerable amount of the kinetic energy of flow into unavailable heat energy. The term "shock wave" for this phenomenon is therefore appropriate.

In an investigation conducted by the N.A.C.A.,[1] shock waves were visualized by schlieren photographs which

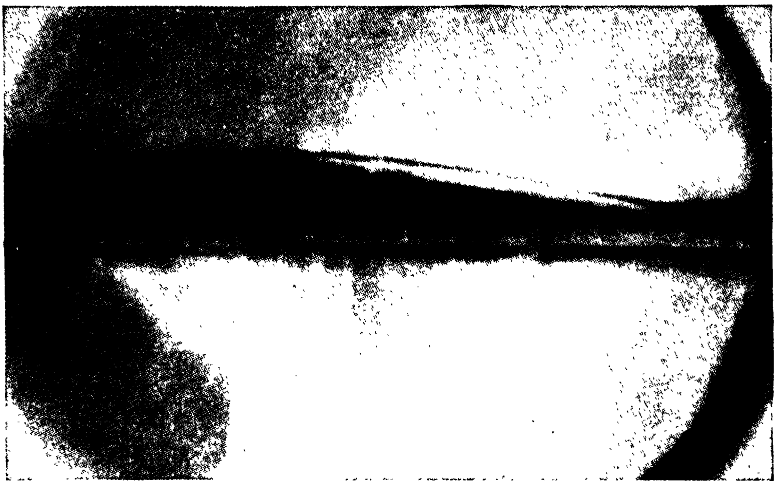

FIG. 8.4.—Schlieren photograph of an N.A.C.A. 4412 airfoil at a Mach number of 0.756 and an angle of attack of −2 deg. (*N.A.C.A Technical Report* 646.)

show variations in air density as changes in light intensity, as described in Chap. 4. One of these photographs is presented in Fig. 8.4 where the pressure disturbances may be seen as lines extending outward from the airfoil in a direction approximately perpendicular to its surface. This and several associated photographs taken at different Mach numbers show a general agreement with theoretical considerations. The shock wave originates near the point in the flow patterns where the local velocity reaches a maximum; then, as the velocity of flow is increased the maxi-

[1] JOHN STACK, W. F. LINDSEY, and ROBERT E. LITTELL, The Compressibility Burble and the Effect of Compressibility on Pressures and Forces Acting on an Airfoil, *N.A.C.A. Technical Report* 646.

mum local velocity rises to a higher value in the supersonic range and the shock disturbance is swept backward to a new position of equilibrium nearer the trailing edge of the airfoil. Shock effects first appear in many of these tests when the maximum local velocity exceeds the speed of sound. This result is to be expected since the speed of sound defines only the lower limiting velocity at which shock waves are possible. Flow at low supersonic speeds may occur without measurable shock effects.

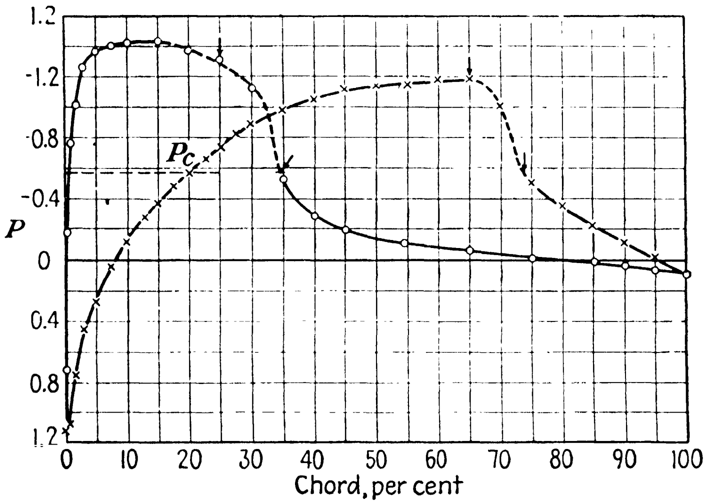

FIG. 8.5.—Pressure distribution for an N.A.C.A. 4412 airfoil at a Mach number of 0.756 and an angle of attack of -2 deg. (*N.A.C.A. Technical Report* 646.)

Pressure-distribution measurements were made under the same conditions of flow as those which prevailed for the schlieren photographs. The pressure-distribution diagram of Fig. 8.5, which corresponds to the photograph of Fig. 8.4, shows a sharp rise in pressure (decrease in negative pressure) on the upper surface of the airfoil in the region of the pressure disturbances. This adverse pressure gradient produces a separation of the flow from the upper surface of the wing which gives rise to a sudden loss of lift in what is generally termed a "shock stall" or, less frequently, a "compressibility burble." The increase in the wake of

the wing resulting from a shock stall will often cause a severe buffeting of the tail surfaces and alter their effectiveness.

The effect of compressibility disturbances on the force and moment coefficients of an N.A.C.A. 4412 airfoil is clearly shown in Fig. 8.6. The disturbances evidently form for this airfoil at a Mach number of the undisturbed flow between 0.6 and 0.8 and give rise to a sharp decrease in the lift coefficient. The drag coefficient experiences an almost

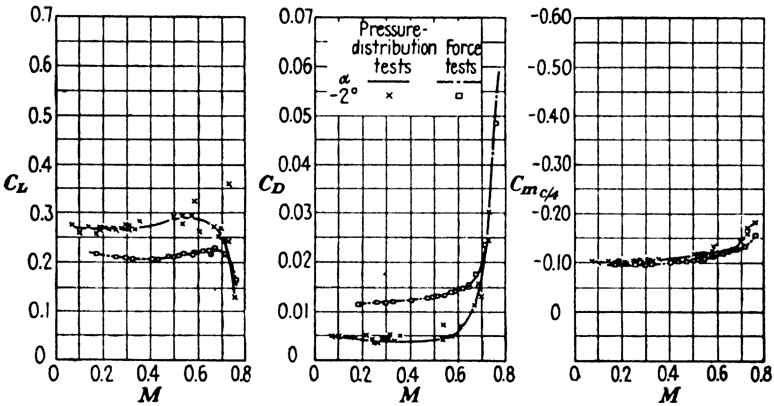

FIG. 8.6.—Variation of force and moment coefficients with Mach number for an N.A.C.A. 4412 airfoil at an angle of attack of −2°. (*N.A.C.A. Technical Report* 646.)

vertical increase to a value of more than five times its low-speed value. The change in the pitching-moment coefficient is less marked and is also of less importance since the pitching moment of the wing is only a small factor in the longitudinal balance of an airplane.

When an airplane experiences a shock stall, the sudden reduction of lift of the wing causes the nose to drop and the airplane goes into a dive. The pilot may meet with serious difficulty in regaining control since the stick forces necessary to restore the airplane to level flight may be excessively large. Dive-recovery flaps have been successfully used to furnish additional lift to a wing after a shock stall to aid in the restoration of control.

Compressibility Effects on Propellers.—The design and operation of aircraft propellers is limited by the desirability of maintaining the local velocity over the tips of the blades less than the velocity of sound for the avoidance of shock waves. The local velocity at the propeller tip depends on the air speed of the airplane, the rotational speed and diameter of the propeller, and the thickness and angle of attack of the tip airfoil section. The usual design procedure is to use a very thin airfoil section at the tip and a small angle of attack.

The increased drag and decreased lift of the tip sections caused by the appearance of a shock wave are, of course, reflected in lowered thrust and efficiency for the complete propeller. The shock effects add also to the noise and vibration produced by the propeller.

A series of tests conducted by the N.A.C.A. on full-scale propellers showed an initial drop in propulsive efficiency at a Mach number between 0.5 and 0.7. At a Mach number of 0.8, the propellers tested showed a loss of about 20 per cent of the thrust power.[1]

Reduction gears are generally used in aircraft engines of the higher horsepowers to permit the operation of both engine and propeller at their optimum speeds.

PROBLEMS

1. In a wind tunnel operating at a test velocity of 200 m.p.h. with standard atmospheric conditions in the working section, what is the compressibility correction to the pressure difference between the working section and the entrance to the converging section? The velocity at the entrance section is 45 m.p.h. at this tunnel speed. What is the approximate error in the velocity as calculated from this pressure difference by the incompressible form of Bernoulli's equation?

2. The velocity of sound in a gas as developed in Chap. 3 may be expressed $C = \sqrt{\frac{kp}{\rho}}$. Show that the velocity of sound in *air* may be expressed as $C = 49.2\sqrt{T}$.

[1] DAVID BIERMAN and EDWIN HARTMAN, The Effect of Compressibility on Eight Full-scale Propellers Operating in the Take-off and Climbing Range, *N.A.C.A. Technical Report* 639.

3. The differential pressure reading of a standard pitot-static tube is 4.43 in. Hg when exposed to the air stream in the test section of a wind tunnel. Calculate the air speed in miles per hour for both compressible and incompressible flows based on (*a*) standard sea-level atmospheric conditions, (*b*) standard atmospheric conditions at 20,000 ft. altitude.

4. An airplane weighing 20,000 lb. with a wing loading of 30 lb. per sq. ft. cruises at 300 m.p.h. at 20,000 ft. altitude. What would be its equivalent lift coefficient as measured in a relatively low-speed wind-tunnel test (not considering scale effect)?

5. Using the low-speed pressure distribution of Fig. 8.3, determine the critical velocity at which a shock wave would form on an N.A.C.A. 23012 airfoil at an angle of attack of 12 deg. Where would the shock wave originate in percentage of chord from the leading edge?

CHAPTER 9

PROPERTIES OF AIRFOIL SECTIONS

Evolution of Airfoil Shapes.—Present-day airfoils are the product of a long period of development which has been mostly experimental in character. Airfoil sections representing several steps in this development together with the approximate dates of their introduction are shown in Fig. 9.1. The flexibility of the thin profile used by the Wright brothers was put to good use; the pilot of the Wright airplane could maintain lateral control through an increase in the curvature of the wing by pulling downward on the trailing edge on one side of the fuselage or the other. Later sections like the early R.A.F. design, which was extensively used during World War I, show a trend toward greater thickness contributing to structural strength and rigidity. The two Göttingen sections carry this trend still further and, in addition, are of especial interest because they conform to theoretical Joukowsky profiles with lift and lift distributions which can be predicted by mathematical methods. Joukowsky airfoils, however, show no marked aerodynamic advantage over airfoils developed by the cut-and-try process and present some structural problems, particularly in the construction of their thin trailing edges. The Clark Y section has proved very popular right up to the present time because of its good aerodynamic qualities and its flat lower surface, the latter contributing to manufacturing convenience, particularly for propellers. The C-62 is a specialized, racing airfoil which has extremely low drag at the angle of attack where its sharp nose is pointed directly into the relative wind and high drag for other positions. The M-6 is of interest because its profile is turned up or *reflexed* a very small but important amount

near the trailing edge. This gives the airfoil more favorable pitching-moment characteristics, as will be discussed later in this chapter.

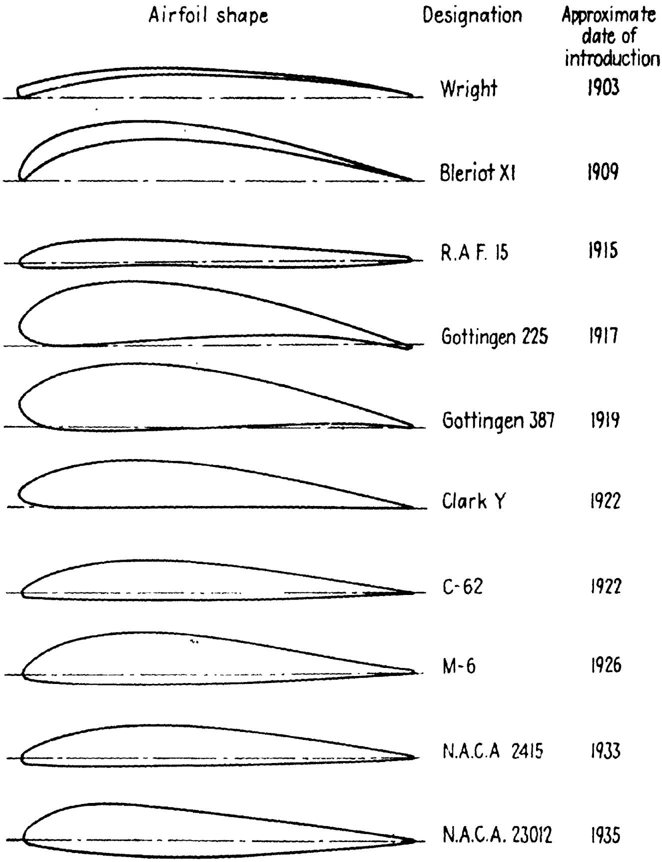

FIG. 9.1.—Historical development of airfoil sections.

Systematic Families of Airfoils.—In 1933 the characteristics of a series of related airfoils were published by the N.A.C.A. as measured in the variable-density tunnel at Langley Field. The profiles of the airfoils were defined in terms of their maximum thickness and the shape of their

mean lines drawn halfway between their upper and lower surfaces. The basic thickness variation of airfoils of this family was patterned after airfoils of proved aerodynamic efficiency, giving the profile of Fig. 9.2. For convenience, an equation was developed to express the basic ordinate y of the airfoil profile in terms of the distance from the leading edge x. The ordinates of thicker or thinner airfoils were then derived by multiplying each basic ordinate by a constant factor.

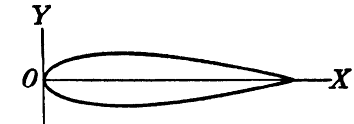

$$\pm Y = 0.29690\sqrt{X} - 0.12600X - 0.35160X^2 + 0.28430X^3 - 0.10150X^4$$

FIG. 9.2.—Basic thickness variation of the N.A.C.A. four-digit airfoil family.

The shape of the mean line of airfoils of this family is specified by giving the value of the *maximum* departure of the mean line from the chord line, known as the maximum "camber," together with its position along the chord line, as shown in Fig. 9.3. The airfoil shape of Fig. 9.2,

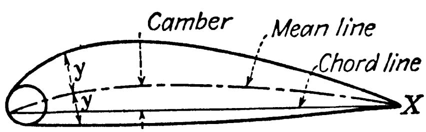

FIG. 9.3.—Cambered airfoil of the N.A.C.A. four-digit family.

since it has zero camber, is known as a "symmetrical airfoil."

Airfoils of this family are designated by numbers of four digits; the first indicating the *camber* of the mean line in per cent of chord; the second, the *position of the maximum camber* in tenths of the chord; and the third and fourth, the *maximum thickness* in per cent of the chord. Thus the N.A.C.A. 0015 airfoil represents a symmetrical airfoil of 15 per cent maximum thickness; and the N.A.C.A. 4221 airfoil has a maximum camber of 4 per cent of the chord, located two-tenths of the chord from the leading edge and has a maximum thickness of 21 per cent of the chord.

Subsequent investigations to the four-digit tests indi-

cated the advisability of moving the camber of an airfoil farther forward. A family of airfoils with forward camber was accordingly tested and the results presented in

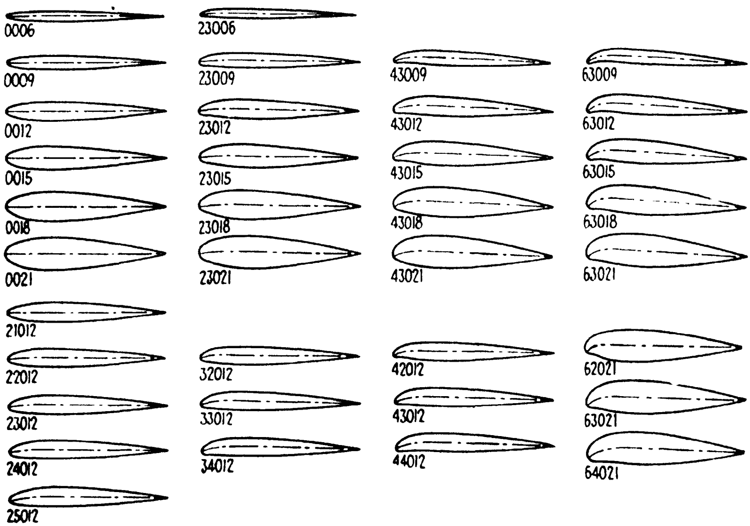

FIG. 9.4.—Airfoil profiles of the N.A.C.A. five-digit family. (*N.A.C.A. Technical Report* 610.)

N.A.C.A. Technical Report 610. The airfoils of this family are designated by a number of five digits; the first indicating, as in the four-digit family, the *camber* in per cent of chord; the second and third numbers, the *position of the camber* as approximately *double* the percentage of the chord length from the leading edge; and the fourth and fifth digits, the *maximum thickness* in per cent of chord. The airfoils composing the five-digit family are shown in Fig. 9.4.

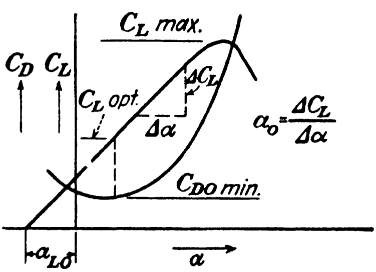

FIG. 9.5.—Airfoil characteristics.

In presenting the test results of airfoils in a form convenient for the designer both curves and tabulated values

of the more important characteristics are used, the tabulated values corresponding to an infinite aspect ratio. Among the characteristics listed are the following (Fig. 9.5):

$C_{L_{max.}}$ = the maximum value of the lift coefficient
α_{L_0} = angle of attack for zero lift
a_0 = the slope of the straight portion of the lift versus α curve
$C_{L_{opt.}}$ = the value of the lift coefficient corresponding to minimum profile drag
$C_{D_{0min.}}$ = the minimum profile drag coefficient

The location of the aerodynamic center with reference to the quarter-chord point.

$C_{M_{ac}}$ = the value of the pitching-moment coefficient about the aerodynamic center

Airfoil Characteristics of a Thin Plate.—Although a thin plate does not make an efficient airfoil shape, its properties may be deduced through ideal fluid theory to guide the

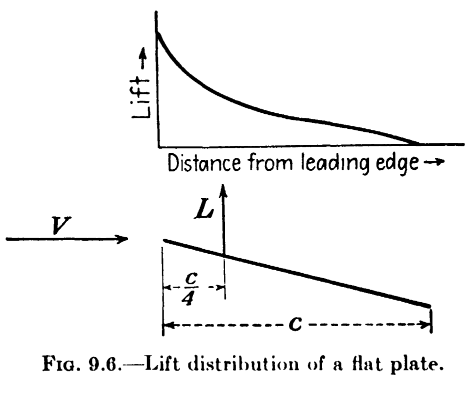

FIG. 9.6.—Lift distribution of a flat plate.

aerodynamicist in the understanding of more practical airfoils. A few of the more significant results of thin-plate theory will accordingly be presented here.

A flat plate inclined at a small angle to a relative air stream forms the simplest type of lift-producing element. As shown in Fig. 9.6, the lift per unit area is greatest near

the leading edge of the plate, the resultant lift force acting through the quarter-chord point at all angles of attack. Consequently, the pitching-moment coefficient C_M, taken about the quarter-chord point, must always equal zero. For small angles of attack the lift coefficient may be related to the angle of attack of the plate *in radians* by

$$C_L = 2\pi\alpha$$

This expression yields the same lift-curve slope as the theoretical Joukowsky profile,

$$a_0 = \frac{dC_L}{d\alpha} = \frac{C_L}{\alpha} = 2\pi$$

For a plate curved in the form of a circular arc and exposed to an air stream parallel to its chord the resultant lift force acts, for reasons of symmetry, at the mid-point of its chord, as shown in Fig. 9.7. If the plate is rotated

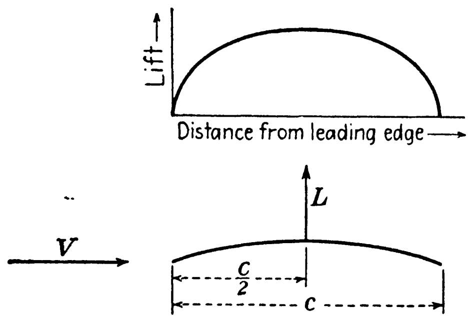

FIG. 9.7.—Lift distribution of a circular-arc plate.

to a positive angle of attack α, the resultant lift distribution represents a superposition of the constant lift distribution of a circular-arc plate at zero angle of attack on the lift distribution of a flat plate at the angle of attack α (Fig. 9.8). In this case, the point where the resultant force acts on the airfoil, the "center of pressure," lies between the center of the chord and the quarter-chord point and moves closer to the quarter-chord point as the angle of attack is increased. The pitching moment of the circular-arc airfoil about an

axis through the quarter-chord point remains constant at all positive angles of attack. This is true because the flat-plate lift component has a zero moment arm about this axis which leaves only the constant contribution of the circular-arc lift force to the pitching moment. The quarter-chord point, in this case, may be termed the

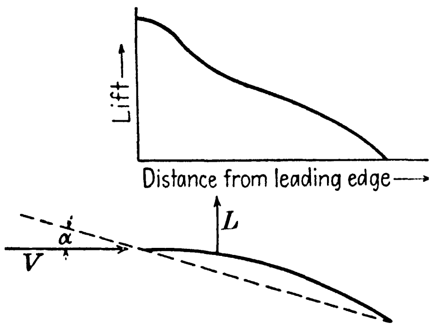

FIG. 9.8.—Lift distribution for a circular-arc plate at a positive angle of attack.

"aerodynamic center" of the airfoil because it represents the point about which the pitching moment remains constant at all positive angles of attack.

When a thin plate of S form is exposed to an air stream at zero angle of attack, a lift distribution like that of Fig. 9.9 results. If an S-shaped plate is superposed on one of

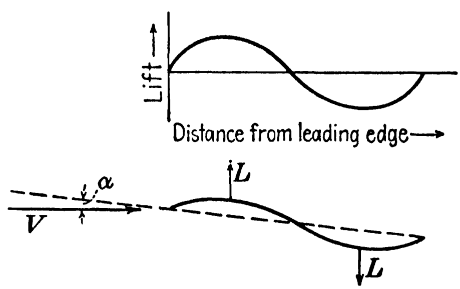

FIG. 9.9.—Lift distribution for an S-shaped plate at a positive angle of attack.

circular-arc form, the lift distribution curves are likewise superposed. This has the effect of moving forward the center of the pressure at zero angle of attack, since the

S-shaped plate contributes to the total lift over the leading half of the chord length and detracts over the trailing half. By choosing S-shaped and circular-arc plates of the proper relative proportions the center of pressure of the resultant plate at zero angle of attack may be shifted to the quarter-chord point where it will remain as the angle of attack is increased. The characteristic "reflexed" shape of such a plate is illustrated in Fig. 9.10.

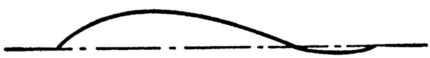

FIG. 9.10.—Reflexed plate with a fixed center of pressure at all angles of attack.

Many of the foregoing considerations find direct application to conventional airfoil sections. Thus we find that the lift coefficients of most airfoils are very nearly directly proportional to the angle of attack, the slope of the lift curve falling within 81 to 95 per cent of the theoretical value of 2π—the lower percentages corresponding to the thicker airfoils; and that for all but reflexed airfoils the center of pressure moves forward toward the quarter-chord point as the angle of attack is increased. Hence the pitching moment of a conventional airfoil about its quarter-chord point must act negatively, that is, in such a direction as to depress the leading edge of the airfoil, at all angles of attack. On the other hand, airfoils with a reflexed mean line may be designed to have zero pitching moment about the quarter-chord point or, by increasing the amount of reversed curvature, may be made to exert a positive pitching moment at all angles of attack.

Discussion of Airfoil Characteristics.—The maximum value of the lift coefficient, $C_{L_{max.}}$, is very responsive to changes in airfoil thickness. The optimum thickness decreases for airfoils of higher camber, varying between a thickness of 14 per cent of the chord for the symmetrical airfoils and about 8 per cent for airfoils with 6 per cent camber.

The angle of zero lift, α_{L_0}, increases negatively with increasing camber from 0 deg. for the symmetrical sections up to 7 deg. for the N.A.C.A. 6712 section.

The value of the lift corresponding to the minimum drag $C_{L_{opt.}}$ increases with the larger cambers. Thickness has an important effect on $C_{L_{opt.}}$, its value decreasing with increasing thickness.

The minimum drag coefficient $C_{D_{0min.}}$ increases with thickness and to a much lesser extent with camber.

As predicted by thin airfoil theory, tests on airfoils with reflexed mean lines yield much lower values of the pitching-moment coefficient C_M than do conventional airfoils. The values of $C_{L_{max.}}$ of the reflexed airfoils are so reduced, however, as to more than offset the improvement in the moment coefficient.

The aerodynamic center is generally located slightly ahead of and above its theoretical position at the quarter-chord point varying from about 22 to 25 per cent of the chord from the leading edge.

Selection of an Airfoil.—The value of $C_{L_{max.}}$ is an important criterion in the selection of an airfoil because of its direct bearing on stalling and landing speeds. The effect of the possible addition of flaps or other high-lift devices should be studied in its relation to the maximum lift coefficient. Care should be exercised to determine the proper value of $C_{L_{max.}}$ corresponding to the Reynolds number of the design landing speed.

The ratio of the lift and drag coefficients is often taken as an index of general airfoil efficiency. The maximum lift coefficient is usually divided by the *minimum* drag coefficient or the drag coefficient corresponding to some important flight attitude, such as that of maximum speed or maximum rate of climb, to provide an important criterion in the comparison of airfoil sections.

The value of C_M should be considered in the selection of an airfoil in its relation to airplane stability. If high-lift devices are employed with the airfoil, the coefficient of the

combination should be investigated. Low values of C_M with little variation with angle of attack are desirable.

Structural considerations may lead to a thicker section than aerodynamic considerations alone since thicker sections may make possible a lighter structure to withstand the external wing loads. Successful field experience with an airfoil section is often an important factor in its selection.

PROBLEMS

1. Calculate the basic ordinate (Fig. 9.2) of the N.A.C.A. four-digit airfoil at the 10 per cent chord station.

2. Compare the characteristics of the following airfoils as given in Table III of *N.A.C.A. Technical Report* 669: N.A.C.A. 0015, N.A.C.A. 2412, N.A.C.A. 23012.

3. An airplane with a wing of 4-ft. average chord has a landing speed of 40 m.p.h. and cruises at the angle of attack for minimum drag at a Reynolds number of about 8,000,000. If the airfoil section is N.A.C.A. 0015, calculate the value of $C_{L_{\text{max.}}}/C_{D_{\text{min.}}}$. Use the scale-effect curves of Fig. 7.12 in obtaining the proper value of $C_{L_{\text{max.}}}$.

4. Derive a relation for the pitching-moment coefficient of a thin flat plate about an axis through its leading edge in terms of the lift coefficient of the plate. What is the value of C_M for an angle of attack of 10 deg.?

CHAPTER 10

HIGH-LIFT DEVICES

The high performance of modern military and commercial airplanes has depended in large measure on the use of higher $\dfrac{\text{weight}}{\text{wing area}}$ ratios, that is, higher *wing loadings*, than in earlier designs. High wing loadings contribute to aerodynamic and structural efficiency but lead also to high take-off and landing speeds, as can be seen by a rearrangement of the fundamental lift equation,

$$L = W = C_L \frac{\rho}{2} SV^2$$

Solving for V,

$$V = \sqrt{\frac{2W}{C_L\rho S}} = \sqrt{\frac{2}{C_L\rho}} \times \sqrt{\frac{W}{S}}$$

$$= \sqrt{\frac{2}{C_L\rho}} \times \sqrt{\text{wing loading}} \qquad (10.1)$$

The flying speed V of a given airplane evidently reaches a minimum value suitable for landing or take-off when the lift coefficient assumes its maximum value $C_{L_{\text{max.}}}$. If $C_{L_{\text{max.}}}$ is increased by auxiliary devices, the landing and take-off speeds will be correspondingly reduced.

The high-lift devices used for increasing $C_{L_{\text{max.}}}$ fall into two general classes: those located near the leading edge of the wing and those located near its trailing edge.

Leading-edge Devices.—As discussed in Chap. 7, a slot built into the leading edge of a wing (Fig. 10.1) will improve the air flow on the upper surface of the wing at high angles of attack. This is accomplished by a high-velocity jet of air which passes through the slot from the high-pressure area beneath the wing to the region of subatmospheric pressure above the wing. The jet impinges on the bound-

ary layer of the upper surface, thereby transferring enough energy to the boundary layer flow to postpone separation to a higher angle of attack. The effectiveness of a slot is indicated by the comparative lift curves of Fig. 10.2.

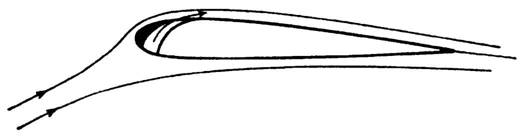

FIG. 10.1.—Wing with fixed slot.

The fixed slot suffers from two serious disadvantages: a higher landing gear is required to accommodate the

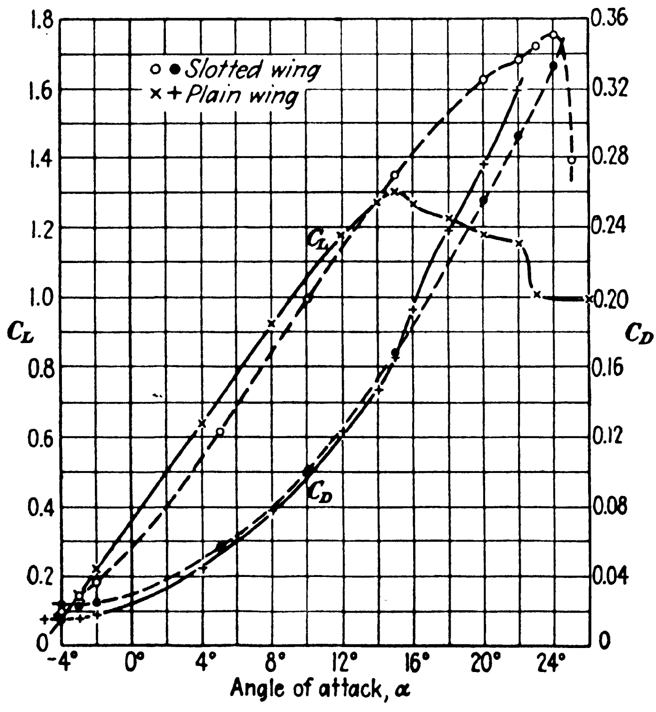

FIG. 10.2.—Characteristics of a Clark Y wing with a fixed slot. (*N.A.C.A. Technical Report* 407.)

increased angle of attack at the burble point, and the slot produces high drag at low angles of attack. An effort was made by the N.A.C.A. to reduce the drag by locating the

slot between regions on the upper and underside of the airfoil which were at equal pressures for low angles of attack. This succeeded in eliminating flow through the slot at low angles of attack, but the drag remained high

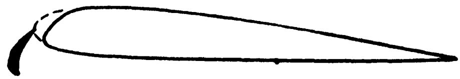

FIG. 10.3.—Wing with automatic slot.

owing to the effect of the discontinuities at the slot openings in producing turbulent flow in the boundary layer of the wing.

FIG. 10.4.—Wing with auxiliary airfoil at the leading edge.

A solution to the high-drag problem of fixed slots is to make the portion of the wing forward of the slot—the *slat*—movable so that the slot can be closed at low angles of attack, as shown in Fig. 10.3. This can be accomplished automatically since the pressures acting on the slat are positive at low angles of attack and negative at angles of attack near the stall.

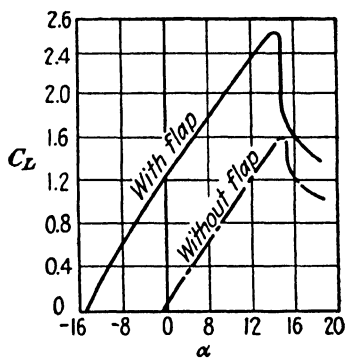

FIG. 10.5.—Effect of a typical flap on the lift coefficient of a wing.

An auxiliary airfoil fixed in a position ahead of and above the wing of an airplane (Fig. 10.4) may give an increase of $C_{L_{max.}}$ of as much as 40 per cent over that of the wing alone. However, tests show that the auxiliary airfoil assumes a relatively large proportion of the total load which is difficult to sustain with an efficient structure.

Plain and Split Flaps.—The displacement of a flap near the trailing edge of an airfoil increases the angle of zero lift

α_{L_0} negatively. This displaces the C_L versus α curve to the left, giving a higher value of $C_{L_{max.}}$ at the burble point (Fig. 10.5). Various types of flaps are used to accomplish this purpose.

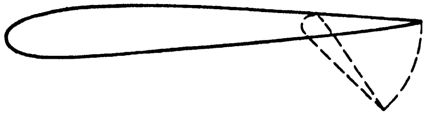

FIG. 10.6.—Wing with plain flap.

The *plain* flap of Fig. 10.6 will increase the $C_{L_{max.}}$ of the wing alone by as much as 0.85, if designed with very small clearance between the leading edge of the flap and the airfoil, or if a rubber diaphragm is used to seal this crack. If only a small gap is left open, the $C_{L_{max.}}$ *increment* will be much reduced, as shown by the curves of Fig. 10.7. High hinge moments are usual with this type of flap since it is generally impractical to locate the hinge line far enough aft on the flap to balance the moments of the air loads on the flap and still maintain the required small clearance with the wing.

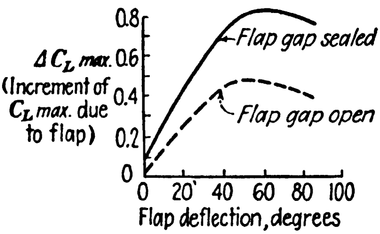

FIG. 10.7.—Influence of a gap at the leading edge of a flap.

The *split* flap of Fig. 10.8 is in most general use in modern airplanes, mainly because of its simplicity of construction.

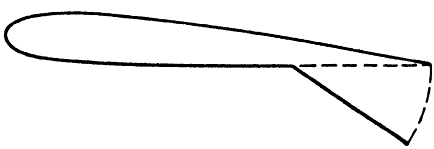

FIG. 10.8.—Wing with a split flap.

Here again, no gap at its juncture with the wing is required for most effective operation.

Slotted Flaps.—Although an ordinary gap at the leading edge will reduce the effectiveness of a plain or split flap, the

use of a *properly designed* slot between an airfoil and a flap is advantageous (Fig. 10.9). Slotted flaps may be designed to give a high lift with a low drag at small flap deflections and the same lift with much greater drag at large flap deflections. This furnishes a convenient means of controlling the steepness of an airplane's glide path; shallow glides may be made with the low-drag flap setting; and steep glides may be made with the high-drag setting. Steep glides are desirable in landing on small fields surrounded by obstacles with the maximum margin of field left for the landing run.

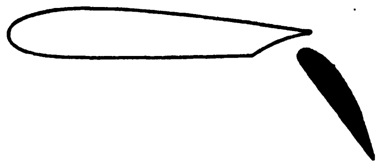

FIG. 10.9.—Wing with a slotted flap in the deflected position.

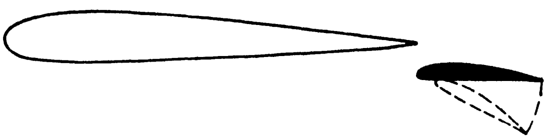

FIG. 10.10.—Wing with external airfoil flap.

The external airfoil flap of Fig. 10.10 has the advantage of contributing to the lift of an airplane at all times as well as functioning as an effective slotted flap when deflected for landing or take-off. Flaps of this kind have been successfully used on German airplanes.

FIG. 10.11.—Fowler flap in a deflected position.

In the Fowler flap of Fig. 10.11, the flap moves backward and rotates downward when deflected. This action not only realizes the benefits of a slotted flap but increases the effective wing surface as well, to give a higher $C_{L_{max}}$

increment than any other flap. The main drawback of the Fowler flap lies in the inherent complexity of its operating linkage.

Table V has been prepared to summarize the characteristics of various high-lift devices. It may be noted that

TABLE V
COMPARISON OF HIGH-LIFT DEVICES
(Applied to an N.A.C.A. 23012 Wing except as noted)

Device	Diagram	$\Delta C_L max$	$C_L max$ at R=3,500,000	Reference
Fixed slot	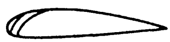	0.45	2.00	T.R. #407
Movable slot	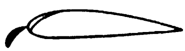	0.54	2.09	T.R. #400
Auxiliary airfoil		0.47	2.02	T.R #472
Plain flap	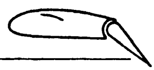	0.75	2.30	T.R. #554
Split flap	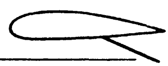	1.00	2.55	T.R. #554
External airfoil		0.78	2.33	T.R. #541
Slotted flap	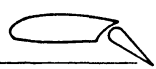	1.10	2.65	T.R. #664
Fowler flap	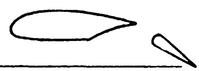	1.25	2.80	T R. #534
Fowler flap and leading-edge slot	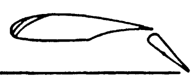	2.08	3.39	T.N. #459
			Clark Y Wing	

the combination of a leading-edge slot and a Fowler flap provides the largest increase in $C_{L_{max.}}$.

Scale Effect of Flaps.—The scale effect of wings equipped with high-lift devices is particularly important since the Reynolds number corresponding to the landing condition is often much lower than that of airfoil and airfoil-flap test data. As shown in Fig. 10.12, the $C_{L_{max.}}$ *increment* con-

tributed by a flap is practically independent of R so that the correct value of $C_{L_{\max.}}$ for an airfoil-flap combination can be obtained by adding the $C_{L_{\max.}}$ increment of the flap

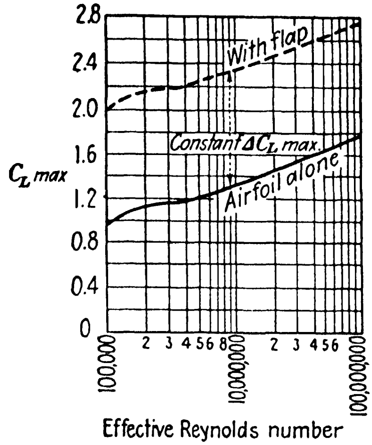

FIG. 10.12.—Scale effect of a typical flap on an N.A.C.A. 23012 wing.

to the value of $C_{L_{\max.}}$ for the basic airfoil at the proper Reynolds number.

PROBLEM

An airplane weighing 1,160 lb. with an N.A.C.A. 23012 wing of 175 sq. ft. of surface is to be fitted with a high-lift device to lower its landing speed. If the average chord of the wing is 5 ft., calculate the *minimum* landing speed of the airplane corresponding to each of the following: (*a*) automatic slot, (*b*) plain flap, (*c*) split flap, (*d*) Fowler flap, (*e*) N.A.C.A. 23012 airfoil alone.

CHAPTER 11

PROPELLER THEORY AND DESIGN

The useful thrust force of a propeller is created by the increase of momentum in a rearward direction of the air passing through its disk of rotation. The increase of momentum is made apparent by the velocity of the propeller "slip stream" with respect to the surrounding air.

The Momentum Theory of Propeller Performance.—In visualizing the operation of a propeller, it is convenient to consider a propeller with no translational velocity which rotates in an advancing column of air, as illustrated in Fig. 11.1. The velocity V_1 of the air far in advance of the propeller, as at section 1 of Fig. 11.1, is then equal in magnitude and opposite in sign to the air speed of the airplane to which the propeller is attached. The air is accelerated to the velocity V_2 at section 2, directly in front of the propeller, by the subatmospheric pressure maintained by the rotation of the propeller. In passing through the propeller to section 3, the pressure of the air is raised to a positive value p_3 without any increase in velocity, so that $V_2 = V_3$. Finally, the positive pressure p_3 accelerates the air until the pressure returns to atmospheric with a relatively high velocity V_4, the final velocity of the slip stream.

The thrust T of such a propeller may be readily computed by means of the fundamental momentum equation,

$$F = T = M\Delta V$$

where

$$M = \rho A_2 V_2 = \rho \frac{\pi d^2}{4} V_2$$

$$\Delta V = V_4 - V_1$$

so that

$$T = \frac{\rho \pi d^2}{4} V_2(V_4 - V_1) \tag{11.1}$$

where d = propeller diameter.

The useful power output P_0 is

$$P_0 = TV_1 = \rho \frac{\pi d^2}{4} V_2(V_4 - V_1)V_1 \qquad (11.2)$$

The power input, P_i, is given by the difference in kinetic energies of the air before and after acceleration by the

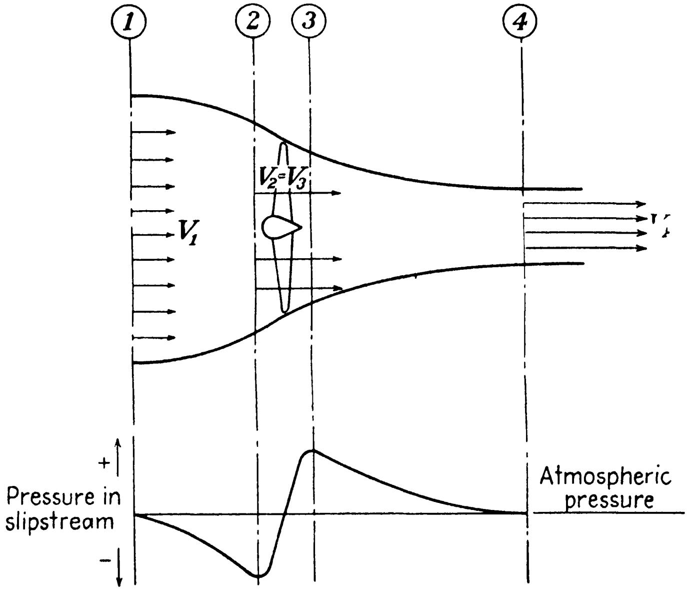

FIG. 11.1.—Variation of velocity and pressure in the slip stream of a propeller.

propeller (assuming no frictional losses), that is,

$$P_i = \tfrac{1}{2}MV_4^2 - \tfrac{1}{2}MV_1^2$$

Reducing and substituting for M,

$$P_i = \frac{\rho}{2} \times \frac{\pi d^2}{4} V_2(V_4^2 - V_1^2)$$

The propeller efficiency η (eta) may be written

$$\eta = \frac{P_0}{P_i} = \frac{\dfrac{\pi d^2}{4} V_2 \rho (V_4 - V_1) V_1}{\dfrac{\pi d^2}{4} \dfrac{\rho}{2} V_2 (V_4^2 - V_1^2)}$$

Simplifying,

$$\eta = \frac{2V_1}{V_1 + V_4} \tag{11.3}$$

Equation 11.3 shows that the efficiency of a propeller may be improved by an increase of the forward speed V_1 and by a reduction of the final velocity of the slip stream V_4 toward its limiting value V_1. But, *for a given thrust* T, it may be seen from Eq. (11.1) that the difference between V_4 and V_1 can be reduced only by a proportionate increase in the propeller diameter or the density of the air. It may be concluded that high air speeds, large propeller diameters, and high values of air density are conducive to increased propeller efficiency.

Propeller diameters are limited in practice by the necessity of maintaining ground clearance with landing gears of reasonable height and by the desirability of maintaining low enough tip speeds to avoid serious compressibility effects.

The foregoing analysis of propeller action might be extended to show that the velocity of flow through the propeller disk is the arithmetic mean of the velocity of the air far in advance of the propeller and the final velocity of the slip stream. That is,

$$V_2 = V_3 = \frac{V_1 + V_4}{2}$$

This simple relation provides the key for the computation of the mass of air acted upon by a propeller since the area of the propeller disk and the density of the air can usually be determined.

The momentum theory sets an upper limit of efficiency and provides a clear physical picture of propeller action. For application to practical design, however, the blade-element theory is more useful.

The Simple Blade-element Theory.—Any circumferential section of a propeller blade forms an airfoil section, the lift and drag of which contribute to both the forward

thrust and the torque required to rotate the propeller. As shown in Fig. 11.2, the *resultant velocity* acting on a blade section varies with its radius. This is true because the tangential velocity component ($V_T = \omega r$) increases with

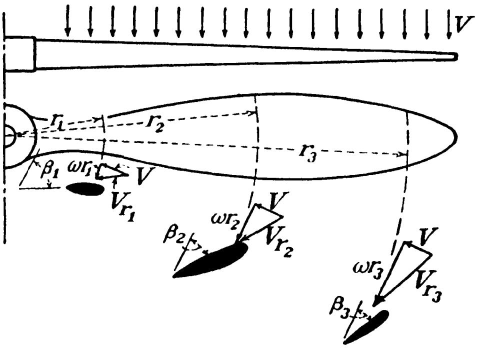

β = blade angle (angle between chord line of blade element and the plane of rotation)
V = component of velocity normal to the plane of rotation
ωr = tangential velocity at radius r
V_r = resultant velocity over blade element at radius r

FIG. 11.2.—Variation of resultant velocity with radius along a propeller blade.

the radius, and the velocity of flow normal to the plane of rotation remains constant.

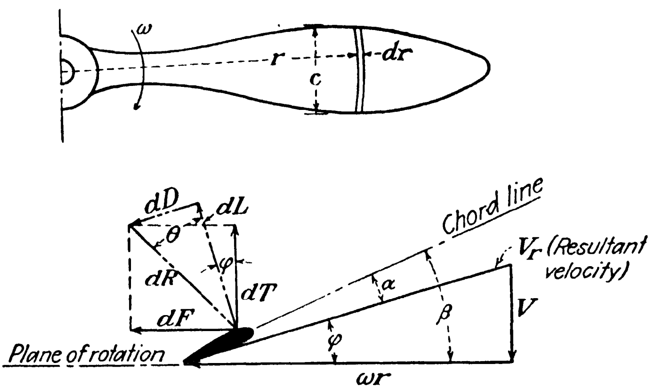

FIG. 11.3.—Forces and velocities at a blade element.

The velocity and force components acting on a typical section of dr thickness are shown in Fig. 11.3. The angle between the plane of rotation and the resultant velocity is designated as φ. The blade section makes an angle of

attack α, with the resultant velocity so that the blade angle β (beta) between the airfoil chord line and the plane of rotation may be written

$$\beta = \varphi + \alpha \tag{11.4}$$

The lift on each segment dL can be evaluated through the fundamental lift equation,

$$dL = C_L \frac{\rho}{2} cdrV_r^2$$

The resultant force dR becomes

$$dR = \frac{dL}{\cos\theta} = \frac{C_L \frac{\rho}{2} cdrV_r^2}{\cos\theta}$$

and

dT = thrust force on the segment $= dR \cos(\varphi + \theta)$

$$dT = \frac{C_L \frac{\rho}{2} cdrV_r^2 \cos(\varphi + \theta)}{\cos\theta}$$

But

$$V_r = \frac{V}{\sin\varphi}$$

Substituting and rearranging,

$$\frac{dT}{dr} = \frac{C_L \frac{\rho}{2} cV^2 \cos(\varphi + \theta)}{\sin^2\varphi \cos\theta}$$

and for a propeller of N blades the total thrust T may be obtained through integration between hub and blade tip.

$$T = N \int_0^{\text{tip}} \frac{dT}{dr}\, dr = \frac{\rho}{2} V^2 N \int_0^{\text{tip}} \frac{C_L \cos(\varphi + \theta) c dr}{\sin^2\varphi \cos\theta} \tag{11.5}$$

The force in the tangential direction dF may be written

$$dF = dR \sin(\theta + \varphi)$$

The torque dQ produced by this segment then becomes

$$dQ = dF \times r = dR \sin(\theta + \varphi) r$$

and, substituting as before,

$$Q = \frac{\rho V^2 N}{2} \int_0^{\text{tip}} \frac{C_L r \sin(\varphi + \theta) c\,dr}{\sin^2 \varphi \cos \theta} \tag{11.6}$$

The integrations indicated in Eqs. (11.5) and (11.6) are generally performed graphically giving curves similar to those of Fig. 11.4, known as "torque" and "thrust grading" curves. The areas beneath these curves multiplied

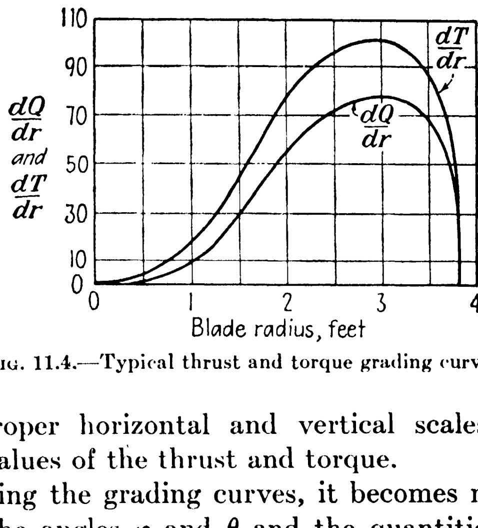

FIG. 11.4.—Typical thrust and torque grading curves.

by the proper horizontal and vertical scales yield the required values of the thrust and torque.

In plotting the grading curves, it becomes necessary to evaluate the angles φ and θ and the quantities C_L and c corresponding to various values of the radius. The angle φ may be evaluated through the relation

$$\tan \varphi = \frac{V}{\omega r} = \frac{V}{2\pi r n} \qquad (n = \text{revolutions/sec.})$$

For a given propeller the angle β is known, so that α can be found through a rearrangement of Eq. (11.4).

$$\alpha = \beta - \varphi \tag{11.7}$$

For a new design, the value of α is generally assumed corresponding to a high L/D ratio and β is then computed using Eq. (11.4). The angle θ may be determined, since $\cot \theta = L/D = C_L/C_D$ (Fig. 11.3). Values of C_L

and C_D are found from airfoil characteristic curves corresponding to the previously determined value of α. The value of c, the chord length, is known for a given propeller and generally assumed for a new design. These computations are generally systematized in tabular form to provide coordinates for several points on the torque and thrust grading curves.

Propeller Efficiency.—Having determined the torque and thrust, the propeller efficiency can be written

$$\eta = \frac{\text{output}}{\text{input}} = \frac{TV}{2\pi nQ} \quad (n = \text{revolutions/sec.}) \tag{11.8}$$

The efficiency of an *element* η_e can similarly be written

$$\eta_e = \frac{dT \times V}{2\pi n dQ} = \frac{dR \cos(\varphi + \theta)V}{dR \sin(\varphi + \theta)2\pi nr}$$

but

$$\tan \varphi = \frac{V}{2\pi nr}$$

and, therefore,

$$\eta_e = \frac{\tan \varphi}{\tan(\varphi + \theta)} \tag{11.9}$$

The value of φ corresponding to maximum efficiency may be found by differentiating the efficiency η_e with respect to φ and equating the first derivative to zero. This yields the result

$$\varphi = 45° - \frac{\theta}{2} \tag{11.10}$$

Since most of the elements of practical propellers operate at values of φ below the value of best efficiency, it is desirable to keep $\tan \varphi$ or its equal $V/2\pi nr$ as high as possible. This is favored by operation of the propeller in high pitch corresponding to high-speed flight.

Limitations of the Simple Blade-element Theory.—The simple blade-element theory is suitable only for approximate design calculations because of its neglect of the following items: (1) aspect-ratio corrections, (2) interference between blades, (3) effect of the flow over one blade

element on adjoining blade elements, (4) variation of the velocity of flow behind the propeller with blade position, (5) tip losses, (6) radial components of flow through a propeller.

Various modifications and extensions of the simple blade-element theory have been employed for the purpose of including all or some of the foregoing items in propeller-design analyses. Weick[1] advocates the use of airfoil characteristic curves computed backward from tests of model propellers by means of the simple blade-element theory. Lift and drag coefficients obtained from these curves are then, of necessity, exactly corrected for the neglected factors in the simple blade-element theory when applied to the particular model propellers tested and prove reasonably accurate for *similar* full-scale propellers. Theoretical performance values of full-scale propellers based on calculated airfoil characteristics of this kind show good agreement with experimental results.

Presentation of Propeller Test Results.—The performance of a propeller is generally determined by wind-tunnel or flight tests and presented in the form of characteristic curves. Dimensionless coefficients are used to increase the convenience and range of application of these results.

The advance ratio $J = \frac{V}{nd}$ is of fundamental importance because of its direct relation to the angle φ ($\tan \varphi = \frac{V}{\pi nd}$ at the blade tip) and its consequent effect on the angles of attack of the blade elements.

Both the thrust and the power absorbed by a propeller depend upon the air density ρ, the revolutions per second n, and the propeller diameter d. Stated symbolically,

$$P = f(\rho,n,d) = C_P\rho^a n^b d^c$$

and

$$T = f'(\rho,n,d) = C_T\rho^x n^y d^z$$

[1] FRED WEICK, "Aircraft Propeller Design," McGraw-Hill Book Company, Inc., New York, 1930.

where C_P and C_T are known as the power and thrust coefficients, respectively. The values of the exponents may be evaluated by dimensional analysis, giving

$$C_P = \frac{P}{\rho n^3 d^5} \tag{11.11}$$

and

$$C_T = \frac{T}{\rho n^2 d^4} \tag{11.12}$$

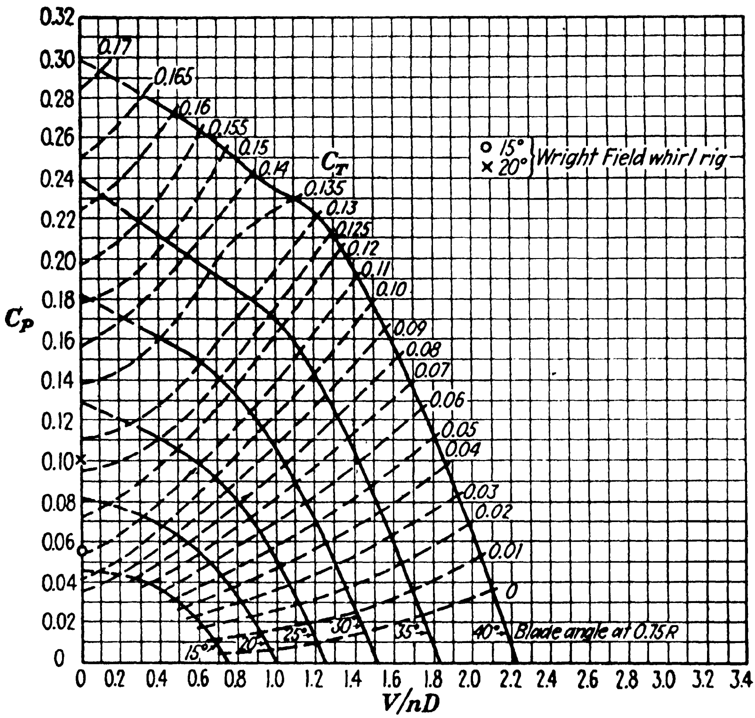

FIG. 11.5.—Power coefficient curves for propeller 6131, three blades, radial engine nacelle. (*N.A.C.A. Technical Report* 642.)

In terms of these coefficients the propeller efficiency may be expressed

$$\eta = \frac{TV}{P} = \frac{C_T \rho n^2 d^4 V}{C_P \rho n^3 d^5} = \frac{C_T}{C_P} J \tag{11.13}$$

In selecting a propeller for an airplane, the designer must generally choose a suitable diameter to correspond to given horsepower, r.p.m., and forward speed. So a dimension-

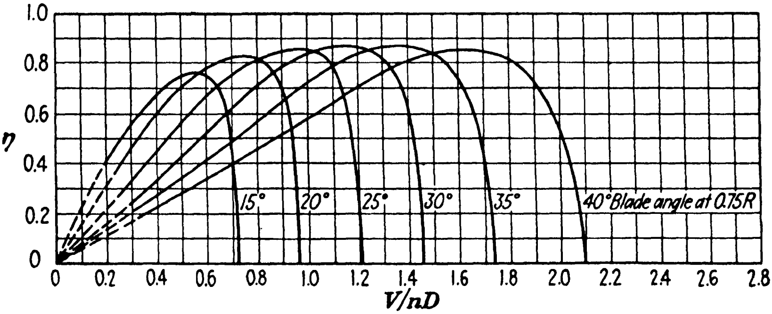

FIG. 11.6.—Efficiency curves for propeller 6131, three blades, radial engine nacelle. (*N.A.C.A. Technical Report* 642.)

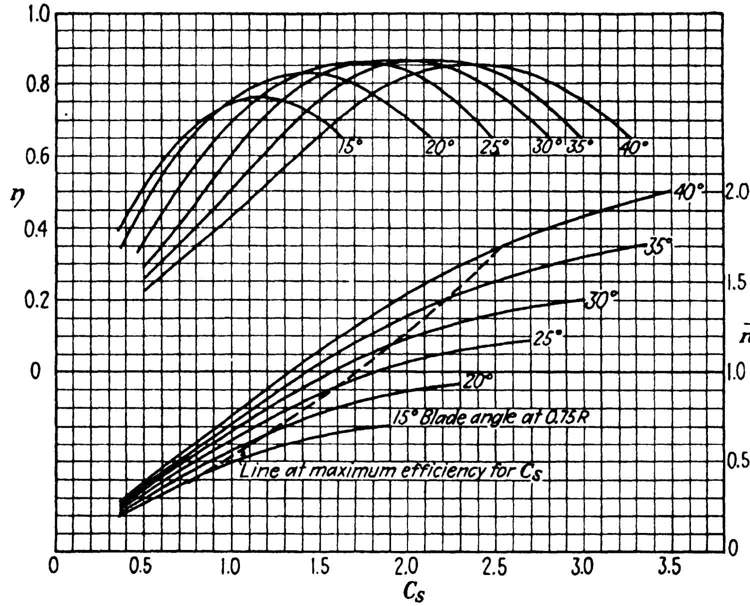

FIG. 11.7.—Design chart for propeller 6131, three blades, radial engine nacelle. (*N.A.C.A. Technical Report* 642.)

less ratio that does not contain the diameter, designated as C_s, is employed in propeller-design charts. C_s may be conveniently expressed in engineering units by the

equation

$$C_s = \frac{0.638 \text{ m.p.h.}}{\text{b.hp.}^{1/5}\text{r.p.m.}^{2/5}}$$

Performance and design charts for a typical propeller are presented in Figs. 11.5 to 11.7. It should be noted that the blade angles specified on these curves are taken at blade sections located three-fourths of the outside radius from the axis of rotation.

Propeller-engine Characteristics.—As the operation of a propeller is closely related to that of its engine, some general aspects of engine performance will now be considered.

At any given altitude, the horsepower output of a typical aeronautical engine will vary with r.p.m. as shown in Fig. 11.8. The *rated* horsepower and r.p.m. are designated by the manufacturer for optimum continuous operation. The propeller is generally designed to operate at maximum efficiency under rated conditions at the cruising speed of the airplane. Operation with a fixed-pitch propeller at forward speeds greater or less than cruising speed results in lowered engine efficiency and probably lowered propeller efficiency as well. Reduced efficiency of the engine-propeller unit is particularly serious for take-off and climbing conditions, where maximum performance is desired. On the other hand, if the propeller-blade angle is set to provide most efficient operation at take-off, the cruising and high-speed efficiencies suffer.

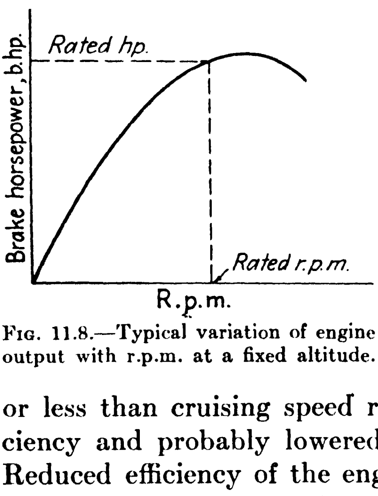

FIG. 11.8.—Typical variation of engine output with r.p.m. at a fixed altitude.

The answer to these difficulties is to change the pitch of the propeller blades to suit the forward velocity of the airplane, either by manual adjustment from the cockpit with a *controllable-pitch* propeller or by automatic means

with an *automatic* or *constant-speed* propeller. These devices permit the operation of the engine under rated conditions with efficient operation of the propeller at all normal air speeds.

The operation of a constant-speed propeller would be depicted as a horizontal line of constant C_p on Fig. 11.5. The lower take-off and climbing speeds obviously correspond to low-pitch settings of the blades, and cruising and top-speed operations correspond to the higher pitch settings.

Engine Performance.—The variation of brake horsepower with altitude of a typical aeronautical engine equipped with a single-stage supercharger is illustrated in

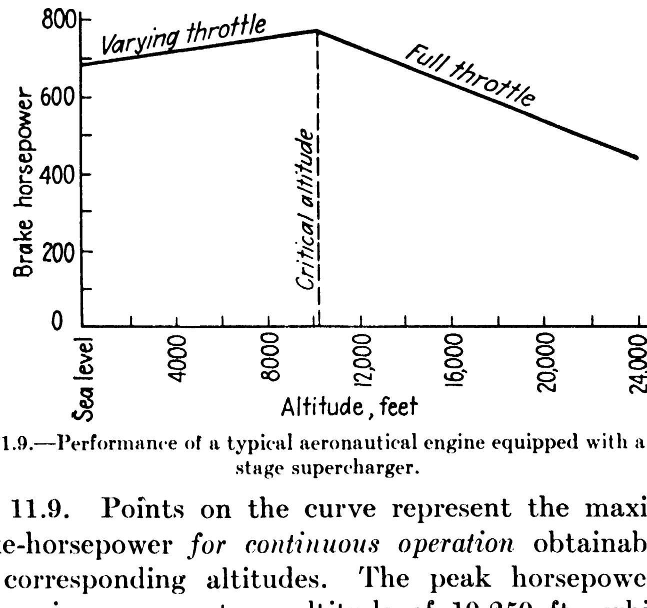

Fig. 11.9.—Performance of a typical aeronautical engine equipped with a single-stage supercharger.

Fig. 11.9. Points on the curve represent the maximum brake-horsepower *for continuous operation* obtainable at the corresponding altitudes. The peak horsepower for this engine occurs at an altitude of 10,250 ft., which is known as the "critical altitude," since it represents the lowest altitude for continuous full-throttle operation. In climbing to the critical altitude from the ground, the throttle is gradually opened because full-throttle operation at low altitudes would overheat the engine and result in its eventual failure.

The maximum horsepower of the engine of Fig. 11.9 increases up to the critical altitude since the back pressure of the atmosphere and the temperature of the inlet air decrease with altitude.

The horsepower available at the propeller can readily be determined if the proper engine and propeller curves are available since

$$\text{Hp.}_{\text{available}} = \text{engine b.hp.} \times \eta \qquad (11.14)$$

PROBLEMS

1. A single-engined monoplane equipped with an 8-ft. propeller cruises at a speed of 200 m.p.h. under sea-level atmospheric conditions. If the final velocity of the slip stream relative to the fuselage is 250 m.p.h., calculate (*a*) the ideal efficiency of the propeller, (*b*) the mass of air handled by the propeller, (*c*) the ideal thrust of the propeller.

2. In the propeller of Prob. 1, what is the drop in pressure below atmospheric directly in front of the propeller? Find the rise in pressure directly behind the propeller. (Write Bernoulli's equation between sections 1 and 2 and between sections 3 and 4 of Fig. 11.1.)

3. A helicopter weighing 1,500 lb. is supported by a 20 ft. diameter rotor. Find the ideal horsepower absorbed by the rotor for hovering flight.

4. Find what ideal horsepower would be required for the helicopter of Prob. 3 if two 10 ft. diameter rotors were substituted for the 20-ft. rotor.

5. The air velocity leaving a 3-ft. propeller fan was observed to be 30 ft. per sec. at a point in front of the fan where the pressure had returned to atmospheric. What is the ideal input horsepower to the fan?

6. A two-bladed propeller 7.50 ft. in diameter having an R.A.F. six-blade section rotates at 2,000 r.p.m. corresponding to an air speed of 85.2 m.p.h. Using the simple blade-element theory, determine the torque, thrust, and output horsepower of this propeller. (The torque and thrust grading curves for this propeller are given in Fig. 11.4.) The area under the dT/dr curve measures 130.4 sq. in. and the area under the dQ/dr curve is 86.68 sq. in. corresponding to a vertical scale of 1 in. = 10 lb. per ft. and a horizontal scale of 1 in. = 0.33 ft. for the dT/dr curve and a vertical scale of 1 in. = 10 ft.-lb. per ft. for the dQ/dr curve. The curves represent the total effect of both blades.

7. Determine the efficiency of the blade element at $0.75R$ of an 8 ft. diameter propeller rotating at a speed of 2,000 r.p.m. corresponding

to a forward speed of 200 m.p.h. and a blade angle at $0.75R$ of 30 deg. for an N.A.C.A. 23012 section.

8. A 6 ft. diameter propeller rotates at 1,800 r.p.m. in air at standard density at an air speed of 200 m.p.h. If the propeller designation is 6131, with a blade angle of 40 deg. at $0.75R$, find its efficiency and the horsepower absorbed under these operating conditions.

9. Using the propeller curves of Figs. 11.5 and 11.6, determine the horsepower available at the propeller corresponding to the following conditions:

Altitude	15,000 ft.
Air speed	400 m.p.h.
Propeller diameter	10 ft.
R.p.m	2,000

Full-throttle operation; most efficient propeller setting.

10. A military airplane cruises at a speed of 300 m.p.h. under sea-level atmospheric conditions corresponding to rated engine power of 1,200 hp. at 1,800 r.p.m. If a three-bladed propeller (6131) is selected for this airplane, what is its optimum diameter for the cruising condition? What are its blade angle and thrust at this speed?

11. Select the diameter and blade setting of a three-bladed propeller of type 6131 suitable for a 350 m.p.h. cruising speed corresponding to a 2,000-hp. output at 1,800 r.p.m.

CHAPTER 12

PERFORMANCE

The performance of an airplane is commonly specified in terms of its maximum and minimum speeds, its maximum rate of climb, and the highest altitude or ceiling at which it can effectively be used. For some types of airplane other performance items may be of importance, such as the minimum time required to climb to various altitudes, the maximum range and endurance, and the length of the landing and take-off runs.

Equilibrium in Unaccelerated Flight.—The forces acting on an airplane during a *steady* climb along a path inclined upward at any angle θ to the horizontal, as illustrated in Fig. 12.1, must remain in equilibrium. These forces may be resolved into lift, drag, thrust, and gravitational components acting through the center of gravity of the airplane.

For equilibrium in a direction normal to the flight path,

$$L = W \cos \theta \tag{12.1}$$

For small angles of climb, $\cos \theta$ is very nearly equal to unity so that Eq. (12.1) reduces to the familiar relation,

$$L = W \tag{12.2}$$

For equilibrium in a direction parallel to the flight path,

$$T - D = W \sin \theta \tag{12.3}$$

Multiplying both sides by V,

$$TV = DV = WV \sin \theta$$

$V \sin \theta$, the vertical component of the velocity of the plane, equals the time rate of vertical displacement, the *rate of climb*, that is,

$$V \sin \theta = \frac{dh}{dt}$$

where h represents the altitude of the airplane at any time t. Substituting in Eq. (12.3),

$$TV - DV = W\frac{dh}{dt} \tag{12.4}$$

The expression TV is recognized as the power output of the propeller (Chap. 11) and is usually referred to as the *power available.* DV is the power consumed by the total

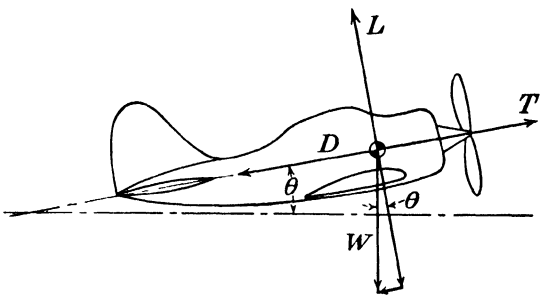

FIG. 12.1.—Forces acting on an airplane during a steady climb.

drag of the airplane, the *power required.*

Solving for the rate of climb in Eq. (12.4),

$$\frac{dh}{dt} = \frac{TV - DV}{W}$$

$$= \frac{\text{power available} - \text{power required}}{\text{weight of airplane}} \tag{12.5}$$

These relations can best be studied and applied by graphical means.

Performance Curves.—The power required by an airplane in level flight at sea level may be readily computed for any given air speed provided that drag data on the complete airplane or on its various components are known (Chap. 7). By performing this calculation for a number of different air speeds, a power-required curve such as that of Fig. 12.2 can be plotted.

A power-available curve can readily be drawn on the same coordinates since the power available at any air speed

simply equals the product of the delivered horsepower of the engine times the propeller efficiency.

A study of the curves of Fig. 12.2 indicates that the available and required powers are equal at the two velocities marked by the crossing of the curves. The intersection at the right of the figure indicates the maximum velocity of the airplane for level flight $V_{max.}$, since at greater speeds the power required would be in excess of that

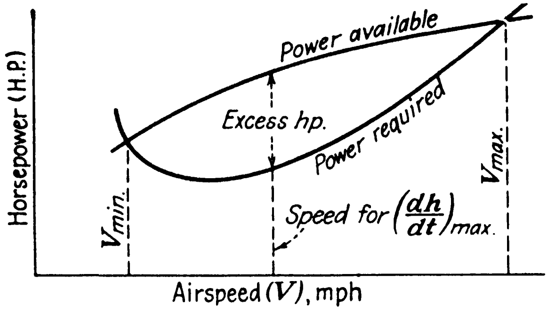

FIG. 12.2.—Typical performance curves for sea-level conditions.

available. By the same reasoning, the intersection at the left of the diagram represents the minimum speed for level flight.

According to Eq. (12.5) the maximum rate of climb $(dh/dt)_{max.}$ must correspond to the maximum vertical separation of the power-available and power-required curves. This can be located experimentally giving the position shown in Fig. 12.2. The difference between the horsepower available and that required is often termed the "excess power."

Performance at Various Altitudes.—Both power-available and power-required calculations could be carried out in exactly the same way for any other altitude than sea level using the proper value of the mass density, resulting in a different pair of curves for each altitude, as shown in Fig. 12.3. A great deal of computational work may be saved, however, by relating the power required at any altitude to the power required at sea level.

For the same values of the lift and drag coefficients, and therefore of the angle of attack, both velocity and horsepower increase with altitude and the density decreases. Letting $HP_{alt.}$, $V_{alt.}$, and $\rho_{alt.}$ represent conditions at any altitude *above* sea level and HP_0, V_0, and ρ_0 the correspond-

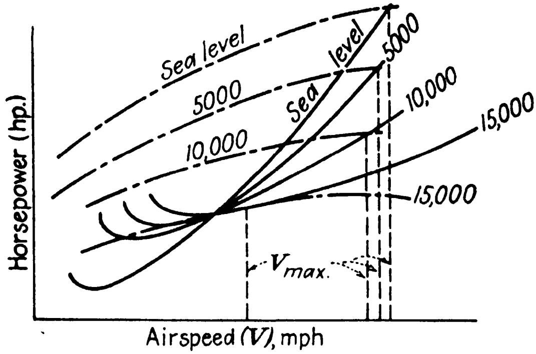

FIG. 12.3.—Performance curves at various altitudes.

ing conditions *at the same angle of attack* at sea level, then, from the fundamental lift equation,

$$V_0 = \sqrt{\frac{W}{C_L \frac{\rho_0}{2} S}}$$

and

$$V_{alt.} = \sqrt{\frac{W}{C_L \frac{\rho_{alt.}}{2} S}} = \sqrt{\frac{W}{C_L \frac{\rho_0}{2} S \times \frac{\rho_{alt.}}{\rho_0}}}$$

Dividing the second equation by the first,

$$\frac{V_{alt.}}{V_0} = \sqrt{\frac{\rho_0}{\rho_{alt.}}}$$

and

$$V_{alt.} = V_0 \sqrt{\frac{\rho_0}{\rho_{alt.}}} \qquad (12.6)$$

It follows from Eq. (12.6) that $\frac{\rho_{alt.}}{2} V^2_{alt.} = \frac{\rho_0}{2} V^2_0$. Hence

the dynamic pressures at the two elevations are equal so that the usual pitot-tube air-speed *indicator* would read the same at the higher velocity, $V_{alt.}$, and its associated lower density, $\rho_{alt.}$, as at the corresponding sea-level conditions V_0 and ρ_0. The *indicated* air speed must then be multiplied by the square root of the density ratio, in accordance with Eq. (12.6) to obtain the true air speed at any altitude above sea level. The stalling speed of an airplane, however, depends upon the dynamic pressure rather than on the air speed alone, so the stalling speed

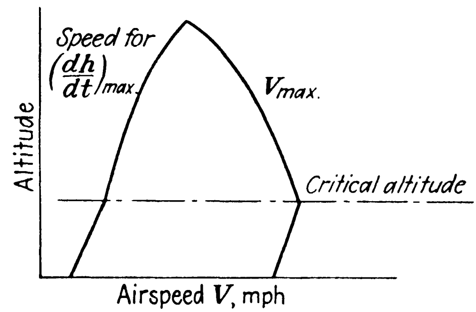

FIG. 12.4.—Speed for maximum rate of climb and maximum speed of level flight for an airplane with a single-stage supercharger.

always occurs at the same indicated air speed regardless of altitude.

The horsepower required at sea level may be expressed as follows:

$$HP_0 = \frac{D \times V}{550} = \frac{C_{D_T}\rho_0 S V_0^3}{550 \times 2}$$

and at any altitude,

$$HP_{alt.} = \frac{C_{D_T}\rho_{alt.} S V_{alt.}^3}{550 \times 2}$$

and, therefore,

$$\frac{HP_{alt.}}{HP_0} = \frac{\rho_{alt.} V_{alt.}^3}{\rho_0 V_0^3}$$

Substituting $V_0 \sqrt{\rho_0/\rho_{alt.}}$ for its equal $V_{alt.}$ [Eq. (12.6)] and reducing,

$$HP_{alt.} = HP_0 \sqrt{\frac{\rho_0}{\rho_{alt.}}} \tag{12.7}$$

Hence, according to Eqs. (12.6) and (12.7), the coordinates of points on the power-required curve at any altitude may be computed by multiplying coordinates of the sea-level curve by the square root of the density ratio, $\sqrt{\frac{\rho_0}{\rho_{alt.}}}$.

The power-available curves must be computed independently for each altitude since there is no simple variation of power available with altitude.

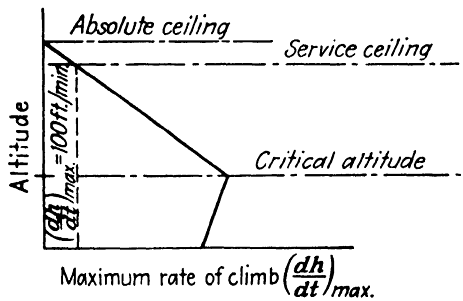

FIG. 12.5.—Variation of the maximum rate of climb of an airplane with altitude.

From the completed curves of Fig. 12.3, the maximum and minimum air speeds and the maximum rate of climb can readily be determined. It may be noted that the power-required and -available curves for 15,000 ft. do not come together except at one point of tangency. The rate of climb at this elevation is consequently zero, fixing the *absolute ceiling* of the airplane at 15,000 ft. The airplane could reach this elevation only by flying at the velocity corresponding to the point of tangency.

With the results obtained from the curves like those of Fig. 12.3, the variation of maximum speed, the maximum rate of climb, and the speed for maximum climb may be plotted against altitude as presented in Figs. 12.4 and 12.5.

In Fig. 12.5, the *service ceiling* has been designated in accordance with its usual definition, the altitude at which the maximum rate of climb equals 100 ft. per min.

Time to Climb to Altitude.—During an infinitesimal interval of time dt, an airplane may climb a distance dh, provided

$$dh = \text{velocity} \times \text{time} = \frac{dh}{dt} \times dt$$

Solving for dt,

$$dt = \frac{dh}{dh/dt}$$

The *minimum* time T to climb to any altitude H from sea level must correspond to the *maximum* rate of climb $(dh/dt)_{\text{max.}}$, that is,

$$T = \int_0^T dt = \int_0^H \frac{dh}{\left(\frac{dh}{dt}\right)_{\text{max.}}} \tag{12.8}$$

The time T can therefore be evaluated if the maximum rate of climb can be expressed in terms of the altitude h. This relation can often be established by fitting a straight line or a simple curve to the variation of maximum rate of climb with altitude (Fig. 12.5).

Range.—The calculation of the maximum distance or *range* of an airplane with a given gas capacity is complicated by the changing weight, air speed, and propeller efficiency resulting from the consumption of gasoline as the airplane proceeds toward its destination. A method developed by Breguet yields approximate results when average values are used for some of the variables involved. His analysis considers first the weight of fuel consumed dQ, during an interval of time dt.

$$dQ = \frac{C \times \text{b.hp.} \times dt}{3{,}600} \tag{12.9}$$

where C is the specific fuel consumption in pounds per brake

horsepower per hour. But

$$\text{b.hp.} \times \eta = \frac{DV}{550} = \frac{LV}{\frac{L}{D} \times 550}$$

and, therefore,

$$\text{b.hp.} = \frac{LV}{\eta \times \frac{L}{D} \times 550} \tag{12.10}$$

Substituting in Eq. (12.9),

$$dQ = \frac{CLVdt}{\eta \times \frac{L}{D} \times 550 \times 3{,}600}$$

and so

$$Vdt = \frac{dQ}{L} \times \frac{\eta}{C} \times \frac{L}{D} \times 550 \times 3{,}600$$

Letting dR represent the distance flown during the time interval dt,

$$dR = Vdt = \frac{DQ}{L} \times \frac{\eta}{C} \times \frac{L}{D} \times 550 \times 3{,}600$$

and

$$R = \int_0^R dR = 550 \times 3{,}600 \times \frac{\eta}{C} \times \frac{L}{D} \int \frac{dQ}{L} \tag{12.11}$$

But the total lift L must vary with the weight of the plane. At any time t sec. after the take-off

$$L = W_i - Q$$

where W_i represents the initial weight of the airplane and Q the weight of fuel consumed after t sec. The *total* weight of fuel carried by the airplane at take-off Q_t will be assumed to be completely consumed during the trip. Substituting in Eq. (12.11),

$$R = 550 \times 3{,}600 \times \frac{\eta}{C} \times \frac{L}{D} \int_0^{Q_t} \frac{dQ}{W_i - Q}$$

Integrating and changing the units of R to miles,

$$R = \frac{550 \times 3{,}600}{5{,}280} \times \frac{\eta}{C} \times \frac{L}{D} \int_{Q_t}^{0} \log_e (W_i - Q)$$

$$= 375 \times \frac{\eta}{C} \times \frac{L}{D} \log_e \frac{W_i}{W_i - Q_t} \qquad (12.12)$$

Converting to the logarithmic base 10,

$$R = 863.5 \times \frac{\eta}{C} \times \frac{L}{D} \log_{10} \frac{W_i}{W_i - Q_t} \qquad (12.13)$$

where R = range, miles
η = average propeller efficiency during trip (generally about 80 per cent)
C = specific fuel consumption, lb. per b.hp.-hr. (varies between 0.42 to 0.50 for usual conditions)
L = average lift of wings
D = average *total* drag of airplane

Take-off.—The length of the take-off run of an airplane depends upon several variables. Rigorous analysis is difficult, if not impossible, particularly since the uncertain factors of pilot technique and ground friction enter into the problem.

In general, the problem involves the balancing of a variable propeller thrust force against the sum of the air drag, ground drag, and acceleration forces. The variation of these forces with forward speed for a typical high-performance airplane during its take-off run is illustrated in Fig. 12.6. It is worth noting that the acceleration force is predominant in absorbing the propeller thrust.

For specific design problems, reference is made to *N.A.C.A. Technical Report* 450[1] in which charts and computation procedures are presented to cover practical conditions.

Rapid Methods of Performance Prediction.—The plotting of power-available and power-required curves for several altitudes in determining the performance of an air-

[1] WALTER S. DIEHL, The Calculation of the Take-off Run.

plane forms a rather long and tedious procedure. Several methods of reducing this labor by using formulas and charts for the calculation of airplane performance have accordingly been devised. These so-called "rapid methods of performance prediction," which are described in detail in N.A.C.A. publications, prove very valuable to those who have frequent occasion to calculate airplane performance. The

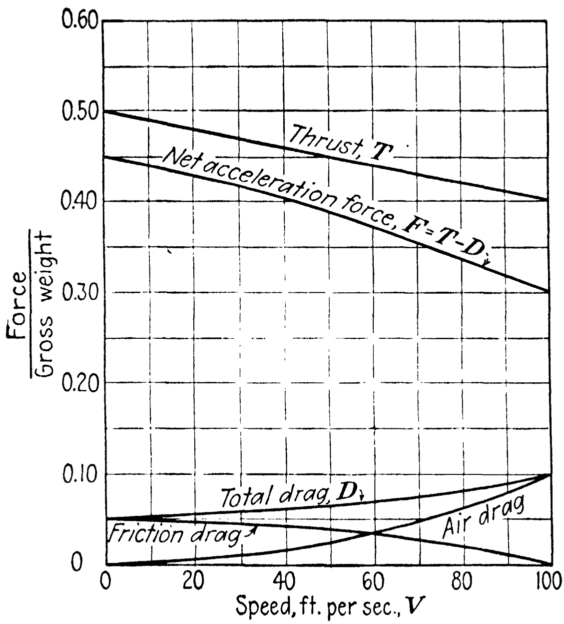

FIG. 12.6.—Forces acting on an airplane during its take-off run. (*N.A.C.A. Technical Report* 450.)

procedures are rather involved, however, and add little to the physical picture of the performance problem, and so are not presented here.

Flight Tests on Performance.—Flight tests are employed in performance checks of new airplane designs, contract acceptance trials, routine inspection, and full-scale tests of new design details. The test pilot generally determines the maximum speed and the maximum rate of climb at various altitudes, the landing speed, and the lengths of the

landing and take-off runs. In addition, the pilot makes at least qualitative measurements of stability, controllability, and maneuverability, and may study special characteristics such as recovery from a spin, gas consumption, and structural strength.

In securing reliable flight-test data, all the instruments used must be carefully calibrated, and the results should be converted to standard conditions.

PROBLEMS

1. An airplane weighing 2,000 lb. is powered by a 65-hp. engine. Calculate the angle of climb of this airplane when flying at an air speed of 70 m.p.h. at its rated horsepower with a propeller efficiency of 80 per cent. The total drag at this speed for the complete airplane is 100 lb.

2. An airplane weighing 10,000 lb. flies at an air speed of 200 m.p.h. during a steady climb under standard sea-level conditions. The airplane is equipped with a 9 ft. diameter, three-bladed propeller rotating at 1,800 r.p.m. Using the curves of Fig. 11.6 of Chap. 11 for the propeller characteristics at the blade angle for highest efficiency, and an engine output of 1,380 hp., calculate the rate of climb and the angle of climb. The required horsepower for overcoming drag at this air speed is 500 hp.

3. The horsepower required and available at sea level for various air speeds for an airplane weighing 8000 lb. is as follows:

V, m.p.h.	Hp. required	Hp. available
60	176	230
80	104	286
100	134	325
120	187	357
140	270	385
160	374	402

Determine graphically (*a*) the maximum speed, (*b*) the maximum rate of climb, and (*c*) the speed for the maximum rate of climb for this airplane at sea level.

4. The rate of climb of a given airplane is found to equal 1,000 ft. per min. at sea level and 700 ft. per min. at 5,000 ft. altitude. Assuming that the rate of climb varies linearly with altitude, determine the absolute and service ceilings for this airplane.

5. A military pursuit plane has the following specifications:

Total rated hp	1,200 at sea level
Total rated r.p.m. of motor and propeller	2,000
Propeller diameter	11 ft.
Propeller type	6131, 3 blades
Gross weight	7,155 lb.
Wing span	36.6 ft.
Wing area	223.7 sq. ft.
Wing section	N.A.C.A. 23012
C_D tail (based on tail area)	0.01
Tail area	50 sq. ft.
Fuselage cross-sectional area	15 sq. ft.
C_D fuselage (based on fuselage area)	0.10

The propeller is fully automatic and maintains a constant power coefficient.

Determine by graphs (*a*) the maximum speed of the airplane at sea level, (*b*) the maximum rate of climb at sea level, (*c*) the speed for maximum climb at sea level. Tabulate all the quantities calculated for obtaining points on the curves.

6. Calculate the range of an airplane with the following specifications:

Loaded gross weight	15,000 lb.
Fuel capacity	760 gal. (Assume gasoline weighs 6 lb./gal.)
Average L/D ratio for trip	15
Average propeller efficiency	80 per cent
Average fuel consumption C	0.45 lb./b.hp.-hr.

CHAPTER 13

CONTROL SURFACES

Reference Axes and Nomenclature.—In dealing with the motion of an airplane in three dimensions, a coordinate system is generally established with its origin at the center of gravity (C.G.) of the airplane. Three mutually perpendicular axes are commonly used with positive directions toward the front, the right wing, and downward as indicated in Fig. 13.1. Rotation about the X axis is termed

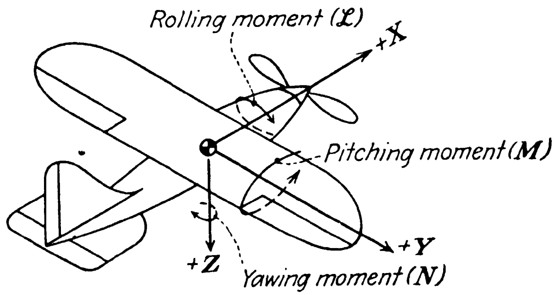

FIG. 13.1.—Reference axes for an airplane.

"roll," about the Y axis "pitch," and about the Z axis "yaw" with the positive directions shown in Fig. 13.1.

The various control surfaces employed on a conventional airplane are illustrated in Fig. 13.2. It should be noted that the *ailerons* exercise control *primarily* about the X axis in *roll*, the *elevator* about the Y axis in *pitch*, and the *rudder* about the Z axis in *yaw*. As will be discussed in later articles of this chapter, however, the effects produced by the rudder and the ailerons overlap, since each produces rotation about both the X and the Z axes.

Trim tabs are used to balance or trim an airplane so that little or no control force need be exerted by the pilot for normal level flight.

Movable Control Surfaces.—The change in the lift of an airfoil-control surface combination when the control surface is deflected is illustrated in the pressure-distribution curves of Fig. 13.3. It is apparent that downward deflec-

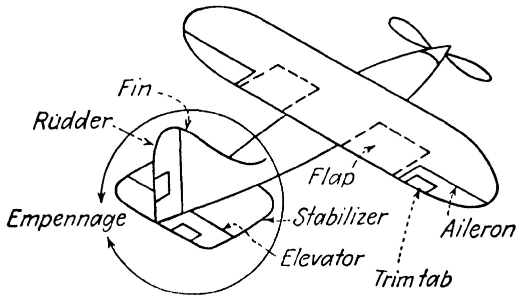

FIG. 13.2.—Control surfaces of a conventional airplane.

tion of the control surface not only increases the lift of the control surface itself but also adds considerably to the lift of the fixed wing to which it is attached. This effect is important since any increase in lift of the movable surface

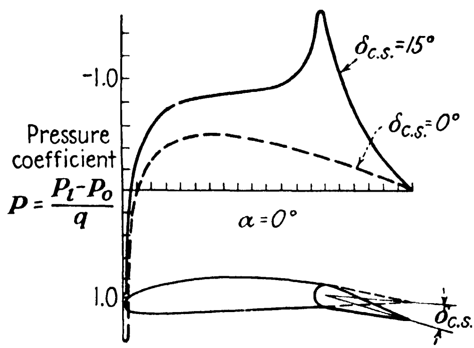

FIG. 13.3.—Effect of control-surface deflection on the pressure distribution over the upper surface of a Clark *Y* airfoil. (*N.A.C.A. Technical Report* 574.)

must, in part, be counteracted by the corresponding force exerted on the control system by the pilot, making it desirable to shift as much of the lift to the fixed surface as possible. For this reason, control surfaces are almost invariably attached to the trailing edge of fixed lifting

surfaces and are given relatively narrow chords compared with the chords of the fixed surfaces.

To reduce further the control effort, a control surface may be given *aerodynamic balance* by properly distributing the exposed area of the surface about its hinge line. Various methods for achieving aerodynamic balance are illustrated in Fig. 13.4, of which the *sealed* and the *inset-hinge*

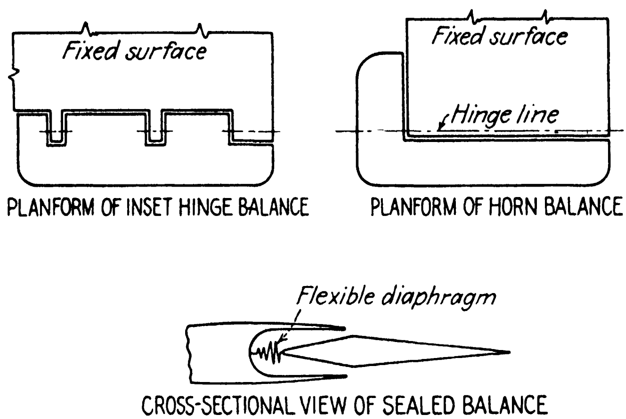

FIG. 13.4.—Types of aerodynamic balance for control surfaces.

types of balanced control surfaces are the most effective. The operating hinge moment for each of these surfaces is reduced by the difference in the air pressures acting on the two sides of the surface forward of the hinge line.

Although the emphasis has so far been on the *reduction* of control effort, it should be noted that, for normal reaction to the controls, the effort should be proportioned so as to increase in an approximately linear manner with the deflection of the surfaces. The proportioning of the control surfaces of a new design to give the proper "feel" to the controls is usually accomplished with the help of wind-tunnel data obtained from hinge-moment tests. The design requirements for the controls of high-performance aircraft are particularly stringent since in these airplanes the pilot exerts only a small percentage of the effort necessary

to deflect the control surfaces, the remainder being supplied by aerodynamic balance.

The Ailerons.—The ailerons are located on the outer portions of the wings and are arranged to deflect in opposite directions to produce rolling moments most effectively. An ordinary aileron, if deflected downward, will increase the lift of the aileron-wing combination; if deflected upward, the aileron will decrease the combined lift. An unwanted by-product of this action is a much greater increase in the drag of the wing with the lowered aileron, producing a yawing moment in the direction *opposite* to that of a properly banked turn. This "adverse yawing moment" may be counteracted with the tail control surfaces, or it may be eliminated in the design of the ailerons or the aileron operating linkage.

The *Frise* aileron is designed to equalize the drag on the ascending and descending ailerons by causing the leading edge of the ascending aileron to project into the air stream

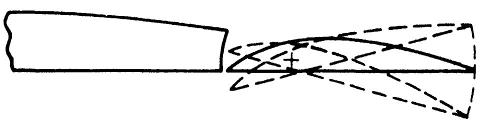

FIG. 13.5.—The Frise aileron.

beneath the wing, as shown in Fig. 13.5. It suffers the disadvantage of increasing the total drag of the airplane.

An alternative method of eliminating or at least reducing the adverse yawing moment of the ailerons is to deflect the ascending aileron a greater amount than the descending one with some form of *differential linkage*. Differential linkages are also employed to improve the hinge-moment characteristics of ailerons.

Ailerons lose their effectiveness as the stall is approached, making lateral control difficult at high angles of attack. Slots are sometimes used in connection with ailerons to postpone the stall, thereby extending the upper limit of aileron usefulness.

Spoilers offer a means of lateral control which remains effective at the stall. As the name implies, a spoiler in an erect position spoils the air flow over a wing by causing premature separation of the flow (Fig. 13.6). In this manner, the pilot may decrease the lift of the wing which he desires to lower. It is seen also that the increased drag is on the descending wing which is conducive to a properly banked turn. On the other hand, spoilers do not act so smoothly as ailerons, and their action causes some loss in altitude, so that ailerons are more satisfactory at low angles of attack and at low altitudes.

FIG. 13.6.—A spoiler on the upper surface of a wing.

The Empennage.—The tail surfaces are subject to the same considerations as the ailerons concerning the need and methods for aerodynamic balance and the limitations on hinge moment. The designer is faced with the additional problem of locating the horizontal and vertical tail surfaces in such a position as to avoid, as completely as possible, the fluctuating flow in the wake of the wing, the engine nacelles, and the fuselage. Wind-tunnel test results are generally used in this connection to indicate the optimum elevation of the horizontal tail and to aid in the selection of single or twin vertical surfaces.

The area of the vertical tail surfaces should be made adequate to provide sufficient lateral stability and to maintain control under all operating conditions. Conditions that may prove critical for the vertical tail include the operation of a multiengine airplane with one or more engines not functioning; recovery from a tail spin; and control on the ground during taxiing.

The size of the horizontal tail surfaces depends upon the requirements for longitudinal stability and control for all normal operating conditions. The condition that often

proves critical in the design of the horizontal tail is the need for getting the tail down for a three-point landing.

Trim, Balance, and Control Tabs.—The position of the center of gravity of an airplane shifts somewhat with varying arrangements of passengers and cargo, with the consumption of gasoline, and with changes in angle of attack. Since an airplane can proceed in level flight with neutral control surfaces at only one position of the center of gravity,

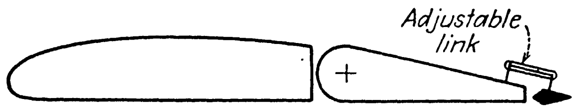

FIG. 13.7.—Fixed trim tab.

each new position of the center of gravity requires a sustained deflection of one or more of the control surfaces. This adjustment of the control surfaces is usually effected by *trim tabs* to relieve the pilot of unnecessary fatigue.

The simplest type of trim tab is the *fixed tab* shown in Fig. 13.7. Accurate adjustment is difficult since the tab

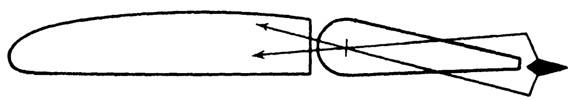

FIG. 13.8.—Controllable trim tab.

must be deflected on the ground to conform with expected flight requirements. In light airplanes, the fixed tab sometimes consists of a strip of sheet metal attached to the trailing edge of a control surface which may be readily bent in either direction.

The *controllable trim tab* of Fig. 13.8 may be adjusted by the pilot from the cockpit to meet conditions of flight accurately.

Balancing tabs may be used to lighten the forces required of the pilot in the operation of the controls. The tabs are arranged, as shown in Fig. 13.9, to rotate relative to a control surface as the control surface is deflected by the pilot so that the lift force exerted on the tab assists in pull-

ing the control surface into a deflected position. The presence of a lift force on a tab in a direction opposite to the lift force of the main control surface is made evident by the pressure-distribution diagram of Fig. 13.10. In this dia-

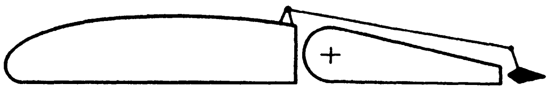

FIG. 13.9.—Balancing tab.

gram only the increments of the pressure coefficients contributed by the deflections of the aileron and tab from their neutral positions are shown, so the areas above and below the X axis are directly proportional to the changes in the lift force produced by the deflections. It may be noted

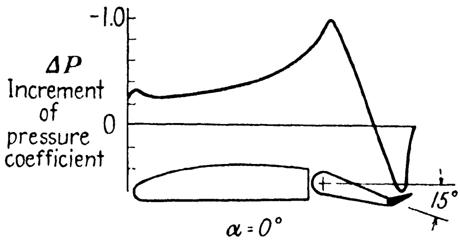

FIG. 13.10.—Increment of pressure coefficient produced by deflection of aileron and tab.

that the negative lift of the tab detracts only slightly from the total increment of lift produced by the aileron, although the moment of the negative lift about the aileron hinge line is nearly sufficient to hold the aileron in its deflected position.

The *servo control* tab is a logical extension of the balancing tab in which the pilot operates the tab alone which, in turn, deflects the main control surface. Servo control and balancing tabs may be employed to augment or replace aerodynamic balance in lightening control forces.

If the wings of an airplane are not sufficiently stiff in torsion, a condition of *aileron reversal* may develop at high speeds. In this condition the ailerons act as servo control tabs for the wings so that the deflection of the trailing edge

of an aileron downward, for instance, will twist the attached wing to a lower angle of attack and result in a net loss of lift for the wing-aileron combination. The aileron controls must therefore be manipulated in a direction opposite to the usual manner in rolling the airplane. At lower speeds such an airplane would evidence very ineffective aileron control.

Flutter of Wing and Tail Surfaces.—Vibration arising from periodic aerodynamic forces is termed "flutter," as exemplified by the fluttering of a flag in the wind. Flutter

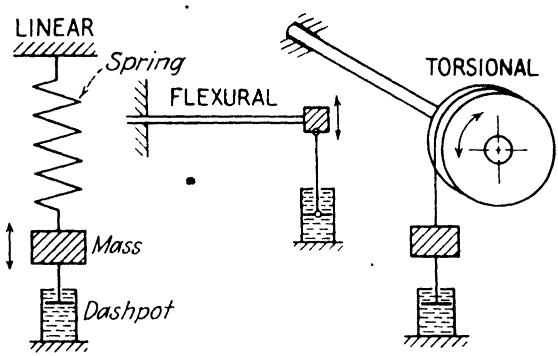

FIG. 13.11.—Comparable vibratory systems.

is not to be confused with engine vibration which may also induce troublesome vibrations in an aircraft structure. Flutter is an independent phenomenon which generally occurs at frequencies bearing no relation to the speed of rotation of the engine crankshaft.

Although the analysis of the flutter characteristics of an airplane structure is rather complicated from a mathematical standpoint, the fundamental principles may be deduced through relatively simple physical reasoning. As a first step, the requirements for a simple vibration will be considered. Figure 13.11 shows comparable types of vibrations in linear, flexural, and torsional systems. An examination of these three types of vibration will disclose fundamental similarities; in each there is a *restoring* spring force due to the elasticity of the vibrating members; the

restoring force is partly counteracted by the *inertia* force acting on the mass of the vibrating parts and is further opposed by the *damping* force or forces in the system. Finally, the vibration is maintained by an external *exciting* force which acts in the direction of motion of the vibration.

In investigating the possibility of flutter of any portion of an airplane, it need only be shown that aerodynamic exciting forces will be set up to reinforce any initial vibration, since elastic, inertia, and damping forces are always present in all parts of an airplane. The exciting forces

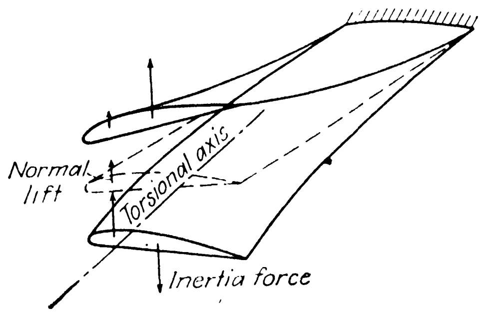

FIG. 13.12.—Wing flutter in a torsion-bending mode (deflections greatly exaggerated).

occur generally as a variation in the lift of wing or tail surfaces due to a periodic change in the angle of attack of the surfaces as the vibration proceeds.

The flutter of a wing in *combined torsion and bending* is illustrated in Fig. 13.12. The inertia force, shown acting through the center of gravity of the wing, tends to twist the wing so as to reduce its angle of attack during the upper part of the vibration and to increase its angle of attack during the lower part of the vibration. This produces a fluctuating lift force in phase with the vibration which may maintain or increase the vibration of the wing.

A more usual type of wing flutter combines the angular displacement of an aileron with the deflection of the attached wing in torsion or bending in the *torsion-aileron* or *bending-aileron* modes of vibration. Figure 13.13 illus-

trates the torsion-aileron case at an instant when the trailing edge of the wing is approaching the upper limit of its angular deflection. Since the angular velocity of the wing is rapidly decreasing at this phase of the vibration, the inertia force acting on the center of gravity of the aileron must act to deflect the aileron upward, thereby decreasing the lift on the wing and accelerating the wing downward on its return stroke. Near the bottom of the vibration the aileron is deflected downward to increase the lift and move the wing upward again. The bending-aileron mode may

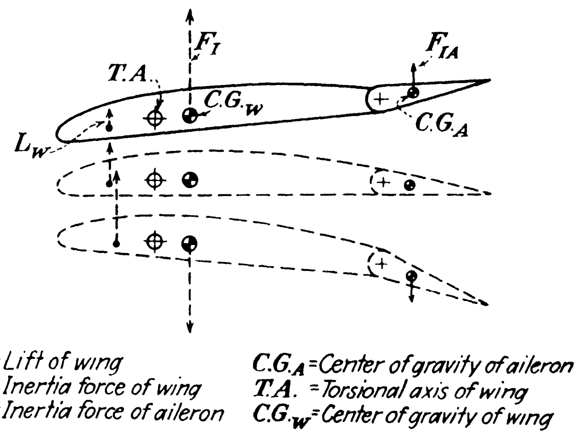

FIG. 13.13.—Wing flutter in torsion-aileron mode. (The three phases of the vibration are shown separately for clarity.)

be described along parallel lines with the wing vibrating in bending instead of torsion.

The foregoing types of vibration may also combine to give a *torsion-flexure-aileron* vibration. This mode may take place at a lower air speed than the other two modes and in this way prove critical, limiting the safe top speed of an airplane.

Although the discussion has so far been limited to the flutter of wings, tail surfaces flutter in similar modes. The combined vibration of a fixed tail surface with its movable control surface, paralleling flexure-aileron wing flutter, occurs most frequently.

The aeronautical designer generally endeavors to keep the critical flutter speed of a new airplane above its maximum operating speed. Higher critical flutter speeds may be promoted by increasing the stiffness of wing and tail surfaces in both flexure and torsion and by mass-balancing control surfaces to locate their centers of gravities at, or forward of, their hinge lines. Increasing the torsional stiffness of a wing tends also to prevent loss of aileron effectiveness and aileron reversal at high speeds.

CHAPTER 14

LONGITUDINAL STABILITY

An airplane may be considered as a free body in space since it is capable of movement in any direction and of rotation about any axis. This concept has already been implied in the derivation of the fundamental performance equations which are based on the equilibrium of the forces parallel and normal to the flight path of an airplane. It remains to develop the conditions for equilibrium of the remaining forces and moments and to determine their effect on flying qualities and controllability.

Stability and Trim.—For straight, level flight at constant speed, the moments about any axis must be in equilibrium. In aeronautical terms this may be expressed by stating that the airplane must be in *trim*, in pitch, yaw, and roll.

In addition to the need for trim, a satisfactory airplane should be *stable* about all three axes. This requires that the airplane return to its equilibrium position of steady rectilinear flight if deviated momentarily by some outside influence, such as a gust of wind. An *unstable* airplane, on the other hand, continues to move away from its original position if disturbed, unless arrested by the action of the pilot. A stable plane will practically "fly itself" in steady rectilinear flight whereas an unstable plane requires almost continuous effort on the part of the pilot to maintain a straight course.

Since stability depends upon the action of a restoring moment to return an airplane to its original position after a deviation by an outside influence, the degree of stability may be found by computing the magnitude of the restoring moment, using the equations of statics. This type of stability is consequently termed "static stability."

An airplane may be statically stable and still exhibit undesirable flying qualities by excessive oscillation about its original position after an outside disturbance. The nature of this oscillation determines the *dynamic* stability or instability of the airplane as discussed later in this chapter.

Longitudinal Stability from Wind-tunnel Tests.—The longitudinal stability of an airplane may be investigated in the wind tunnel by obtaining values of its pitching-moment coefficient C_M for the entire airplane about its center

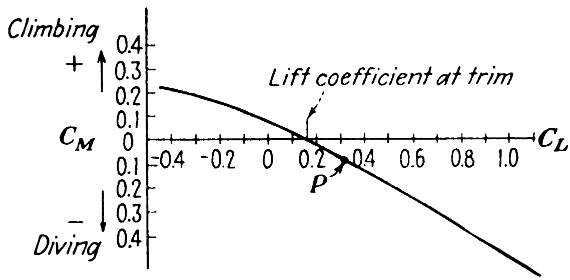

FIG. 14.1.—Pitching-moment curve for a longitudinally stable airplane.

of gravity corresponding to various lift coefficients, and then plotting C_M versus C_L as in Fig. 14.1. These data should preferably be obtained with a powered model since slip-stream and thrust effects have considerable influence on longitudinal stability.

Referring to Fig. 14.1, the airplane will be in trim at the value of the lift coefficient corresponding to the intersection of the pitching-moment curve with the C_L axis, that is, where $C_M = 0$. The horizontal stabilizer would normally be adjusted to trim the airplane at its cruising speed with zero elevator deflection at this attitude.

Assuming that the airplane is in trim in level flight at its cruising speed, an upward gust of wind would deflect its nose upward and at the same time increase both the angle of attack and the lift coefficient. This increased value of C_L might be represented by the point P of Fig. 14.1. The point P corresponds to a diving moment which would tend

to restore the airplane to an even keel. In the same way, a down gust would cause a decrease in C_L and produce a climbing moment to restore again the original condition of level flight. Thus a curve with a negative slope such as that of Fig. 14.1 corresponds to an airplane that is longitudinally stable. It may be observed further that a curve with a steeper slope would indicate even greater stability since a larger restoring moment would result from a given change in C_L.

On the other hand, if a similar analysis is conducted for the curve of Fig. 14.2, it will be seen that any gust will

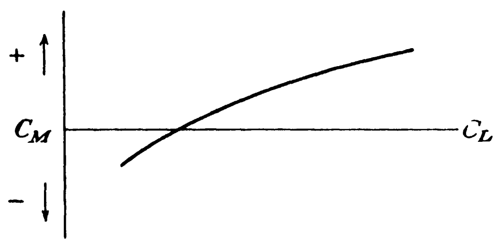

FIG. 14.2.—Pitching-moment curve for a longitudinally unstable airplane.

cause a change in C_L which will set up a moment to rotate the airplane *away* from the original position of trim. A pitching-moment curve of positive slope therefore represents an *unstable* airplane.

Since the static longitudinal stability of an airplane depends upon the slope of the pitching-moment curve and is positive when the slope is negative, the static longitudinal stability at any value of the lift coefficient (or α) can be expressed by the magnitude of dC_M/dC_L at the proper value of C_L, negative values of this derivative corresponding to stability and positive values to instability.

The pitching moment of a complete airplane may be built up by adding algebraically the moment contributions of its components—the wings and tail providing the larger contributions with the fuselage, nacelles, and landing gear of relatively minor importance, as indicated by the curves of

Fig. 14.3. Wind-tunnel tests are often conducted of airplane models with the empennage removed to determine the required stabilizing moment to be contributed by the tail.

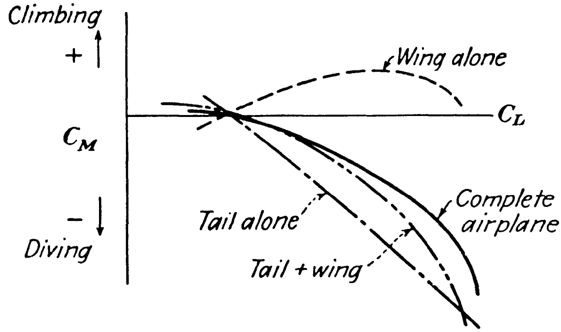

FIG. 14.3.—Pitching moment of the components of an airplane.

Stability of the Wing.—The forces and moments acting on a normal cambered airfoil at a positive angle of attack are illustrated in Fig. 14.4. For convenience, the resultant force acting on the airfoil has been resolved into lift and

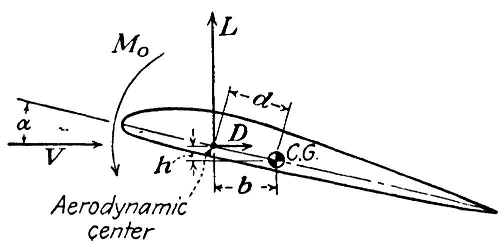

FIG. 14.4.—Investigation of the stability of an airfoil with normal camber.

drag components and moved forward to the aerodynamic center with the addition of a couple M_0, to give the same combined effect as the original resultant force acting at the center of pressure of the airfoil. The center of gravity of the complete airplane has been located on the chord line aft of the aerodynamic center.

For equilibrium, $\Sigma M = 0$ about an axis through the center of gravity, that is (with clockwise moments positive),

$$M = Lb + Dh - M_0$$

or, in coefficient form,

$$C_M \frac{\rho}{2} SV^2c = C_L \frac{\rho}{2} SV^2b + C_D \frac{\rho}{2} SV^2h - C_{M_0} \frac{\rho}{2} SV^2c$$

Dividing by $\frac{\rho}{2} SV^2c$,

$$C_M = C_L \frac{b}{c} + C_D \frac{h}{c} - C_{M_0}$$

Taking the distance between the center of gravity and the aerodynamic center as d,

$$b = d \cos \alpha \doteq d;$$
$$h = d \sin \alpha \doteq d \times \alpha \quad \text{(for small values of } \alpha\text{)}$$

Substituting,

$$C_M = C_L \frac{d}{c} + C_D \frac{d}{c} \alpha - C_{M_0} \tag{14.1}$$

Differentiating with respect to C_L for the evaluation of the longitudinal stability dC_M/dC_L and recalling that the moment coefficient around the aerodynamic center C_{M_0} is constant (by definition) and also that C_D is approximately constant over the usual working range of C_L so that

$$\frac{dC_{M_0}}{dC_L} = 0 \qquad \text{and} \qquad \frac{dC_D}{dC_L} = 0$$

$$\frac{dC_M}{dC_L} = \frac{d}{c}\left(1 + C_D \frac{d\alpha}{dC_L}\right) \tag{14.2}$$

An inspection of Eq. (14.2) shows that dC_M/dC_L can be negative for longitudinal stability only when the distance d is negative, since neither C_D nor $d\alpha/dC_L$, the reciprocal of the lift-curve slope, can be negative. In other words, the center of gravity of the airplane must be located *ahead* of the aerodynamic center for longitudinal stability of the *wing alone*. However, if d is given a negative value in Eq. (14.1), the airfoil cannot remain in equilibrium with negative pitching moment about the aerodynamic center (Fig. 14.4) since all the moments acting on the airfoil would have the same sign. Since a normal cambered airfoil *does*

have a negative C_{M_0}, we are led to the conclusion that such an airfoil cannot be in trim and be longitudinally stable at the same time.

With a reflexed airfoil, however, the moment coefficient about the aerodynamic center is positive, permitting both stability and trim for a center of gravity position ahead of the aerodynamic center. These characteristics are illus-

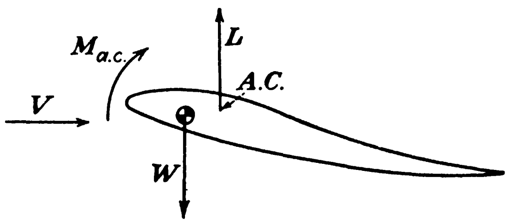

FIG. 14.5.—Stability and trim of a reflexed airfoil.

trated in Fig. 14.5. Airplanes of the flying wing type must consequently employ a reflexed airfoil section. Conventional airplanes are generally designed with the center of gravity behind the aerodynamic center so that the wing alone is unstable, requiring the overshadowing stability of horizontal tail surfaces to restore stability to the complete airplane, as indicated by the curves of Fig. 14.3.

Influence of the Horizontal Tail.—The tail surfaces are very important to the balance and stability of an airplane

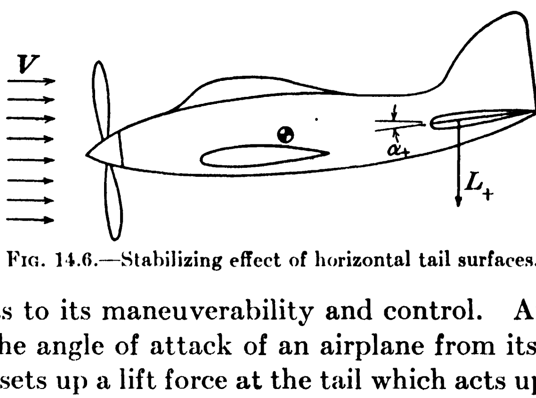

FIG. 14.6.—Stabilizing effect of horizontal tail surfaces.

as well as to its maneuverability and control. Any deviation in the angle of attack of an airplane from its trimmed position sets up a lift force at the tail which acts up or down to restore the airplane to its original position (Fig. 14.6).

Since the lever arm of the tail force about the center of gravity is generally large, the resulting restoring moment exerts a powerful influence on the stability of the complete airplane.

The lift force acting on the tail at any given angle of attack is subject to the following uncertain influences which make its accurate evaluation very difficult:

1. The effect of the down-wash of the wing on the effective angle of attack of the tail, as shown in Fig. 14.7.

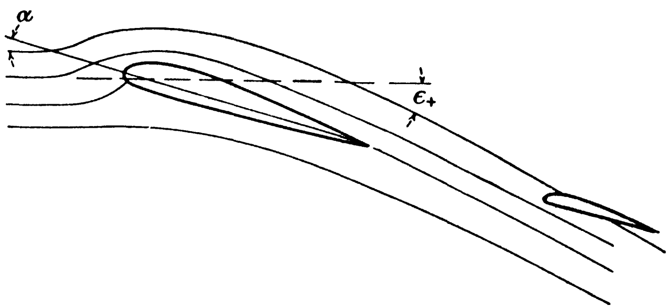

FIG. 14.7.—Effect of wing down-wash on the horizontal tail.

2. The inaccuracy resulting from the divergence of the tail lift distribution from the elliptic distribution underlying the usual aspect-ratio correction formulas. This divergence results principally from the low aspect ratio of the tail.

3. The reduced air speed over the tail caused by the frictional drag of the air passing over the wings and the fuselage.

A rough approximation of the down-wash produced at the tail by the wing is twice the down-wash at the lifting line of the wing, that is,

$$\epsilon_t = \frac{2C_L}{\pi A.R.} \times 57.3 \tag{14.3}$$

where ϵ_t = the reduction in the angle of attack of the tail produced by the down-wash of the wing

C_L = lift coefficient of wing

$A.R.$ = aspect ratio of wing

The correction to elliptic lift distribution together with the reduction in air speed over the tail surfaces may be taken into account with an empirical tail-efficiency factor η_t. Values of η_t usually range between 0.60 and 0.80, depending mainly upon the relative positions of wing and tail.

After the pitching moment due to the tail and the wing has been determined with the center of gravity on the chord

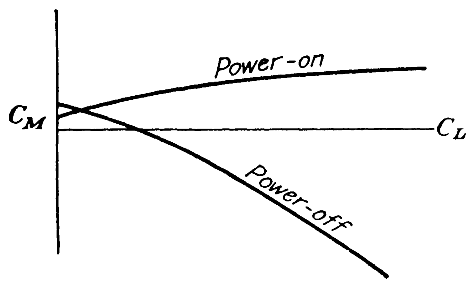

FIG. 14.8.—Effect of propeller slip stream on the pitching moment of a typical high-performance airplane.

line, it remains to consider the relatively small moment contributions of the fuselage, nacelles, and landing gear and the effect of shifting of the center of gravity vertically to a position above or below the chord line. These are usually given as empirical factors which may be applied to the stability as determined from the combined pitching-moment curves of the wing and tail.

For high-powered airplanes the effect of the propeller slip stream is a very important factor in longitudinal stability as indicated by the curves of Fig. 14.8. The power-off stability may be modified by correction factors based on the slip-stream effect of comparable airplanes to obtain a more accurate value of power-on stability, but the actual testing of a powered model yields much more reliable results. Powered tests are therefore conducted to investigate the stability of most high-performance airplanes.

Dynamic Stability.—The static longitudinal stability of an airplane measures its *tendency* to return to an equilibrium

position after a disturbance; its dynamic longitudinal stability measures the *manner* of return of the airplane to its equilibrium position. Thus an airplane may be statically stable and yet oscillate about its equilibrium position with an increasing amplitude as shown in Fig. 14.9*a*. Such an airplane is dynamically unstable since undue effort is required of the pilot in maintaining a level flight path. Figure 14.9*b*, on the other hand, shows a dynamically stable motion since the amplitude of oscillation after an initial disturbance diminishes rapidly, owing to the damp-

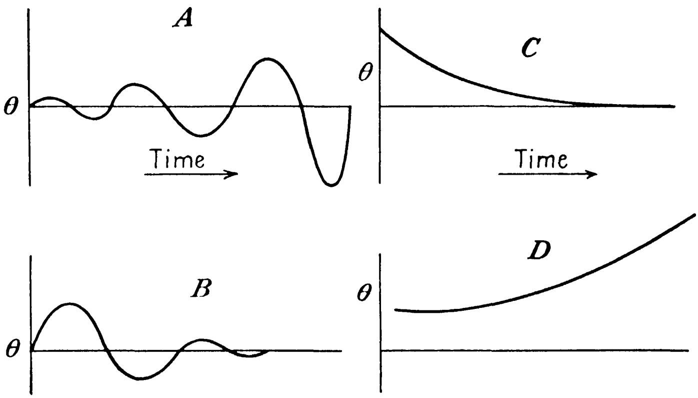

FIG. 14.9.—Types of longitudinal oscillations of an airplane.

ing effect of the airplane, particularly of the tail surfaces. Extreme damping produces the so-called "dead-beat" motion of Fig. 14.9*c* where the airplane returns with no oscillation to its original position. This motion is rarely encountered in practice. Figure 14.9*d* illustrates the angular motion of an airplane which is both statically and dynamically unstable. Such an airplane would obviously be very dangerous to operate.

The mathematical treatment of dynamic longitudinal stability is very involved and laborsome. A practical method of investigating the dynamic stability of an airplane is presented in *N.A.C.A. Technical Report* 521.[1]

[1] C. H. ZIMMERMAN, An analysis of Longitudinal Stability in Power-off Flight with Charts for Use in Design.

Numerous design charts are offered in this report to facilitate the determination of both static and dynamic longitudinal stability.

PROBLEMS

1. Determine, approximately, the static longitudinal stability of the airplane furnishing the pitching-moment curves of Fig. 14.1 at (*a*) trim, (*b*) $C_L = 0.5$, (*c*) $C_L = 1.0$.

2. A tailless airplane weighing 20,000 lb. is designed to cruise at 300 m.p.h. The effective wing area of this airplane is 1,000 sq. ft. with a mean chord length of 12 ft. The value of C_M about the quarter-chord point of its reflexed airfoil is equal to 0.02. Determine the position of the center of gravity along the chord line for both static longitudinal stability and trim under standard sea-level atmospheric conditions. (Assume that the drag exerts no resultant moment about the center of gravity.)

3. Calculate the tail moment at cruising speed of an airplane with the following characteristics:

Cruising speed	200 m.p.h.
Wing angle of attack	3 deg.
(Wing and tail chord lines are parallel)	
Lift coefficient of wing at cruising speed	0.3
Aspect ratio of wing	8
Aspect ratio of tail	3
Tail efficiency, η_t	80 per cent
Distance from center of gravity to quarter-chord point of tail	12 ft.
Tail surface	40 sq. ft.
Tail profile	N.A.C.A. 23012

CHAPTER 15

LATERAL STABILITY

Since the lateral motions of roll and yaw are intimately interrelated, they will be combined in the discussion of the lateral stability of an airplane. The study of lateral stability may be approached by applying the conditions for equilibrium to the various aerodynamic and inertial forces acting on an airplane after a small disturbance from level flight. This leads to a long and mathematically involved analysis, so that only the physical significance of some of the more important aerodynamic factors will be discussed here. Conditions below the stall will be considered first.

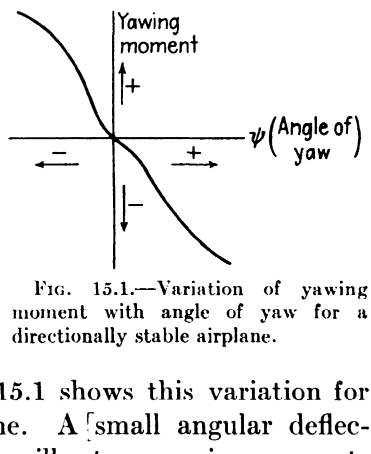

FIG. 15.1.—Variation of yawing moment with angle of yaw for a directionally stable airplane.

Yawing Moment Due to Yaw.—One of the more important of the aerodynamic factors in the theoretical discussion of lateral stability is the variation of yawing moment with angle of yaw. The curve of Fig. 15.1 shows this variation for a directionally stable airplane. A small angular deflection in yaw in either direction will set up yawing moments tending to return the airplane to its initial position. This effect is, of course, produced by the force exerted by the relative wind on the airplane, particularly on the fuselage and the vertical tail, when the airplane is yawed to its direction of flight. Figure 15.2 shows representative positions of the center of pressure of the wind force and the center of gravity of an airplane. Such an airplane may

be said to have "weathercock stability" since it will always tend to turn into the relative wind like a weather vane. The size and location of the vertical tail surfaces are the

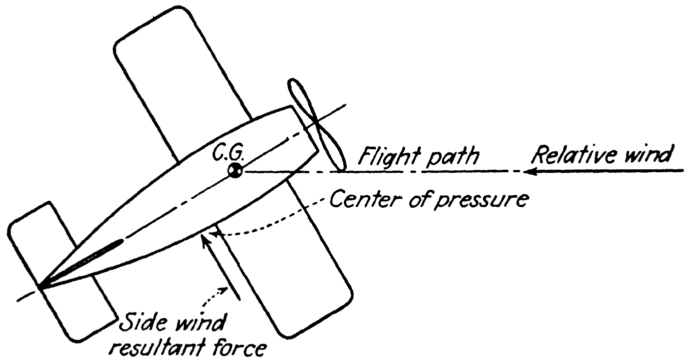

FIG. 15.2.—Relative positions of the center of pressure and the center of gravity for weathercock stability.

predominating influences in determining the degree of weathercock stability.

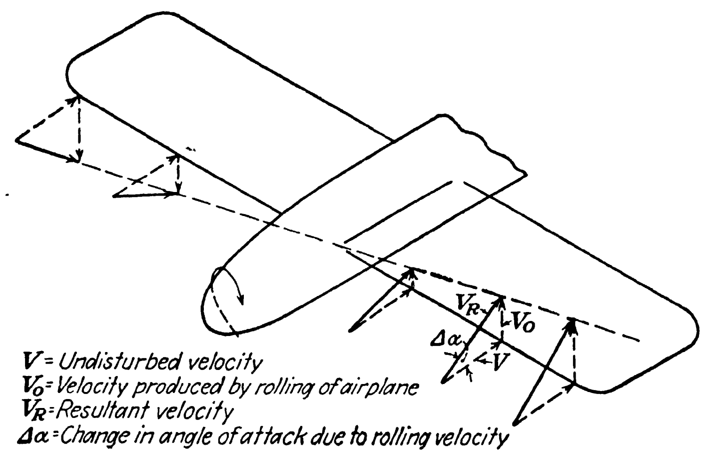

FIG. 15.3.—Changes in angle of attack along a wing during a roll.

Yawing Moment Due to Rolling Velocity.—An airplane executing a pure rolling maneuver is subject to a varying angle of attack along its wing span, as shown in Fig. 15.3. The relative wind at any section along the wing is composed

of a component equal and opposite to the velocity of rotation of the wing at that section added vectorially to the undisturbed velocity of the approaching air stream. The angle of attack of the descending wing therefore increases as the wing tip is approached, while the angle of attack for the rising wing diminishes toward the tip and may even become negative. The lift forces are consequently inclined forward on the dropping wing and backward on the rising wing, creating a yawing tendency in the direction of the ascending wing.

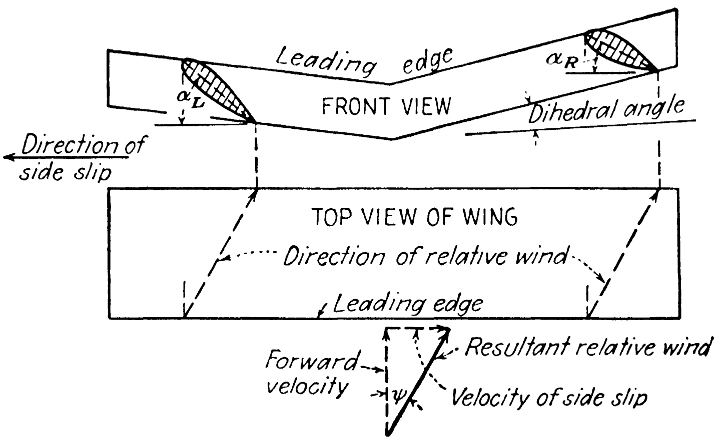

FIG. 15.4.—Influence of dihedral during a sideslip.

Rolling Moment Due to Sideslip.—The wings of conventional airplanes are usually constructed with *dihedral* by sloping the wings upward at a small dihedral angle, as shown in Fig. 15.4. An airplane with dihedral will oppose any sidewise components of the relative wind—sideslip velocities—by tending to tip its wings to provide a lift component in the direction opposite to the motion.

In describing the action of dihedral, an airplane in rectilinear level flight will be considered after a gust of wind has lowered one wing, as illustrated in Fig. 15.4. An airplane in such an attitude would sideslip in the direction of the low wing causing the resultant relative wind to pass obliquely over both wings. Air particles would

accordingly pass over oblique airfoil sections making an increased angle of attack α_L on the lower wing with respect to the relative wind. This increased angle would be reflected in an increased lift on the low wing which would tend to restore the airplane to its normal level-flight attitude.

Since dihedral depends upon sideslip velocity for its action, it has no effect in a *properly* banked turn.

Rolling Moment Due to Yawing.—When an airplane yaws, the velocity of air flow over the advancing wing is increased and over the receding wing is diminished by the superposition of the yawing velocity on the undisturbed

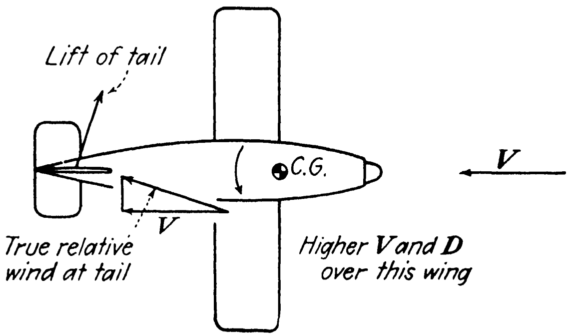

FIG. 15.5.—Damping effects in yaw.

velocity of approach. This difference in velocities produces a corresponding difference in the lift forces on the two wings which tends to roll the airplane in the direction of the turn. The aileron deflection required for a properly banked turn is thereby reduced.

Damping in Roll and Yaw.—The rolling of an airplane sets up an opposing rolling moment which increases with the velocity of roll. As indicated in Fig. 15.3, this opposing or damping moment results from the increase angle of attack—and therefore lift—on the down-moving wing and the decrease in angle of attack and lift on the up-moving wing.

A damping moment is also set up in yaw, which is dependent on the yawing velocity. This moment arises

from two effects: the change of angle of attack with yawing velocity at the vertical tail surfaces which produces a sidewise lift force (Fig. 15.5), and the increased drag on the forward-moving wing coupled with decreased drag on the backward-moving wing owing to the corresponding difference in air speeds.

Damping in both roll and yaw make important contributions to the stability of a conventional airplane.

Static and Dynamic Stability.—Static lateral instability may occur in two ways: an airplane with zero or negative weathercock stability may, after an initial deviation, continue to fly in a yawed attitude or turn to a greater angle of yaw; and an airplane with too little dihedral may, after an initial deviation in roll, sideslip and then either turn over on its back or go into a dive. The remedy to the first type of instability is to add to the weathercock stability through an increase in the vertical tail area or a lengthening of its effective moment arm; more dihedral will obviously preclude the latter type of instability.

An airplane with too much weathercock stability coupled with small dihedral may exhibit a form of dynamic instability known as "spiral instability." Such an airplane, if deviated by an outside disturbance, will yaw, bank, and sideslip simultaneously wherein each component motion contributes to the others to produce a tightening, spiral dive. Generally the pilot checks the motion before it proceeds very far, but it may catch him unaware during night flights or at other times when the visibility is low.

On the other hand, if an airplane is designed with large dihedral and small weathercock stability, it may evidence an undesirable and uncomfortable stable oscillation known as the "Dutch roll." This motion is well named since it resembles that of a (Dutch) ice skater. It is characterized by a roll followed by a yaw to the right, a stable return taking it past the equilibrium position into a yaw and roll to the left, followed by another return to the right, and so on.

The dihedral and weathercock stability of a satisfactory airplane should be proportioned so as to fall within the two extremes marked by spiral instability and Dutch roll. Generally, an airplane is designed to come closer to the spiral instability condition which is considered less objectionable.

The Dutch roll is stable not only statically but dynamically as well, since the amplitude of its oscillations dies out

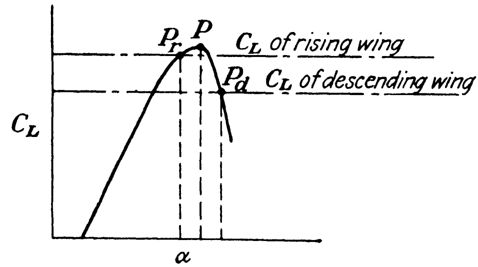

FIG. 15.6.—Autorotation.

in time through aerodynamic damping. Similar oscillations in roll and yaw, which *increase* in amplitude and are therefore dynamically *unstable*, produce oscillatory divergence. Oscillatory divergence, like the Dutch roll, may be avoided through the use of small dihedral and large weathercock stability.

Autorotation.—An airplane operating at or near the stall may exhibit a particularly violent form of instability known as "autorotation." This phenomenon may be described as an uncontrolled roll, accelerated by a difference in lift of the wing on the two sides of the fuselage.

To illustrate the manner in which the accelerating moment develops, consider an airplane operating near its burble point as defined by point P of Fig. 15.6. If a gust of wind or other disturbance should give the airplane an initial rolling velocity, the angle of attack of the descending wing will be increased and of the rising wing decreased corresponding to points P_d and P_r of Fig. 15.6. It will be seen that the lift coefficient of the descending wing is less than that of the rising wing which tends to *increase* the

rotation. Use of the ailerons, moreover, will not usually check the rotation since the influence of the aileron on the up-moving wing will be substantially offset by the reduction of the lift coefficient produced by the aileron on the down-moving wing.

Autorotation may be demonstrated in the wind tunnel by pivoting an airfoil on an axis parallel to the air stream, as shown in Fig. 15.7, and setting the airfoil at a high angle of attack. If given an initial rotation in either direction, the airfoil will continue to autorotate in that direction.

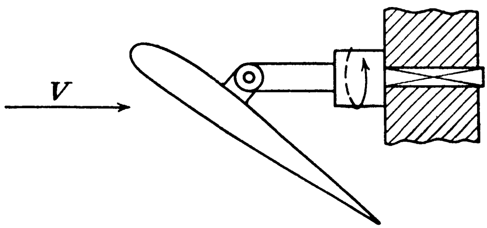

FIG. 15.7.—Wind-tunnel model for demonstration of autorotation.

The Tail Spin.—Autorotation may lead to a more complicated and often more dangerous maneuver known as a "tail spin," or more simply as a "spin."

In a spin, an airplane follows a helical course downward with a very high mean angle of attack and with one or both wings stalled and the control surfaces largely ineffective. A very complex motion is executed in pitch, roll, and yaw to maintain equilibrium between the inertial and aerodynamic forces acting on the airplane. The general method of recovery is to utilize the partial effectiveness of the control surfaces to decrease the angle of attack and to restore thereby smooth flow over the wings and control surfaces in a normal dive.

Spins have resulted in a large number of serious accidents and so have been the subject of a great deal of investigation and research. The N.A.C.A. maintains a special spin tunnel in which light airplane models are supported in free flight on a vertical jet of air. The controls in these models may be deflected electrically and the spin characteristics

noted either visually or photographically. In this way, the spinning properties of a new design may be estimated and the model redesigned if unsatisfactory.

PROBLEMS

1. An airplane with a wing span of 40 ft. executes a pure roll at an angular velocity of 0.5 radian per second. Calculate the change in angle of attack of the wing-tip section corresponding to its cruising speed of 150 m.p.h.

2. Show that the theoretical damping moment in roll L_p of an airplane with a rectangular wing may be expressed:

$$L_p = \frac{dC_L}{d\alpha} \times p \times \frac{\rho}{2} \times c \times V \times \frac{b^3}{12}$$

where $\frac{dC_L}{d\alpha}$ = lift-curve slope

p = angular velocity of roll

ρ = mass density of air

c = wing chord

V = undisturbed velocity; approximately equal to resultant velocity acting on wing elements (in magnitude)

b = wing span

Assume that change in angle of attack at any wing element $\Delta\alpha$ produced by rotational velocity is small so that

$$\tan \Delta\alpha \doteq \Delta\alpha$$

CHAPTER 16

UNCONVENTIONAL AIRCRAFT

The restriction of the minimum flying speed of an airplane to the stalling speed of its wings is the most serious limitation inherent in the conventional airplane. Especially is this true near the ground where the stalling speed proves inconveniently, and often dangerously, high for take-offs and landings. Present-day requirements for high performance and maneuverability in the air only increase the problem, in spite of the extensive use of high-lift devices.

A solution lies in moving the lifting surfaces of an aircraft relative to its fuselage so that the lifting surfaces may remain unstalled for even a forward speed of zero. Two types of aircraft employing this principle have been successfully flown, the *helicopter* and the *autogiro*. The helicopter is characterized by a power-driven lifting rotor, the autogiro by a lifting rotor which is driven in flight by aerodynamic forces alone.

The Helicopter.—The fundamental idea underlying the helicopter—that of coupling an engine to a lifting rotor for the attainment of vertical controlled flight—was not overlooked by the ancients any more than by our own scientists and inventors. The many problems and complications attending the development of this idea have, however, postponed its successful realization until quite recently. The complications may best be reviewed through a general consideration of the aerodynamic aspects of helicopter flight.

For the take-off the rotor of a helicopter should develop enough lift to sustain the weight of the craft during vertical flight. The rotor blades cannot operate at full effective-

ness all along their length, however, since the relative wind velocity over the blades during vertical flight must fall off uniformly with radius to a value near zero at the hub. These circumstances set a definite minimum on the surface area of the blades and, for an efficient blade aspect ratio, a minimum on the rotor diameter as well.

Power considerations also favor rotors of larger diameters. For hovering flight and small rates of climb, the lift of the rotor is equal to the momentum of the air accelerated downward, the momentum depending on the *first* power of the exit velocity, $L = MV$. The energy required by the rotor for the acceleration of the air depends on the *square* of the exit velocity, since it exists principally in the form of kinetic energy, exit K.E. $= \frac{1}{2}MV^2$. It is consequently more economical of power to sustain the weight of a helicopter through the momentum of a large mass of air M and a small exit velocity V, corresponding to a rotor of large diameter.

On the other hand, larger rotors are less desirable from the standpoint of convenience, structural strength, and freedom from vibration and icing troubles. In addition, larger rotors must rotate at lesser rotational speeds to avoid serious compressibility effects at their tips, the slower speeds requiring larger gear reduction elements which add to the total weight of the helicopter. The final rotor diameter selected for a particular design must therefore represent a compromise between conflicting aerodynamic and structural design factors.

Because the rotational speed of a helicopter rotor is generally much lower than that of a conventional airplane propeller, the torque supplied to the rotor is proportionally greater for a given engine horsepower. Since the reaction to the rotor torque tends to turn the fuselage in a direction opposite to the rotor, some external means of torque counteraction is required. A second propeller mounted with its axis of rotation normal to that of the main rotor and provided with adjustable pitch is often used for this

purpose. This arrangement serves also to furnish directional control since the pilot can yaw the aircraft to any desired heading by changing the pitch of the auxiliary propeller. This and several other methods of torque counteraction are illustrated in Fig. 16.1.

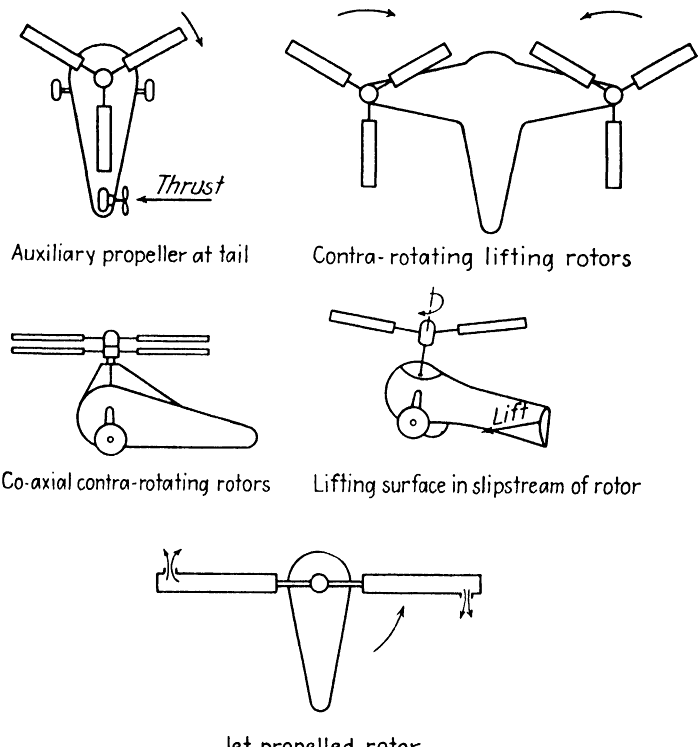

FIG. 16.1.—Various methods of torque counteraction for helicopters.

In forward flight, the air velocity over any blade element of a rotor blade is the vectorial resultant of the forward velocity of the helicopter and the tangential velocity of the blade element, as shown in Fig. 16.2. The tangential velocity of a blade element changes continuously in direction with the rotation of the rotor blade. The resultant velocity over an element must consequently also change

during each revolution, being higher for the advancing than for the receding blade.

If it were not for the "feathering" or the "flapping" of the blades, used singly or in combination, the greater air speed over the advancing blade would create an increased lift for that blade which would tend to roll the helicopter.

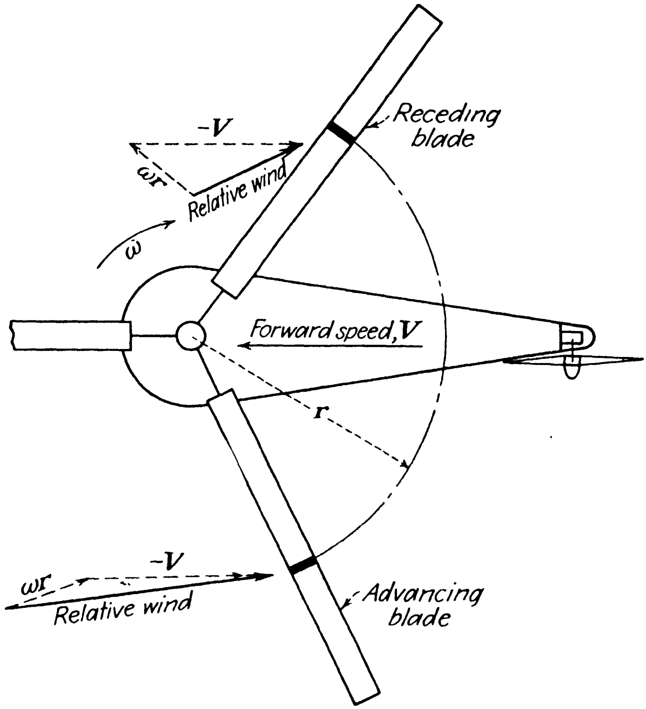

FIG. 16.2.—Relative wind over corresponding blade elements of advancing and receding blades of a helicopter in forward flight.

In feathering, the pitch of a rotor blade is varied during each revolution to compensate for the changing air speed so as to maintain the lift of the blade constant. In flapping, the blades are hinged at the hub so that the blades producing the greater lifts—the advancing blades—are free to rotate upward to a greater angle with the horizontal. This occurs automatically, for equilibrium of the centrifugal and lift forces acting on a blade requires that a blade rotate upward if the lift is increased as shown in Fig. 16.3.

Feathering and flapping are interrelated since a blade feathered to a higher angle of attack will flap upward to a greater angle with the horizontal. Thus, through regulation of the feathering, the path of rotation of the blades—the so-called "rotor disk"—may be tilted in any direction. Figure 16.3 shows how a thrust force in the forward direc-

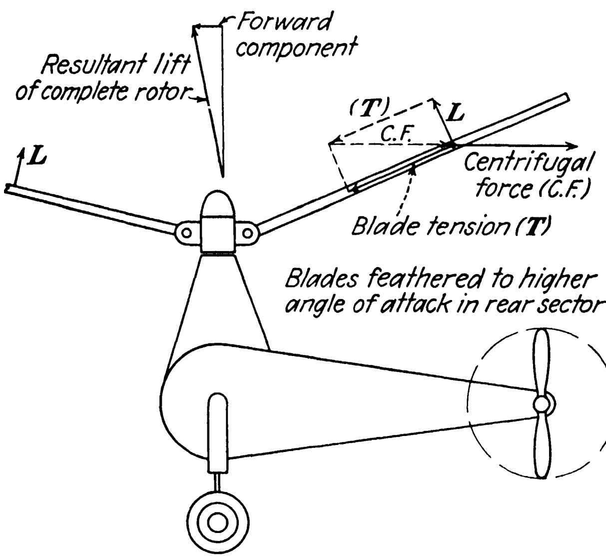

FIG. 16.3.—Production of a forward-thrust force through combined feathering and flapping.

tion may be produced by feathering the blades to a higher angle of attack during the backward sector of rotation. It is interesting to note that the rotor disk may be tilted in this manner in any direction without changing the inclination of the rotor drive shaft. The pioneer Sikorsky helicopter was controlled in this manner.

Since the flapping of a rotor blade sometimes leads to troublesome vibration problems, particularly near the ground, several rotating-wing aircraft designs employ feathering alone. Direct control is used in these designs by tilting the rotor axis in the direction in which flight is desired, as illustrated in Fig. 16.4.

In the event of engine failure, the rotor of a helicopter may be declutched to permit its continued rotation. The

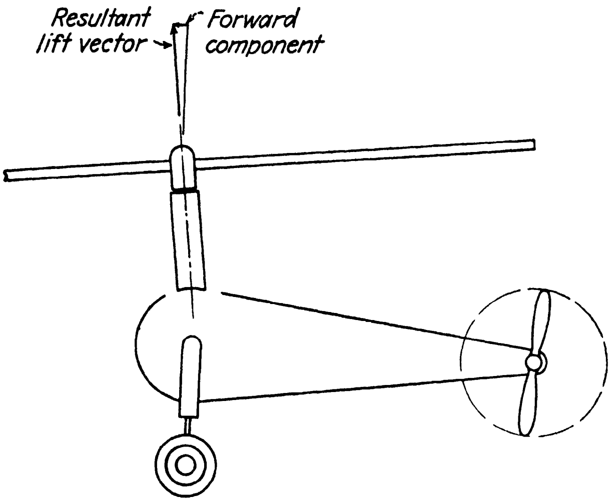

FIG. 16.4.—Direct control of a helicopter through tilting the rotor axis.

rotor then autorotates through the action of aerodynamic forces acting on the blades, as shown in Fig. 16.5. It may be noted that even during vertical descent the resultant aerodynamic force has a component tending to rotate the blade. This rotation serves to reduce the vertical rate of descent of the machine sufficiently to avoid serious injury to either the helicopter or its pilot upon landing. If the helicopter follows an inclined glide path to the ground, the landing shock is greatly lessened.

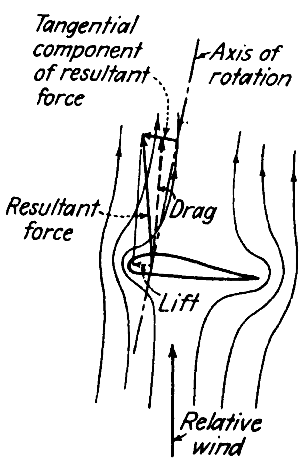

FIG. 16.5.—Action of aerodynamic forces on a typical blade element of a lifting rotor during vertical descent.

Helicopters fill an important need in aviation by virtue of their ability to hover motionless in the air, and to land and take off from small land areas

with little or no horizontal velocity. It is questionable, however, whether the helicopter will ever supplant the airplane. The airplane will probably remain a speedier, less complex, and more efficient heavier-than-air machine for the transportation of freight and passengers.

The Autogiro.—The autogiro utilizes a conventional airplane engine-propeller unit for motive power and a freely rotating lifting rotor for sustentation, as shown in Fig. 16.6. Control is maintained by tilting the rotor axis

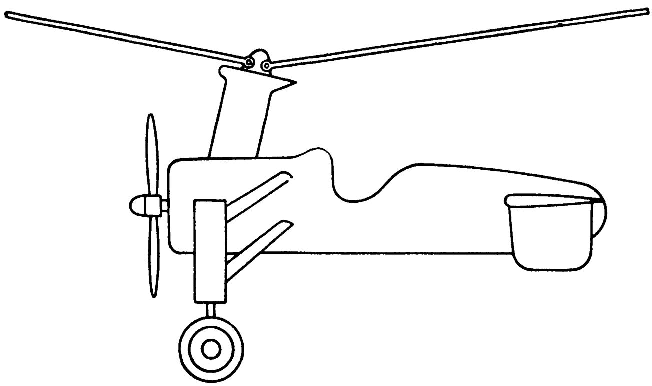

FIG. 16.6.—An autogiro.

and by manipulating conventional rudder and elevator surfaces. The rotor blades are hinged at the hub to permit free flapping.

An explanation of how the rotation of the blades of an autogiro is maintained during level flight may be found in Fig. 16.7 where the forces acting on a typical blade element of a rotor blade are shown. The relative wind for the blade element is drawn in such a direction that it produces a resultant force on the blade element having a forward component with respect to the rotor axis which tends to speed up the rotor. As the rotor speed increases, however, the relative wind tilts downward (since its blade rotation component increases), causing the resultant force on the blade element to tip backward so as to reduce the force component producing rotation. An equilibrium speed of

rotation is thereby reached at which the resultant force remains parallel to the rotor axis.

The autogiro cannot climb vertically except during the course of a "jump" take-off. For this maneuver, a special clutch is engaged between the engine and the lifting rotor while the autogiro is on the ground. The blades are set at low pitch and brought up to fairly high speed; then the clutch is disengaged, and the blades are quickly set at high pitch causing the aircraft to rise vertically for a few feet before assuming its usual inclined path of ascent. In this

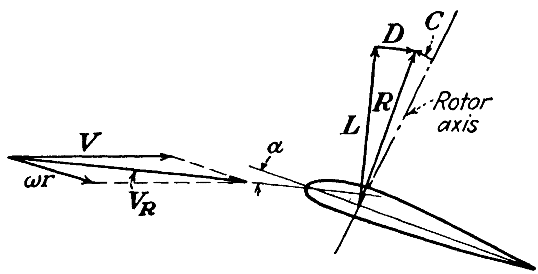

FIG. 16.7.—Forces acting on a blade element of an autogiro rotor during level flight.

manner the autogiro is able to clear obstacles around the edges of small take-off areas.

The autogiro cannot hover for extended periods nor can it land or take off from as restricted areas as the helicopter; on the other hand, the autogiro pioneered in the field of successful rotating-wing aircraft and thus laid the groundwork for the rapid development of the helicopter.

Jet Propulsion.—From a fundamental standpoint, the conversion of the energy in a fuel into useful thrust in a conventional engine-propeller unit is a very roundabout process. First of all, the fuel is burned in the engine cylinders to heat a charge of previously compressed air; then the charge is allowed to expand by doing work on

engine pistons which are mechanically linked with the propeller; finally, the rotation of the propeller increases the rearward momentum of a large mass of air to create the desired thrust force.

Despite this indirectness of operation, the conventional power unit remains the logical choice in most aeronautical applications, mainly because of high efficiency and flexibility of operation. Its high efficiency stems from two sources: the thermodynamic advantage of maintaining high-compression pressures and combustion temperatures in the engine cylinders regardless of the forward speed of the aircraft, and the aerodynamic efficiency of a large-diameter propeller to handle large masses of air.

As aircraft speeds increase, compressibility effects arise in the operation of an ordinary engine-propeller unit which tend to nullify its advantages. Compressibility effects sharply reduce the efficiency of the propeller and contribute to both the high cooling drag of the engine and the profile drag of the engine nacelles. These difficulties at high speeds together with the ever-present mechanical complexity and weight of the conventional drive unit make it profitable to explore the possibilities of other methods of producing a useful thrust force.

The more attractive alternatives and adjuncts to the ordinary reciprocating engine-propeller drive fall under the general heading of jet-propulsion devices, of which the turbine-jet unit is representative. The simplicity of the turbine-jet unit is revealed by an examination of the diagrammatic sketch of Fig. 16.8, where it may be seen that the rotary compressor and its turbine drive contain the only moving parts of the power cycle. In operation at low forward speeds, atmospheric air enters the compressor through the front opening of the unit and is compressed to four or five times atmospheric pressure; at high forward speeds, the *ram* effect of the near-stagnation pressures developed in the relatively slow-speed air at inlet substantially increases the compression pressure.

The air thus compressed is heated by the combustion of the fuel and then passes to the gas turbine, which extracts enough work to drive the compressor. Finally, the air is expanded through the exit channel which transforms as much of the remaining pressure and heat energy as possible into increased kinetic energy of the exit jet.

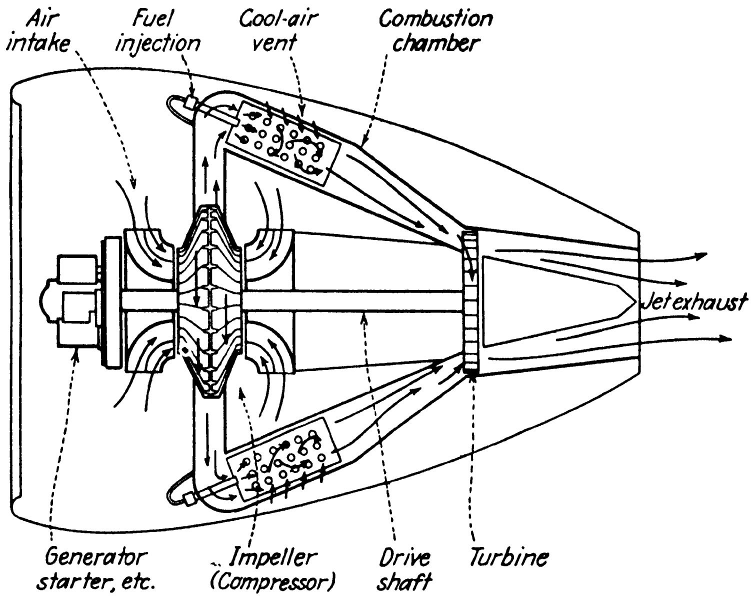

FIG. 16.8.—Diagram of a gas-turbine jet-propulsion unit. (*General Electric Company.*)

The turbine-jet unit may be directly compared with a reciprocating engine-propeller unit, since each accomplishes the same end in fundamentally the same manner. To assist in the comparison, Fig. 16.9 shows corresponding processes in the two thermodynamic cycles. In the compression process the rotary compressor of the jet unit operates at a lower efficiency and produces a lower compression pressure than the reciprocating engine. In a way the lower compression pressure of the jet cycle is advantageous for, although it detracts from the thermal efficiency of the cycle, it makes possible the use of kerosene or other

cheap grades of fuel rather than high-octane gasoline. For the combustion process the continuous flow of the jet engine maintains the burning of the fuel, while the intermittent action of the reciprocating engine calls for a comparatively complicated ignition system. The expan-

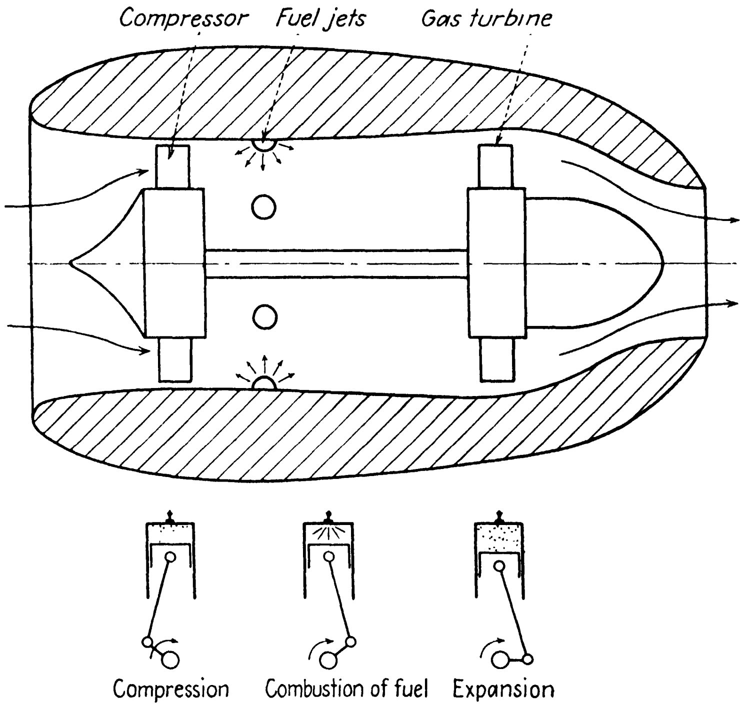

FIG. 16.9.—Comparison of the operation of a turbine jet unit with the events of a reciprocating-engine power cycle.

sion process of the reciprocating engine is more efficient *as far as it goes* because of lower fluid-frictional losses, but the combined expansion in the gas turbine and the exit nozzle is much more complete. For the complete cycle, the thermal efficiency of the jet unit is less than that of the reciprocating engine, particularly at low flying speed. Future improvements in design and materials will, however, almost certainly narrow the gap between them.

The propulsive efficiency is fully as important as the

thermal efficiency since the over-all efficiency is equal to the product of the two. In this the reciprocating engine-propeller unit is far superior to the usual jet unit at low and moderate speeds because of the greater mass of air handled for a given thrust force, the masses of air handled being roughly proportional to the propeller disk area and the jet inlet area, respectively. Compressibility effects,

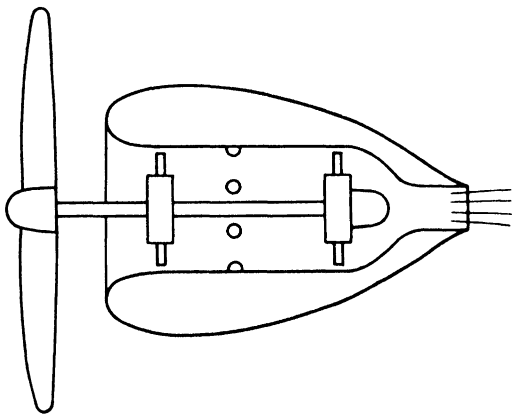

FIG. 16.10.—Gas turbine with propeller and exhaust jet.

however, which seriously impair the efficiency of a conventional propeller above about 450 m.p.h., may be postponed in the jet unit to a much higher forward speed by making the areas through the compressor and the turbine larger than the inlet area. Thus the over-all efficiency of the jet unit overtakes that of the engine-propeller unit at very high speeds.

A compromise design is shown in Fig. 16.10 where the gas turbine of a jet unit is used to drive a variable-pitch propeller as well as the usual rotary compressor. In this way each method of propulsion may assume the greater part of the load in the speed range in which it is most effective.

A very interesting and remarkably simple jet-propulsion device is the resonance motor developed for the German "buzz-bomb." As shown in Fig. 16.11, flap valves in the

entrance section comprise the only moving parts. In operation, air passes through the flap valves into the combustion chamber where fuel is added and an explosion occurs. The gas pressure so generated closes the flap valves and propels the mass of burning gas out of the exit opening at high velocity. The momentum of this exit gas not only produces a useful thrust reaction but assists in drawing a new charge into the combustion chamber, by creating a lowered pressure on the inside of the flap valves.

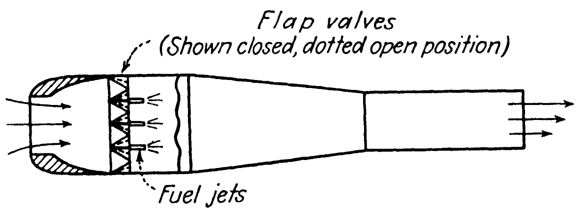

FIG. 16.11.—Diagram of a resonance motor.

The frequency of the explosions is determined by the resonant frequency of the tube which, in the German design, is about 45 cycles per second. The over-all efficiency of the resonance unit is much lower than that of the turbine-jet unit owing to its lower compression pressure and consequent lower thermal efficiency.

A *rocket motor* carries the oxygen required for the combustion of its fuel along with it, as distinguished from jet-propulsion motors, which use oxygen from atmospheric air. Like all other propulsive devices, the rocket develops a reactive thrust force by accelerating a mass of gas rearwardly according to the familiar equation, $F = M\Delta V$. Since in the rocket the accelerated mass of gas is formed wholly from the combustion of the fuel with stored oxygen, the presence of atmospheric air is unnecessary and is indeed detrimental to its efficient operation.

A simple form of rocket motor employing a solid propellant is shown diagrammatically in Fig. 16.12. The device consists essentially of a chamber which serves the twofold purpose of storing the fuel with its oxidizer and of accom-

modating the combustion process; an igniter which initiates combustion; and a nozzle which transforms the heat and pressure energy generated in the combustion process into kinetic energy of the exit jet. Solid-fuel rockets of this kind have proved effective in shortening the take-off runs of airplanes by providing additional thrust until the airplane is air-borne.

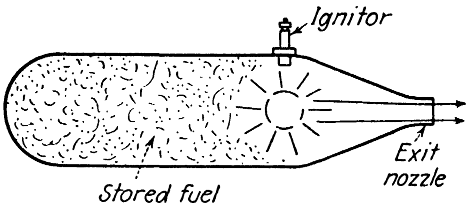

FIG. 16.12.—Diagram of a solid-fuel rocket motor.

Liquid-fuel rocket motors offer higher efficiencies and greater control over the combustion process than the solid-fuel motor which for some applications justify their increased complication. As shown in Fig. 16.13, the fuel, which may be alcohol or a petroleum product, is pumped to a burner where it is united with oxygen to form high-temperature and high-pressure combustion gases which are

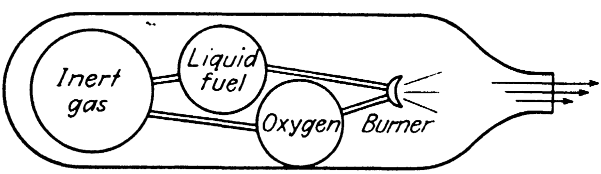

FIG. 16.13.—Diagram of a liquid-fuel rocket motor.

expelled from a nozzle to the rear. The oxygen is usually stored in liquid form, introducing serious difficulties in the care and handling of the rockets. The liquid-fuel rocket has not, as yet, found practical application as a propulsive device for passenger airplanes. It has so far been developed most highly in the German V-2 rocket projectile which is reported to have a top speed of over 3,000 m.p.h. and a range of more than 300 miles.

As with other methods of propulsion, the propulsive efficiency of a rocket motor depends on the relation between its forward and jet speeds. When the forward speed of a rocket equals the speed of efflux of its jet, the ejected gas particles have no motion relative to the earth and therefore no kinetic energy; the theoretical efficiency then reaches its peak value. The jet velocity of a rocket is extremely high, however, so the propulsive efficiency is low for practical flying speeds.

Of the jet propulsion and rocket motors discussed, the gas-turbine jet motor has found the most widespread application in present-day military aircraft. With continued development, the turbine-jet unit may displace the conventional engine-propeller unit in many of the high-speed military and commercial airplanes of the future.

INDEX